

# Contribution to the application of Optical Camera Communications to Wearable Sensor Networks

#### Eleni Niarchou

Doctoral thesis to achieve the academic degree of

Doctor of Philosophy (Ph.D.)

in the doctorate program
EmITIC - Empresa, Internet y Tecnologías de las Comunicaciones

IDeTIC - Instituto para el Desarrollo Tecnológico e Innovación en Comunicaciones
Universidad de Las Palmas de Gran Canaria

Date: September 2025

## **Supervisors**

**Prof. Dr. Rafael Pérez Jiménez** IDeTIC, Universidad de Las Palmas de Gran Canaria

**Dr. Vicente Matus Icaza**IDeTIC, Universidad de Las Palmas de Gran Canaria

#### **Examiners**

**Prof. Dr. Konstantinos Yiannopoulos** University of Peloponnese

**Prof. Dr. Cesar Augusto Azurdia Meza** University of Chile

Anexo	ı

D/D <sup>a</sup> SECRETARIO/A DEL DEPARTAMENTO DEDE LA UNIVERSIDAD DE LAS PALMAS DE GRAN CANARIA,						
CERTIFICA,						
Que el Consejo de Doctores del Departamento en su sesión of fecha	to ne or					
Y para que así conste, y a efectos de lo previsto en el Al 73.2 del Reglamento de Estudios de Doctorado de es Universidad, firmo la presente en Las Palmas de Gran Canaria, a . dede dos mil veinticinco.	ta					

#### Anexo II

#### UNIVERSIDAD DE LAS PALMAS DE GRAN CANARIA

Departamento: Instituto para el Desarrollo Tecnológico e Innovación en

Comunicaciones Programa de Doctorado: Empresa, Internet y Tecnologías de las Comunicaciones					
	Título de la Tesis				
Contribution to the application Sensor Networks.	ation of Optical Camera (	Communications to Wearable			
Tesis Doctoral presentada	a por Dª Eleni Niarchou.				
Dirigida por el Dr. Rafael I	Pérez Jiménez.				
Codirigida por el Dr Vicen	te Matus Icaza.				
El/la Director/a,	El/la Codirector/a	El/la Doctorando/a,			
(firma)	(firma)	(firma)			
Las Palmas de Gra	n Canaria, ade	de 2025			

# Dedication

In loving memory of Prof. Antony C. Boucouvalas.

## Acknowledgments

#### **Funding**

This work has received funding from the Agencia Estatal de Investigación (AEI, Spanish Research Government), under the FPI grant (PRE2021-100311).

#### **Collaborators**

The author thanks the technical contributions and active support from the team members at the Institute (IDeTIC) in Las Palmas de Gran Canaria, Spain, the Department of Electromagnetic Field, Czech Technical University (CTU) in Prague, Czechia, and Instituto de Telecomunicações (IT), Universidade de Aveiro, Aveiro, Portugal, listed as follows:

- Main supervisor: Prof. Rafael Pérez Jiménez (IDeTIC).
- Second supervisor: Dr. Vicente Matus Icaza (IDeTIC).
- Academic staff:
  - Prof. José Rabadan (IDeTIC).
  - Dr. Victor Guerra (IDeTIC).
  - Prof. Stanislav Zvanovec (CTU).
  - Prof. Luis Nero Alves (IT).
- Technical support:
  - Dr. Matej Komanec (CTU).
  - Klara Eollos Jarosikova (CTU).
  - Atiya Fatima Usmani (IT).

Modern society is heavily dependent on a radio-based wireless communications infrastructure, which is almost congested as the demand for high-capacity and low-latency wireless connections grows with the increasing number of devices. Optical wireless communication (OWC), which operates in the optical spectrum, emerges as a promising complementary technology, capable of addressing the capacity challenges of future networks. Within OWC, visible light communication (VLC), is a technology that repurposes existing lighting systems, such as solid-state lighting (SSL) systems in offices, homes, hospitals, and airports, to transmit data using optical spectrum wavelengths through light-emitting diodes (LEDs) used for illumination, with photodiodes (PDs) serving as receivers. Despite the providing advantages of VLC in terms of enhanced security, spectrum availability, and interference immunity, the complexity of integrating this hardware in end-user devices serving as receivers, has made VLC challenging to be adopted in the marketplace.

On the contrary, the plethora of off-the-shelf cameras in end-user devices, such as smartphones and public infrastructure surveillance cameras, eliminates the need for additional hardware at the reception stage and has led to the emergence of a new branch of VLC, known as optical camera communication (OCC). OCC is standardized by the Institute of Electrical and Electronics Engineers (IEEE) and the International Telecommunications Union (ITU) through the IEEE 802.15.7a standard and ITU-T G.9992, respectively. By employing cameras as receivers, OCC enables the operation of cameras both as imaging devices and as communication tools, in a variety of applications, particularly in dynamic and resource-constrained environments such as wireless sensor networks (WSNs) and Internet of Things (IoT) systems. For the first time, OCC allows the development of commercial, low-

cost wireless optical communication systems by leveraging ubiquitously available technology, paving the way for innovative and accessible solutions across numerous industries.

WSNs are composed of spatially distributed sensor nodes that collaborate to monitor and collect data about their environment. They are designed to observe one or more physical parameters, such as temperature, humidity, motion, or light, and transmit wireless data to a central system. WSNs have found widespread applications in industrial automation, environmental monitoring, healthcare, agriculture, and smart cities. The WSNs nodes are typically small-sized, battery-powered devices with sensors, processing units, and wireless communication modules (e.g. LEDs). Therefore, wearable devices can act as mobile or semi-mobile nodes in WSNs.

Smartwatches, fitness bands, smart clothing, and medical patches, are examples of wearable devices that can be seamlessly integrated into daily life. These devices are equipped with sensors and processors enabling them to collect, process, and transmit data about their users and their surroundings. Typically, the commercially available devices use RF technologies such as Bluetooth or near-field communication (NFC), for data transmission, which face limitations in link distance, safety, electromagnetic interference, and spectrum usage. For this reason, the replacement of these modules with LEDs could overcome these limitations.

This thesis experimentally evaluated the feasibility of deploying LED transmitters in the form of wearable devices, in OCC systems and WSNs. The first objective (O1) of the research is to establish efficient indoor and outdoor OCC links by including hybrid solutions that combine image processing and wireless optical communication. Additionally, (O2) to analyze how the channel conditions related to the position and configuration of sensor nodes affect data rate performance. Finally, (O3) proposes the use of an artificial intelligence (AI) algorithm for node recognition and tracking, in networks with multiple camera receivers.

The core of this thesis is based on several contributions published in high-impact journals, following the progression of the research. During the exercise of this thesis, contributions have been achieved in: (i) making the system available for widespread use, as in most experimental OCC setups in this research, commercial devices employed as transmitters (i.e., LED array, LED strip, LED-coupled side-emitting optical fiber) and receivers (i.e., smartphones, Raspberry Pi cameras), (ii) developing an image processing algorithm for accurately detecting transmitted bits within frames, despite the user's movement, (iii) detecting the user's position within the frame, offering valuable insights into the user's exercise intensity, and could potentially identify chronic conditions or detect early signs of injuries, (iv) analyzing critical aspects for the transmitter placement in relationship with the camera receiver position, (v) making the system applicable in high-risk environments, where real-time monitoring of users' physical conditions is critical, with the integration of deep learning into OCC systems, enabling indoor communication and monitoring, even under challenging conditions such as low visibility, user movement and multiple users.

La comunicación óptica inalámbrica (OWC), que opera en el espectro óptico, es una tecnología complementaria prometedora para coexistir con las tecnologías actualmente más utilizadas, capaz de abordar los desafíos de capacidad de las redes futuras a un coste aceptable y con dispositivos ya disponibles comercialmente. Dentro de este campo, la comunicación por luz visible (VLC) es una tecnología que reutiliza los sistemas de iluminación existentes, como los sistemas de iluminación de estado sólido (SSL) en oficinas, hogares, hospitales y aeropuertos, para transmitir datos utilizando longitudes de onda del espectro óptico a través de diodos emisores de luz (LED) utilizados para la iluminación, con fotodiodos (PD) que actúan como receptores. Sin embargo, a pesar de las ventajas que ofrece esta tecnología en términos de su inherente seguridad de los datos, disponibilidad de espectro e inmunidad a interferencias, la complejidad de integrar este hardware en dispositivos de usuario final que actúan como receptores ha dificultado su adopción en el mercado. Esto ha llevado a buscar alternativas en el tipo de receptores a emplear para captar y procesar información transmitida por medios ópticos como son las cámaras. Estas, al contrario que los fotodiodos, están disponibles comercialmente de forma ubicua, en dispositivos de consumo como teléfonos, tablets, monitores de televisión o sistemas de vigilancia. Su uso, si bien limitado a velocidades y distancias bajas, elimina la necesidad de hardware adicional en la etapa de recepción y ha propiciado el surgimiento de una nueva rama de la comunicación óptica por cámara, conocida como comunicación óptica mediante cámaras (OCC) y que ha sido estandarizada por el Instituto de Ingenieros Eléctricos y Electrónicos (IEEE) y la Unión Internacional de Telecomunicaciones (UIT) a través de las normas IEEE 802.15.7a e ITU-T G.9992, respectivamente.

Al emplear cámaras como receptores, estos se convierten en dispositivos duales

que simultanean su funcionamiento como dispositivos de imagen y herramientas de comunicación en diversas aplicaciones, especialmente en entornos dinámicos y con recursos limitados, como las redes de sensores inalámbricos (WSN) y los sistemas del Internet de las Cosas (IoT). OCC ha permitido que, por primera vez, se estén desarrollando sistemas comerciales de comunicación óptica inalámbrica de bajo costo aprovechando tecnología ampliamente disponible, allanando el camino para soluciones innovadoras y accesibles en numerosos sectores. En concreto, en el campo de las WSN, estas mallas de sensores distribuidos espacialmente están diseñadas para observar uno o más parámetros físicos (como temperatura, humedad, movimiento etc.) transmitiendo datos inalámbricos a un sistema central. En este caso concreto, se estudian aplicaciones basadas en el control de la salud o la actividad física, y dentro de estos, destacan por su interés los dispositivos vestibles o wearables, según su denominación más extendida. Vienen caracterizadas por la baja velocidad de transmisión requerida, su pequeño tamaño y baja complejidad en cuanto a unidades de procesamiento, estar alimentados por batería y requerir una alta seguridad y baja latencia. Estos sensores pueden actuar como nodos móviles o semimóviles en las WSN. Los relojes inteligentes, las pulseras de actividad física, la ropa inteligente o los parches médicos, pueden ser en sí mismos ejemplos de dispositivos wearables que se integran a la perfección en la vida diaria, o bien dispositivos que interactúan con otros sensores o actuadores que les permiten recopilar, procesar y transmitir datos sobre sus usuarios y su entorno. Si bien habitualmente estas interacciones se basan en tecnologías de radiofrecuencia como Bluetooth de bajo consumo (LPB) o comunicación de campo cercano (NFC) para la transmisión de datos, estas tecnologías presentan limitaciones en cuanto a la distancia de enlace, la seguridad, la interferencia electromagnética y el uso del espectro, que aconsejan valorar alternativas como los módulos por LED para tratar de superar estas limitaciones.

Esta tesis evalúa experimentalmente la viabilidad de implementar transmisores LED en dispositivos portátiles para sistemas OCC en redes inalámbricas de sensores (WSN). El primer objetivo ha sido establecer enlaces OCC eficientes en interiores y exteriores mediante la inclusión de soluciones híbridas que combinan el procesamiento de imágenes y la comunicación óptica inalámbrica. Además, se analiza cómo las condiciones del canal, relacionadas con la posición y configuración de los nodos sensores, afectan el rendimiento de la velocidad de datos. Finalmente, se propone el uso de un algoritmo de inteligencia artificial (IA) para el reconocimiento y seguimiento de nodos en redes con múltiples receptores de cámara.

El núcleo de esta tesis se basa en varias contribuciones publicadas en revistas de alto impacto, siguiendo el progreso de la investigación. Durante el desarrollo de esta tesis doctoral, se han logrado contribuciones en el uso de sistemas OCC basados en dispositivos comerciales empleados como transmisores (p. ej., matrices o tiras LED o fibras óptica de emisión lateral acoplada a LED) y receptores (como teléfonos inteligentes o cámaras Raspberry Pi); También se ha abordado el desarrollo un algoritmo de procesamiento de imágenes para detectar con precisión los bits transmitidos dentro de los fotogramas, independientemente del movimiento del usuario, y se han analizado aspectos críticos para la colocación del transmisor en relación con la posición del receptor de la cámara, con el fin de mejorar la detección de la posición del usuario dentro del fotograma, lo que ofrece información valiosa sobre la intensidad del ejercicio del usuario y podría potencialmente identificar enfermedades crónicas o detectar signos tempranos de lesiones o ser usado en entornos de alto riesgo donde las emisiones radioeléctricas convencionales pueden estar contraindicadas.

# Contents

De	edicat	tion	vii
Ac	know	vledgments	ix
Αb	strac	rt e e e e e e e e e e e e e e e e e e e	хi
Re	sume	en	χv
Co	nten	ts	xix
1	1.1 1.2 1.3 1.4 1.5	Motivation  Hypotheses Objectives Organization of the document List of publications 1.5.1 Journal articles 1.5.2 Conference proceedings 1.5.3 Collaborations	1 3 4 5 6 6 7 7
2	2.1 2.2	Challenges	9 10 13 13 13
3	<b>The</b> 3.1	Fundamentals 3.1.1 Modulation schemes 3.1.2 Artificial intelligence for optical camera communications Technologies 3.2.1 Transmitters	17 17 17 19 22 22 23
4	4.1 4.2 4.3	Experimental setups	27 27 29 31 31 32 33

5	Exp	erimental Results	37		
	5.1	Publication 1 (P1)	37		
	5.2	Publication 2 (P2)	52		
	5.3	Publication 3 (P3)	66		
	5.4	Summary	75		
6	Conclusions and Future Works				
Bi	bliogi	aphy	83		
A	Con	ference proceedings	93		
В	Coll	aborations 1	105		

Introduction

Optical camera communications (OCC) is a cutting-edge technology within the field of optical wireless communications (OWC) and visible light communications (VLC), particularly under the standard of the Institute of Electrical and Electronics Engineers (IEEE) 802.15.7a [1]. OCC employs light-emitting diodes (LEDs) as transmitters, and image sensors (i.e. cameras) as receivers, with light (visible, infrared, ultraviolet) serving as the signal communication carrier. This technology offers many advantages compared to conventional radio-frequency (RF) technologies, with regard to security, immunity to electromagnetic interference, cost-effectiveness, and energy efficiency [2].

The plethora of cameras on end-user devices, such as smartphones and public infrastructure surveillance cameras, has further simplified the use of OCC, eliminating the need for additional hardware. As shown in Figure 1.1 the global volume in the digital cameras segment of the consumer electronics market is expected to increase steadily between 2024 and 2029, by a total of 8.5 million units (+6.71%), reaching a peak of 135.1 million units in 2029. Besides their elementary functionality of capturing images, cameras are capable of capturing details beyond the human visual limit and enable applications such as communication, localization, and activity/motion detection, which are highly relevant for indoor and outdoor Internet of Things (IoT) applications [3], [4]. By employing cameras as both image capture devices and communication tools, OCC eliminates the need for additional hardware, reducing the cost and complexity of end-user devices while enabling advanced capabilities such as space division multiple access (SDMA) [5] and color-space based modulations [6]. This makes OCC particularly attractive to markets, as implementing an OCC-based application on smartphones would only require a computer vision-based app, as well as, especially valuable in dynamic and resource-constrained environments, such as wireless sensor networks (WSNs).

WSNs [8] are low-cost and ultra-low-power networks consisting of spatially distributed sensor nodes that cooperate to sense and collect environmental information. They should also provide low-latency performance when required for real-time applications [9]. Sensor

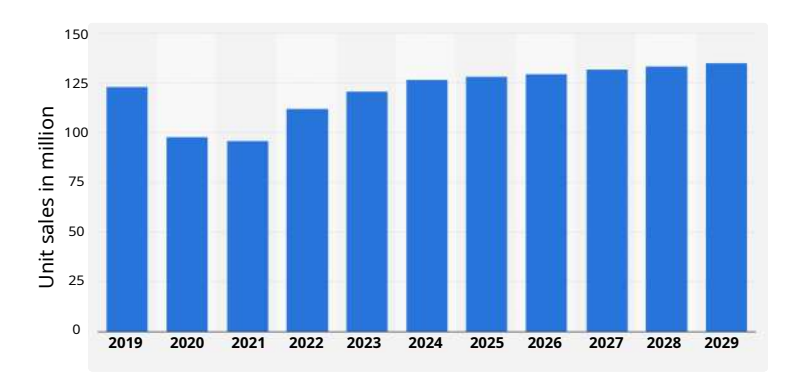
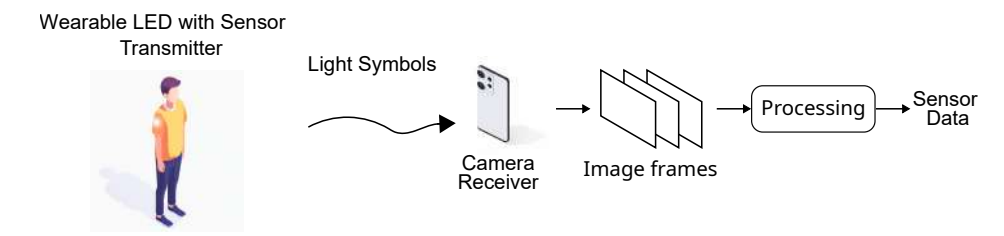


Figure 1.1: Volume of digital cameras Worldwide 2019-2029. Source: Statista [7]

#### Chapter 1 Introduction



**Figure 1.2:** Diagram of application of optical camera communication to wearable sensor networks.

nodes are usually compact, battery-operated devices composed of sensors, processing units, and wireless communication components (e.g., LEDs) that measure one or more physical parameters such as temperature, humidity, motion, or light and transmit the sensed data wirelessly to the central processing system. They find application in the military [10], agricultural plant monitoring [11], environmental monitoring [12], traffic management [13], and health monitoring [14].

Wearable devices in WSNs represent a rapidly advancing technology that enables real-time monitoring of users, as well as the transmission of data about their environments, with applications in healthcare, fitness, and smart environments, by deploying sensors, processors, and communication modules. Examples of such wearable technologies include smartwatches, smart wearables, and glucose monitoring patches-are lightweight and compact, easily wearable in daily life [15]. By combining OCC with wearable technology, the data measured by these devices can be forwarded to cameras for processing with the aid of OCC-enabled LEDs; hence, a secure and power-efficient communication solution is provided. This would have potential in applications that require high data integrity and low latency, such as health monitoring and fitness tracking. In this work, we propose employing OCC in a wearable sensor network with LED-based wearable transmitters, to transmit sensor data to cameras, as shown in Figure 1.2.

By repurposing accessible and commercially available devices, such as LED arrays, LED strips, and side-emitting fibers for transmitters, along with off-the-shelf surveillance cameras and smartphones as receivers, as shown in Figure 1.3, OCC apart from reducing the need for additional specialized hardware, enables a cost-efficient and practical communication and monitoring system. The transmitter side can be implemented using a simple LED circuit consisting of an LED component, a microcontroller unit (MCU), and a power source — which is significantly less complex compared to traditional Bluetooth Low Energy (BLE) circuitry [16] - to transmit the data collected from wearable sensors or patches. On the receiver side, commercially available closed-circuit television (CCTV) cameras or smartphones, beyond their primary role in user activity monitoring, can also capture signals from wearable sensors, transforming them into communication tools.

The integration of OCC with wearable sensor networks offers new opportunities for wearables. OCC provides secure communication, addressing critical challenges such as spectral congestion and energy efficiency in resource-constrained systems. Hence, it is ideal for applications, such as health monitoring systems, fitness tracking devices, and safety-focused applications. The increasing number of wearables and the arrival of 6G, will bring a new era for smart environments and healthcare, characterized by enhanced

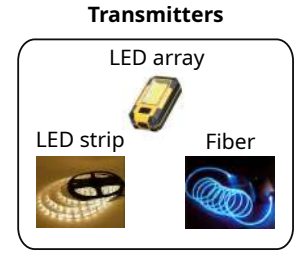




Figure 1.3: Example of commercial devices used as LED transmitters and camera receivers.

sensing, processing, and communication capabilities seamlessly integrated into everyday life.

#### 1.1 Motivation

The OCCAM project, funded by the Agencia Estatal de Investigación (AEI, Spanish Research Government) under the PID2020-114561RB-100 grant, is directed at research challenges in optical communication systems, particularly using monitoring cameras within sensor networks.

The Institute for Technological Development and Innovation in Communications (IDeTIC), part of the University of Las Palmas de Gran Canaria (ULPGC), consists of six divisions, among which the Division of Photonics Technology and Communications holds the OCCAM project. The division has been working on VLC and OCC, with funding from international and national sources. In this context, the OCCAM project is funded by highly active and pioneering researchers in the area.

Previous research in IDeTIC, which has provided the foundation for the development of this thesis, has focused on practical experimental implementations of VLC [17], [18] and, in particular, on OCC in WSN [19]. In addition, the research includes works on discovery and tracking systems for OCC [20], on localization [21], smart cities [22], optical multispectral camera communications [23] and underwater optical wireless communications [24], [25].

#### 1.2 Hypotheses

Taking into account the continuous advances in smart environments and localization systems, this work explores how commercially available devices, such as cameras and LEDs, can be used to receive signals from wearable sensors. The hypotheses of this work are stated as follows.

#### Hypothesis 1 (H1)

The ubiquitous availability of cameras, embedded in many devices such as smartphones, tablets, or surveillance devices that already exist in an indoor or outdoor environment, can be used for receiving signals from wearable sensors.

OCC systems can be implemented using commercially available cameras, such as those in smartphones, tablets, or surveillance cameras in indoor and outdoor environments.

#### Chapter 1 Introduction

Many surveillance cameras already installed in many places, can be utilized not only for video monitoring of user activity but also as means for communication, as these cameras can serve as receivers for signals transmitted by sensors worn by users, therefore limiting the need for additional hardware.

#### Hypothesis 2 (H2)

It is feasible to implement a network where multiple sensors transmit, simultaneously, to the cameras, within an indoor or an outdoor environment.

Cameras can capture data from multiple sources at the same time and therefore, serve as central nodes in a sensor network. The system that could enable real-time tracking and monitoring of many users within the same environment is suitable for complex indoor and outdoor environments where many people might need monitoring.

#### Hypothesis 3 (H3)

The artificial intelligence image processing algorithms combined with data decoding OCC can efficiently track and predict the users' movement.

Computer vision is a supporting technology within AI that enhances the image processing capabilities needed for precise tracking. Various neural networks (NNs) have shown effectiveness in the computer vision applications of deep learning, to track a large number of users in indoor and outdoor environments, and offer predictive modeling for the anticipation of future movements.

#### 1.3 Objectives

#### Objective 1 (O1)

To implement optical communication links based on cameras (OCC) using image sensors in the optical spectrum including hybrid solutions that combine image processing and wireless optical communication.

In order to demonstrate H1, experiments must be conducted in an indoor and outdoor environment to test the feasibility of using commercial off-the-shelf cameras embedded in many devices such as smartphones, tablets, or surveillance devices for receiving signals emitted by wearable sensors using optical spectrum image sensors combined with image processing algorithms and wireless optical communication. This system can eliminate the need for additional hardware, by reusing cameras already installed for video monitoring, making it possible to efficiently track and communicate with users within the indoor or outdoor environment.

This objective is addressed by all the published articles (P1, P2, and P3) presented in Chapter 5 as a compendium, as they explore different image sensors in indoor OCC to validate the integration of image processing and wireless optical communication. In addition, outdoor OCC was studied in the conference paper [26] (see Chapter A), demonstrating its feasibility. To expand the scope of the optical spectrum, it was demonstrated that OCC is not limited to visible light but can also utilize near-infrared (NIR), as shown in the conference paper [27] (see Chapter B).

#### Objective 2 (O2)

To examine the impact of channel conditions related to the position and configuration of the sensor nodes on data rate performance.

Based on the H2 that it is feasible to implement a network in which multiple wearable sensors communicate simultaneously with cameras, this study will evaluate how factors such as the number, positioning, and configuration of sensors as network nodes, as well as the channel conditions related to position (e.g., near-far distances, obstructions, ambient light interference), affect data transmission rates, and overall network performance. To address this, the research tries to optimize network configurations supporting real-time tracking and monitoring of multiple users in complex indoor or outdoor environments by analyzing data rates on the number, positioning, and channel conditions of sensors and cameras, with experimentation in short and long distances and under different light conditions.

This objective is addressed in publications P2 and P3. The importance of sensor positioning and environmental factors is supported by the findings in P2, which highlight how different placements of wearable LED transmitters influence communication performance. Furthermore, P3 demonstrates how deep learning-based detection and tracking of wearable LEDs are affected by factors such as movement and lighting conditions. Regarding distances, P1 demonstrates OCC feasibility at a short link distance of 20-30 cm, while the conference paper for outdoor OCC [26] extends this to 90–120 meters.

#### Objective 3 (O3)

To deploy networks with multiple receivers and apply node recognition and tracking algorithms based on artificial intelligence techniques.

It is proposed in H3 that a system using an OCC combined with Al-based image processing algorithms can track and predict user movements within an indoor environment. Computer vision combined with NNs would allow the cameras to monitor many users and receive signals from their wearable sensors. Predictive modeling further enhances the system's ability to predict movements and optimize applications such as positioning, tracking, and user identification.

This objective is supported by P3, where YOLOv8, a CNN-based object detection algorithm, is utilized to identify and track multiple wearable LED transmitters in dynamic environments. The study demonstrates the ability of OCC in providing communication and tracking capabilities.

#### 1.4 Organization of the document

This thesis is composed of a compendium of indexed journal publications, which serve as the primary experimental contributions of this work. Each article is included in its final post-print version, formatted according to the respective journal's guidelines. To provide context for the project and its methodologies, review relevant literature, outline the foundational principles of the research, and detail the experimental design, the thesis includes preliminary chapters prior to the presentation of the articles.

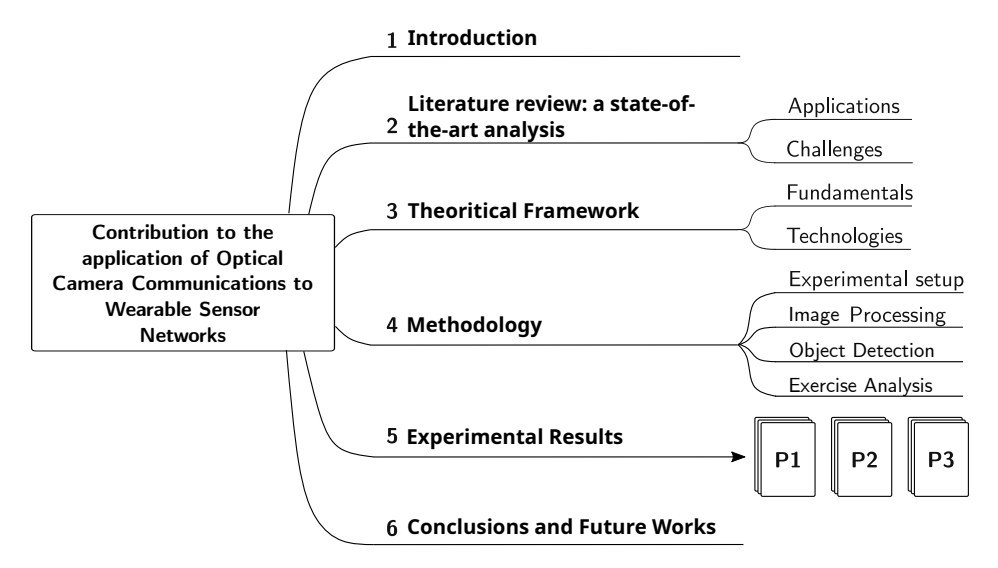


**Figure 1.4:** Thesis structure with the contents of each chapter.

This document is organized as illustrated in Figure 1.4 and follows the structure outlined below. Chapter 1 states the main objectives of the work. Chapter 2 presents a literature review of OCC in wearable sensor networks, emphasizing its applications and challenges. Chapter 3 discusses the principle of OCC and the technologies implemented in this thesis. Chapter 4 describes materials and methods, such as the experimental design, the digital signal processing (DSP), the image processing techniques applied, the object detection algorithm developed, and the exercise analysis. The following chapter, Chapter 5, contains the results in the form of a compendium of publications discussing experiments conducted with OCC using wearable LEDs. Finally, Chapter 6 summarizes the conclusions drawn from the research along with the major contributions and gives possible directions for future research.

#### 1.5 List of publications

The research carried out during this thesis resulted in the publication of three articles in indexed journals and five papers in conference proceedings. Additionally, the author contributed as a secondary collaborator to two other conference papers in partnership with fellow researchers. The following sections provide a complete list of these publications.

#### 1.5.1 Journal articles

The publications included in the compendium (see Chapter 5) are entitled as follows:

- Niarchou, E., Matus, V., Rabadan, J., Guerra, V., Perez-Jimenez, R. (2024).
   "Optical Camera Communications in Healthcare: A Wearable LED Transmitter Evaluation during Indoor Physical Exercise," MDPI Sensors, 24(9):2766.
- Niarchou, E., Eollos-Jarosikova, K., Matus, V., Perez-Jimenez, R., Zvanovec, S., Komanec, M., Rabadan, J. (2024). "Experimental evaluation of wearable LED

- strip and side-emitting fiber for optical camera communications systems," *Optics Express*, 32(14), 25, 091–25, 103.
- Niarchou, E., Usmani, A.F., Matus, V., Rabadan, J., Guerra, V., Alves, L.N., and Perez-Jimenez, R. (2025), "CNN-Based Human Detection and Identification in Indoor Optical Camera Communication Systems Using a Wearable LED Strip." *IET Optoelectronics*, 19: e70005. https://doi.org/10.1049/ote2.70005

#### 1.5.2 Conference proceedings

The camera-ready conference proceedings are included in the Appendix A, and are entitled as follows:

- Niarchou, E., Matus, V., Rabadan, J., Guerra, V., Perez-Jimenez, R. (2023). "Experimental Evaluation of LED-Based Wearable Transmitter for Optical Camera Communications Systems" in 2023 17th International Conference on Telecommunications (ConTEL), Graz, Austria, 11-13 July 2023.
- Niarchou, E., Matus, V., Perez-Jimenez, R., Rabadan, J., Guerra, V. (2024). Experimental Evaluation of LED-Based Wearable Transmitter for Optical Camera Communications Systems in 2024 14th International Symposium on Communication Systems, Networks and Digital Signal Processing (CSNDSP), Rome, Italy, 17-19 July 2024.

#### 1.5.3 Collaborations

The following list contains articles in which the author has participated as a collaborator, included in the Appendix  ${\sf B}$ .

- Younus, O., Niarchou, E., Teli, S., Ghassemlooy, Z., Zvanovec, S., Le Minh, H. (2022) "Near-Infrared based Optical Camera Communications" in 2022 13th International Symposium on Communication Systems, Networks and Digital Signal Processing (CSNDSP), Porto, Portugal, 20-22 July 2022.
- Eollos-Jarosikova, K., Neuman, V., Niarchou, E., Gomez-Cardenes, O., Zvanovec, S., Perez-Jimenez, R. (2023) "Pilot Experiments of Side-Emitting Fiber-Based Optical Camera Communication for Wearable Applications" in 2023 4th South American Conference On Visible Light Communications (SACVLC), Santiago, Chile, 8-10 November 2023.

# Literature review: a state-of-the-art analysis

This chapter provides a comprehensive literature review of OCC technology within the context of wearable sensor networks. It outlines the applications of OCC technologies with wearable devices and the current challenges that need to be addressed. A more specific review of related works is provided in the individual papers.

OCC technology, a branch of VLC technology [2],[3], has attracted interest in engineering and scientific communities due to the use of cameras as optical receivers instead of conventional photodiodes (PDs). With the growing number of devices that have built-in complementary metal oxide semiconductor (CMOS) cameras, such as smartphones, laptops, and tablets, OCC technology has become increasingly viable, because these cameras are more cost-effective than charge-coupled device (CCD) cameras. CMOS cameras, such as those in modern smartphones are capable of capturing high-resolution photos and videos, with an average viewport resolution of  $360\times800~\rm px$  [28], which translates into an actual resolution of  $1080\times2400~\rm px$  (Full High Definition). Their recording speed of 30-60 frames per second (fps) or higher, provides data rates in the range of 10 bps-100 kbps, which is more than adequate for low-speed applications [29] and IoT systems [4]. One critical aspect of OCC technology is the type of camera's image acquisition mechanism, which can be categorized into rolling shutter (RS) or global shutter (GS) (as will be further analyzed in the next chapter), which affects the data rate or the link ranges of OCC systems [3], [30].

Wearable devices, due to their mobility and compact design, can serve as mobile or semi-mobile nodes within WSNs [31]. Each wearable node includes low-power sensors, a wireless transceiver, electronic processing elements (i.e. microcontroller) and the power supply unit, which must be miniaturized, lightweight and long lasting.

The field of wearable devices has received increased popularity due to the widespread availability of consumer electronics such as smartphones, smartwatches, smart rings, fitness bands, smart glasses, smart clothes, and medical patches. These devices are mobile electronic devices that can be worn as accessories, attached to clothing, or directly on the body and are often designed to be lightweight and compact, offering convenience to users and seamlessly integrated into daily life without disrupting normal activities to measure heart pulse, acceleration, temperature, oxygen, and sugar levels. Typically, they are equipped with sensors, processors, as well as communication capabilities, with the aim of providing specific functionalities, such as recognizing human activities, health monitoring and fitness metrics [32], [33], [34], [35], [36].

Recent advances in stretchable conductive inks and hybrid 3D printing have enhanced wearable devices through the potential for producing soft, flexible electronics [37]. This technique combines direct ink writing of conductive materials with automated component placement, to achieve seamless integration of electronic circuits. Wearable sensors therefore become flexible, long-lasting, and adaptive, making them ideal for wearable electronics applications, soft robotics, and biomedical devices.

Despite their utility, most commercially available wearables rely on RF technologies,

such as BLE or near-field communication (NFC) for data transmission [38]. However, these technologies face challenges related to the potential health effects of exposure to electromagnetic radiance, limited range, security, electromagnetic interference, and spectrum availability. To overcome these limitations, by replacing the RF modules with LEDs, OCC enhances security, reduces electromagnetic interference, and provides a more efficient and reliable alternative for wearable sensor networks.

#### 2.1 Applications of wearable sensors

To date, only a limited number of research works have explored the integration of wearable sensors with LEDs as transmitters. In the field of OWC, an all-optical bidirectional wireless communication system has been proposed in [39] for health monitoring that used infrared (IR) for the uplink and visible light (VL) for the downlink, which evaluated the transmission of sensor data from extreme positions, such as the ankle, considering variations in transceiver orientation due to random body part mobility, and addressed trade-offs between emitting power and data rate to maintain a given quality of service. Furthermore, the performance of an optical code-division multiple access in extra wireless body-area networks, which also used an IR uplink, has been analyzed in [40], which evaluated the impact of multiple access interference and link outages due to line-of-sight (LOS) blockages, showing that random  $T_x$  orientations degrade link performance, especially at greater distances from the access point (AP). It demonstrated that using multiple APs improves link reliability, despite the increased system complexity, and highlighted the beneficial role of first-order reflections in enhancing link performance.

Particularly in the field of OCC, wearable sensors are mostly used in healthcare applications. For instance, in [41], a sensor patch collected a patient's heart rate and oxygen saturation data and employed an LED array modulated using color intensities to transmit data to a CCTV camera, for real-time remote monitoring, ensuring reliable reception regardless of LED orientation. A neural network (NN) was utilized to detect individual LEDs, while another NN-based feature extraction method accurately identified colors. The study achieved a data rate of 4.68 kbps with a low bit-error rate (BER) at 1 m and 1.172 kbps at 3 m.

Similarly, in [42] several wearable sensors transmitted multiple clinical data, including electrocardiogram (ECG), photoplethysmogram, and respiration signals, in a home-based rehabilitation system via an LED light source and received by a smartphone camera. The reliability of the system was evaluated by analyzing the relationship between BER and signal-to-noise ratio (SNR) under different lighting conditions. An Android mobile application was also developed for local interface, data analysis, and cloud-based clinician supervision.

Additionally, in [43] body sensors data were transmitted to a CCTV system, in a deep learning-based OCC system integrated with the You Only Look Once (YOLO) object detection model, for real-time health monitoring and indoor location tracking of multiple patients with an LED array. The data were securely transmitted to an edge server and displayed via a web interface for real-time patient updates.

OCC can also be integrated with RF technologies, leading to hybrid systems with enhanced robustness. In scenarios where OCC connections may be disrupted by the mobility of the nodes, BLE integration guarantees seamless communication. For

instance, in [44], OCC integrated with BLE was used for efficient, remote, real-time ECG transmission. A hybrid patch circuit was developed for the collection and transmission of ECG data through an LED array and BLE transmitter while minimizing power consumption. A network selection algorithm was proposed to provide reliable network access, using fuzzy logic for optimal camera selection in multi-camera scenarios. A handover mechanism was also added in order to ensure continuous connectivity for mobile patients. The simulation results demonstrated that the hybrid system improved network selection and reduced outage probability in eHealth applications. Similarly in [45], OCC integrated with BLE was used for real-time health monitoring by transmitting data from body sensors to a central gateway. A hybrid OCC/RF architecture was proposed, where an access point selection algorithm prioritized OCC given its highperformance characteristics. The selection mechanism included parameters such as the angle of view of the camera and the distance between the camera and the patient. The simulation results have proven the feasibility of the proposed system, thus demonstrating its potential to facilitate efficient and reliable health data transmission in eHealth applications.

This thesis proposes the application of OCC in wearable sensor networks. In particular, an LED-based wearable transmitter can be implemented as shown in the example in Figure 2.1, with the sensing node consisting of an MCU and a power source, to transmit data collected by the sensors via LEDs to a surveillance camera, enabling monitoring purposes. This system can be used in high-risk environments where monitoring of physiological health is critical, such as in industries, mining, construction, and by safety and airport ground personnel. The integration of LEDs into wearables or uniforms not only enhances visibility and comfort for the user but also enables transferring critical health information, thus helping to bring about better protection and health monitoring in challenging environments.

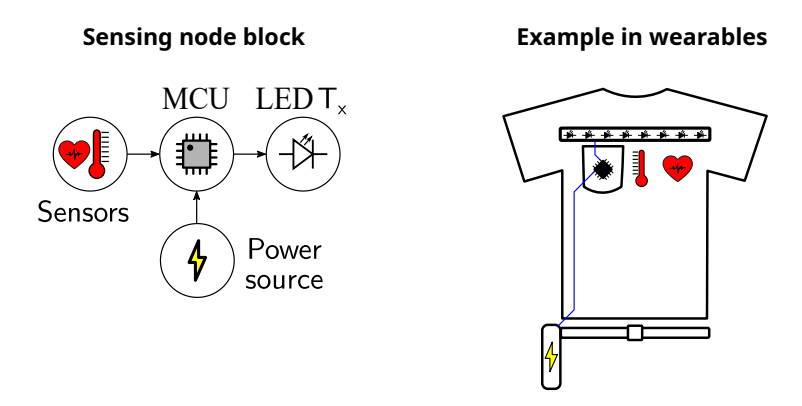


Figure 2.1: Example of sensor node with LED transmitter in wearable sensor networks.

In addition, this system can be applied to monitor the activities of people - both healthy and with chronic health conditions - at homes, gyms, ambulances, hospitals, intensive care units, rehabilitation centers, and nursing homes for the elderly, as shown in Figure 2.2. It can also be used for baby monitoring, providing a non-intrusive solution to track vital signs, movements, and sleep patterns to ensure their safety and well-being. Specifically, it can aid in rehabilitation processes, sports training, elderly treatment,

even in the earliest detection of musculoskeletal or cognitive disorders, as well as in assessing falls and balance.



**Figure 2.2:** Possible applications of our system.

The analysis of human exercise routine data is a research area that can provide valuable insights into health monitoring. For instance, in [46] a smart exercise bike was developed for Parkinson's rehabilitation to investigate the impact of cycling on changes in motor skills for riders with Parkinson's disease, explaining how variability analysis of biomechanical and physiological parameters during exercise can predict improvements in motor function. Furthermore, in [47] a camera-based monitoring system provides insights into cardiovascular health and optimized training protocols, indicating that individuals who exercise regularly have a lower resting heart rate, reduced heart rate variability, less fluctuation in heart rate and heart rate variability during exercise, and quicker heart rate recovery post-exercise compared to non-exercisers. Similarly, in [48] a video-based heart rate detection system was proposed for the monitoring of individuals during intensive exercise, demonstrating precise heart rate monitoring throughout the entire fitness cycle. Additionally, in [49], an autonomous system was designed to monitor the presence patterns of elderly individuals, showing that otherwise hidden but relevant events (e.g., fall incidents and irregular sleep patterns) can be detected and reported to the caregiver, enabling a targeted intervention. Moreover, in [50], a system was proposed capable of determining body posture and identifying the physical condition and health of users, thus saving the trouble of manual angle measurement in traditional physical therapy.

Behavioral analysis has also been explored using machine learning (ML) techniques. For instance, in [51] typing patterns were examined to detect depressive disorders and contribute to a non-invasive, high-frequency tracking of tendencies toward depression during everyday life. Similarly, [52] analyzed keyboard interaction in the evaluation of clinical conditions such as multiple sclerosis, showing that combining keyboard interaction data with ML techniques can be used as an unobtrusive monitoring tool to estimate various levels of clinical disability in individuals with multiple sclerosis based on their daily activities. Keystroke dynamics have also been studied in relation to early loneliness detection and intervention development in [53], indicating that people with very high levels of loneliness tended to use mobile keyboards during late-night hours and showed little variation in smartphone usage behavior between weekdays and weekends.

#### 2.2 Challenges

Despite the aforementioned advantages of OCC technology over other technologies - thanks to the use of cameras as receiving tools and their ability to capture details beyond the capabilities of the human eye — there are still some challenges that need to be addressed.

#### 2.2.1 Transmitter detection and tracking

The detection process of the transmitting source within the image frame, defined as the region of interest (ROI), as well as its tracking throughout a video sequence, are major challenges in OCC systems and computer vision [20], [54], because cameras lack the human ability to detect, recognize, and track objects within images or videos. As a result, recognizing human activities in surveillance systems is a consequent challenge, in numerous practical applications, including elderly care monitoring, rehabilitation activity tracking, sports performance analysis, and identification of security intrusions [55], [56].

In scenarios involving low visibility, multiple users, and user mobility it is important the accurate detection and tracking in communication and monitoring systems. In low visibility environments, it is challenging to accurately detect and continuously track the users, especially when their LEDs are off. Furthermore, systems must differentiate between overlapping signals and track each transmitter effectively to avoid interference when dealing with multiple and mobile users. Ensuring the system's performance in such scenarios requires advanced ML strategies and the use of multiple camera receivers that capture from different angles.

The detection and tracking processes rely on algorithms that employ pattern recognition techniques, such as correlation analysis or ML methods, to identify the transmitter's ROI within the image effectively. However, the computational demands of these algorithms could affect the link latency. The method of ROI detection differs depending on the camera's image acquisition mechanism, RS or GS, as shown in Figure 2.3. Commercial CMOS cameras implement the RS technique for image acquisition, exposing rows of pixels sequentially, and sampling light at different times as the shutter remains open. This creates illuminated stripes in the image based on the light source's state during row exposure. In these cameras, the ROI is detected in the image as a template corresponding to the LED's transmitted signal, through a correlation process (Chapter 4). On the other hand, GS cameras, expose all pixels simultaneously when capturing a frame, resulting in light sampling at the camera's frame rate (typically 30-120 fps). In these cameras, the ROI is identified as the transmitter's location within the frame, with ML methods. The GS technique is primarily implemented by CCD cameras. However, depending on the data rate requirements, it can also be employed by CMOS cameras [3].

#### 2.2.2 OCC in resource-constrained environments

The combination of computer vision, a subfield of artificial intelligence (AI) that will be further analyzed in the next chapter, with OCC functionality is a challenging issue, resulting from the above challenge to detect the transmitter's ROI and track it throughout a video sequence. In resource-constrained environments, where computational power

#### Image frame in RS effect



#### Image frame in GS effect

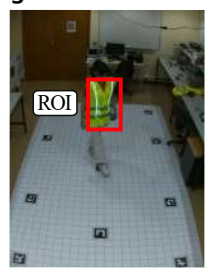


**Figure 2.3:** The detected region of interest (ROI) within an image frame, captured in different acquisition mechanisms, rolling shutter (RS) and global shutter (GS).

is limited, computer vision complements image processing techniques through neural networks (NNs).

Object detection [57], an important and challenging field in computer vision, serves as the foundation for more advanced applications, such as image segmentation [58], object tracking [59], and behavior recognition [60]. Convolutional Neural Networks (CNNs) have been widely used for object detection since the 1990s and have proven effective for deep learning-based tasks in the field [61]. Beyond object detection, CNNs have been applied in a variety of areas, such as image and pattern recognition [62], speech recognition [63], video analysis [64], human activity recognition [65] and human fall detection [66]. Lately, CNN-based object detection has been applied in autonomous driving [67], virtual reality (VR) [68], and intelligent video surveillance [69], demonstrating its potential for OCC applications, especially in dynamic and resource-limited environments.

The application of neural networks in OCC has demonstrated significant improvements in system performance. For instance, in [70] an NN-based decoder was introduced to enhance the decoding of the modulation scheme in OCC, demonstrating robustness against blurring, noise effects, and various channel conditions. NNs have also been implemented in [71] to improve the performance of a smartphone camera-based device-to-device system, by exploiting two-dimensional data transmission capability in OCC. In [72], NNs estimate camera position using coordinate information transmitted by LED, and in [73] trained neurons perform repetitive analysis to provide efficient and reliable motion detection in OCC. Moreover, in [74] an NN-based technique can estimate target vehicle's position in OCC.

CNNs have been employed in various OCC applications. For instance, in [75] CNN has been applied to vehicle systems for recognizing and detecting LED array patterns of target objects or ROIs, which provides correct recognition even at remote distances, as well as signal blockage and adverse weather conditions. Similarly, in [76] CNN was used in the mobile OCC decoding scheme to extract features from bright and dark stripes, reversing stripe distortion and reducing bit error rates (BERs) in dynamic environments. Also, in [77] a CNN was used at the OCC receiver to estimate the optimum decoding strategy, enabling efficient decoding of data symbols from images of LED transmitters under varying real-world scenarios.

Among these, the You Only Look Once (YOLO) algorithm, a CNN-based framework,

firstly introduced in 2016 [78], is regarded as a cutting-edge solution for real-time object tracking.

To date, the YOLO architecture has evolved through eleven versions, from YOLOv1 to YOLOv11, with each version addressing specific challenges in object detection. The first generation of YOLO in [79] was processing images at high speed (45 fps for the base model and 155 fps for the smaller model), while in [80] was modified by enhancing the loss function, adding a spatial pyramid pooling layer, and incorporating a convolutional inception model, resulting in better object detection performance. Later, YOLOv2 was proposed for real-time human detection in [81].

An improved method of YOLOv3 was used in [82] for initializing the width and height of predicted bounding boxes, which improves convergence speed, selects more representative initial values, and achieves better performance in terms of recall, mean average precision, and F1-score compared to the original method. In [83], YOLOv3 was used for object detection in image datasets, while YOLOv4 was applied to video datasets, for detecting multiple objects in video surveillance, achieving accuracy of 98% and 99%, respectively. YOLOv4 was applied in [84] with image processing techniques for the extraction of the color barcode area from electronic displays for the OCC system.

YOLOv5 was applied in [54] for LED detection and decoding in a multiple-input multiple-output camera on–off keying (MIMO C-OOK) scheme that increases the data transmission rate and decreases the BER effectively, under long-range and mobility constraints.

YOLOv6 was utilized in [85] for real-time object detection, with transfer learning to balance detection accuracy and inference speed, to enable efficient operation in practical scenarios and pave the way for future applications in IoT and vision aid systems for visually impaired individuals.

YOLOv7 was used in [86] for small target detection of aircraft, vehicles, and ships in remote sensing images using image segmentation and high-level detection features, where achieved superior performance with an average precision of 77%, outperforming all YOLOv5 variants in accuracy and with higher robustness.

YOLOv8 was applied in [87] for real-time OCC systems operating under high-mobility conditions, to showcase the flexibility of the proposed approach in a rapidly evolving setting. Moreover, in [43], YOLOv8 proved effective for real-time health monitoring and indoor location tracking applications, mainly for Internet of Medical Things (IoMT), showing its capability in numerous fields. In [88] the YOLOv8-based transmitter tracking algorithm was proposed for precise tracking of light sources in dynamic environments, with a deep learning decoder in order to reduce BER values for a 2D-MIMO scheme, and thereby to improve the overall system performance. Versions v1 to v8 were evaluated in [89] in the context of human fall detection, taking into account their structures, datasets, metrics, and performance, with focus on advances from YOLOv5 onwards.

YOLOv9 was compared to its previous version in [90] for thermal-based person detection in surveillance and monitoring applications, whereas it was used alone in [91] for real-time monitoring of vehicles in urban surveillance systems. In [65] YOLOv9 was evaluated for human activity recognition, showing significant improvements in accuracy (98.23%), precision (98.53%), recall (98.65%), and F1-score (98.75%) over previous versions.

YOLOv10 was evaluated in [92] for real-time pedestrian detection in autonomous

#### Chapter 2 Literature review: a state-of-the-art analysis

vehicles. In [93] for underwater object detection, improving detection achieving a 3.04% improvement in mean Average Precision (mAP). In [94] an improved version of YOLOv10 was used for infrared image classification and detection of power equipment, achieving significant improvements in detection performance with a 13.3% higher mAP than the original version.

The latest version YOLOv11 was used for miner detection in underground coal mines in [95].

The next chapter provides the theoretical framework, presenting the fundamental technical knowledge on which this thesis is based.

This chapter provides the theoretical framework on which this research and its resulting published articles are based. It covers fundamental concepts such as signal modulation schemes that exploit the characteristics of the devices implemented and AI strategies for optimizing OCC receivers. The key technologies implemented in the transmission and reception stages of the OCC systems, including LED-based transmitters and camera receivers, are also presented.

## 3.1 Fundamentals

This subsection presents the essential principles of OCC, including signal modulation schemes that exploit the characteristics of LED-based transmitters and camera-based receivers, as well as the role of AI in optimizing the performance of the proposed systems and introducing new capabilities.

## 3.1.1 Modulation schemes

Modulations and coding schemes are the key drivers in the performance of a communications system. Unlike the conventional photodetector (PD)-based VLC systems, OCC systems use a camera as a receiver. Hence, the light emitted from LEDs is captured as images or video frames by the camera. Consequently, the conventional modulation schemes that were designed for PD-based VLC systems may not be suitable for OCC systems. Therefore, new modulation schemes are required to accommodate both lighting and OCC functionalities. Moreover, since OCC operates as an asynchronous communication system, synchronizing requires special methods. The OCC system primarily utilizes four modulation schemes: on-off keying (OOK), undersampled-based modulation, rolling shutter (RS) effect-based modulation, and liquid-crystal display (LCD)-based modulation [2].

OOK is the simplest amplitude shift keying (ASK) modulation, where digital data are represented by the presence or absence of a carrier wave [96]. In the simplest form, the presence of a carrier for a certain interval of time represents a binary one, while the absence of a carrier represents a binary zero, as shown in Fig.3.1. Since communication is based on light modulation, OOK is highly compatible with VLC systems. A straightforward method to achieve this is by switching the LED on and off, so that the receiver detects the light signals as binary 1 or binary 0, respectively. However, due to the relatively low frame rate of commercial cameras (e.g.,  $\leq$  60 fps), OOK can introduce flickering. To ensure flicker-free lighting, the modulation frequency must be higher than the critical flicker fusion frequency (CFF) of the human eye (i.e., 50-90 Hz [97]). Additionally, RGB OOK modulation can be used to enhance data rates by utilizing multiple color channels for transmission [98].

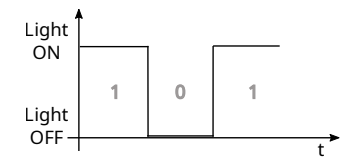


Figure 3.1: On-off keying (OOK) modulation scheme.

Undersampled modulation [99], a type of subcarrier intensity modulation (SIM), enables flicker-free communication by transforming a baseband signal into a passband signal with a frequency above the CFF. A special case of this is undersampled frequency shift OOK (UFSOOK), in which distinct square wave patterns trigger modulation of the baseband signal into higher frequencies to represent binary 1 or 0. The camera undersamples the signal, detecting steady or blinking states of the LED to decode the transmitted data. Several variations of undersampled modulation have been proposed for greater spectral efficiency, such as undersampled phase shift OOK (UPSOOK), undersampled m-ary pulse amplitude modulation (UPAM), and modulation with wavelength-division multiplexing (WDM) or color shift keying (CSK). These schemes follow a similar structure with a baseband modulation module and a square-wave SIM modulator. WDM creates multiple parallel transmission channels, different from each other in the modulation scheme, while CSK uses RGB LEDs to produce non-flickering white light. These techniques, do not require high frame rate cameras, thereby enabling long-distance, and high-spectral-efficiency communication and enhancing data rates through techniques such as multi-amplitude and multi-wavelength transmission.

RS effect-based modulation extracts information from all pixels of each video frame by exploiting the RS effect of the CMOS camera. In this scheme, the camera scans the image row by row and records dark and bright bands created by the flickering LEDs. When the LED is on, the camera captures the illuminated row, and when the LED is off, a dark row is captured. The width of these bands depends on symbol duration and scanning rate, from which a waveform can be extracted from the video frame, representing multiple bits of information. This modulation offers higher data rates compared to undersampled-based modulation. However, synchronization is necessary between the LED state and camera capture, as not all data blocks may be captured in the same frame by the camera. Other protocols such as Manchester coding and block detection can ensure complete data extraction [100]. Experiments show that this scheme can achieve faster data rates than the camera's frame rate, with additional techniques like binary frequency shift keying (BFSK) modulation and frequency division multiple access (FDMA) allowing multiple LED-based transmitters [101].

In LCD-based OCC, information is transmitted using dynamic 2D images, such as quick response (QR) codes [102], rather than LED lamps. A smart device with a built-in camera captures these changing images to wirelessly receive data. Despite the low frame rate of commercial smart devices, high data rates can be achieved using large QR codes. By incorporating RGB coding, the data rates may be tripled, thereby improving the communication speed. However, the system requires the receiving device be stationary to avoid motion blur, which can hinder decoding. Invisible codes [103] embed data within images or video frames in a way that the coding is invisible to human perception and utilizes spatial and temporal modulation to reduce visible artifacts. These codes

allow screen-camera communication but are limited to short-range applications (typically 10–110 cm).

## 3.1.2 Artificial intelligence for optical camera communications

Al plays an important part in enhancing data transmission, improving signal detection, and optimizing performance of the receiver under various environmental conditions. Al-driven techniques, particularly machine learning (ML) and deep learning (DL), have significantly advanced OCC [104], [105].

Specifically, neural networks (NNs) have been key to the enhancement of image processing in smartphones (supported by Google [106], [107]), implemented with neural processing units (NPUs) [108] for Al-based accelerated processing.

Machine learning techniques [109], especially supervised and unsupervised learning models, have been assessed to enhance OCC performance. These models are trained on large datasets of captured optical signals, detecting and predicting transmission patterns in different lighting conditions, motion scenarios, and signal interference. With classification and regression algorithms, ML models enhance error correction, symbol detection, and channel estimation.

Deep learning, a subset of ML based on artificial neural networks, has shown potential in OCC [110], [87] as it involves processing a huge amount of visual data. NNs, particularly Recurrent Neural Networks (RNNs) and Long Short-Term Memory (LSTM) networks [111], have been modeled temporal dependencies in optical signals enhancing robustness in a dynamic environment. These deep learning models improve the decoding of modulated signals by learning complex relationships between transmitted and received light patterns.

Although NNs and other pattern-recognition algorithms have been developed over the past 50 years, CNNs have developed significantly in recent years. The improved network structures of CNNs lead to memory savings and reduced computational complexity and, at the same time, offers better performance for numerous applications.

While there are CNN models in various configurations, their fundamental architecture has a fixed structure. As detailed in [61], the architecture consists of an input layer, alternate convolutional and pooling layers, one or more fully connected layers, activation functions, and a final output layer.

Image classification [112] in computer vision is an important challenge that involves discriminating among objects based on their visible characteristics. The main steps are image preprocessing, feature extraction, and classification using the pre-trained model, with feature extraction considered to be the most critical. Traditional methods may perform well on simpler tasks and fail on more complex classifications. CNNs, on the other hand, use convolution kernels to learn feature representations from big data sets automatically and offer better generalization for complex tasks in contrast with traditional methods dependent on manual feature extraction.

As mentioned in the previous chapter, object detection can solve complex tasks. Object detection and recognition can be considered to be two major steps: first, to find and localize the positions of target objects in the candidate image, and then to classify the detected objects into predefined classes. Unlike image classification, where attention

## **Chapter 3** Theoretical Framework

is focused on the whole image, an object detection approach focuses on certain regions of interest to recognize particular object classes.

The known strategies for object detection are the region-based object detection algorithm (two-stage detectors) [113] and the regression-based object detection algorithm (one-stage detectors). Two-stage detectors scan the whole image through multiple fixed-size sliding windows for the generation of region proposal boxes. These proposals are then selected for the localization and classification tasks that will detect objects inside the selected regions. On the other hand, one-stage detectors eliminate the need for region proposals by merging three operations into a single CNN—feature extraction, object classification, and position regression—thereby simplifying the object detection into an end-to-end regression task. A typical algorithm of this kind is the YOLO algorithm.

The core idea of YOLO [114] is to divide the image into a number of cells, where each cell predicts the coordinates of bounding boxes, classifies the objects in those boxes, and assigns confidence scores to its predictions. These overlapping boxes are pruned with a non-maximum suppression algorithm to enhance the result, maintaining only the most relevant predicted boxes for distinguishing objects. The YOLO-based object detection model training process involves several steps for accurate and efficient performance [115], [116].

- Data collection and annotation. The first step is to create a dataset of images with the target objects taken under different conditions. Every image needs to be annotated with bounding boxes, known as anchor boxes, and the correct class names so that the model gets important information regarding object locations and identities. Properly annotated datasets ensure the model learns to detect and classify objects correctly.
- Data preprocessing. The next step is then carried out to standardize and enhance the dataset. It includes steps for resizing images to a uniform dimension, normalization of pixel values, and data augmentation techniques like rotation, scaling, flipping, etc. These augmentations help in making the model robust against different appearances of objects in terms of light condition or background noise and hence, enhancing its generalization ability.
- Model configuration. After preprocessing select YOLO architecture versions according to the application requirements. Next, the model has been tuned with optimized hyperparameters like learning rate, batch size, and number of training epochs. On another front, the anchor boxes were defined in such a way that their dimensions correlate well with of the objects from the dataset so as to improve an object's detection accuracy.
- Training. Once the model is configured, training is started on the prepared dataset. The model learns to predict bounding boxes and class probabilities by iteratively minimizing a predefined loss function. The model's detection ability improves after a number of iterations. Training continues until it has stabilized, according to the evaluation metrics on a validation set.

Validation. The validation set helps to enhance the training period and as well acts as a litmus test for ensuring that the model performs well on unseen data. A separate validation set is used to detect overfitting and fine-tune hyperparameter values, ensuring that the trained model generalizes well to different datasets. The performance of the system for prediction, detection, and tracking can be evaluated using appropriate metrics. However, relying on a single evaluation metric is insufficient for a comprehensive assessment of the model's performance [95], [89]. Key evaluation metrics include:

Precision in object detection is the ratio of correctly identified objects. It is calculated by dividing the number of true positives (TP) (correctly identified positive instances) by the sum of true positives and false positives (FP) (incorrectly identified positive instances). Hence, the precision score would vary between 0 and 1, as expressed in Eq. 1.

$$Precision = \frac{True \ Positives}{True \ Positives + False \ Positives}$$
 (1)

Recall measures the ratio of actual positive instances that were correctly identified by the model. It is measured by dividing the number of TP by the total of TP and false negatives (FN) (incorrectly classified negative instances). The recall score ranges from 0 to 1, as demonstrated in Eq. 2.

$$Recall = \frac{True \ Positives}{True \ Positives + False \ Negatives}$$
 (2)

The F1-score is a combined metric which assesses the accuracy of a model by both precision and recall. It provides a balanced measure between correctly identifying instances and the elimination of false detections. The F1-score ranges from 0 to 1, and higher values indicate superior performance, computed using the Eq. 3.

F1 Score = 
$$2 \times \frac{\text{Precision} \times \text{Recall}}{\text{Precision} + \text{Recall}}$$
 (3)

The mean average precision (mAP) at 0.5 is an important metric used to assess the model's overall accuracy, combining both localization and classification performance to measure accuracy across different classes. It is determined by computing the average of the average precision (AP) values for all classes. Initially, the AP for each class is calculated as the area under the precision-recall curve. Afterward, the mAP is obtained by averaging the AP values across the different classes. The formula is Eq. 4:

$$\mathsf{mAP} = \frac{1}{N} \sum_{c=1}^{N} A P_c \tag{4}$$

where N represents the total number of classes, while APc refers to the AP for class c. The intersection over union (IoU) formula, given in Eq. 5, is used to calculate the overlap between predicted and actual bounding boxes [117].

$$IoU = \frac{Area of Overlap}{Area of Union}$$
 (5)

The confusion matrix is a valuable tool in machine learning, offering a comprehensive visualization of a classifier's performance beyond conventional accuracy metrics. It enables the user to visualize the model's strengths and weaknesses, particularly in identifying specific error patterns and biases towards certain classes. By analyzing the different types of errors in the matrix, developers can make informed adjustments to enhance model accuracy and robustness by optimizing either recall or precision based on application needs. The structure of the confusion matrix is shown in Fig. 3.2.

		Real c Positive	lasses Negative
classes	Negative	TP	FP
Detected	Positive	FN	TN

Figure 3.2: Confusion matrix.

Testing and deployment. Finally, in the testing and deployment phase, the trained model for the purpose of object detection on the specified test set to prove its validity. The model would be deployed only after validation for the object detection purpose on novel images/video streams, enabling real-time predictions for practical applications.

# 3.2 Technologies

This subsection explores the key technologies behind OCC, focusing on the critical components of the system: the transmitters and receivers. It examines various transmitter technologies and different types of cameras based on their internal shutter mechanism.

## 3.2.1 Transmitters

Among the various light sources in the existing lighting infrastructure, such as fluorescent lamps, incandescent bulbs, halogen lamps, and LEDs, only the latter can provide data communication. In contrast to other lighting sources, LEDs, due to their ability to switch on and off at high rates imperceptible to the human eye, their higher energy efficiency, compact size, durability, and their ability to operate at visible spectrum, can serve as transmitters in VLC and OCC systems [2].

LED is a semiconductor device that generates light through electroluminescence, a phenomenon in which electrons combine with electron holes in the semiconductor material to release energy in the form of photons. The emitted light's wavelength,

and thus its color, depends on the semiconductor material's energy band-gap, with compounds such as Gallium Arsenide (GaAs) and Gallium Phosphide (GaP) commonly used. LEDs come in various forms—such as phosphor-converted LEDs (pc-LEDs), multi-chip LEDs, organic LEDs (OLEDs), and micro-LEDs ( $\mu$ -LEDs)—each offering unique properties that make them suitable for diverse applications [118].

White light LEDs are the most widely used in illuminating infrastructure, which is the basis of VLC and OCC concepts. Unlike other LED colors, which are determined by the semiconductor materials, white light is generated through three main techniques [119]. The first method uses a blue LED light bulb coated with a phosphor layer. The blue LED emits photons that pass through the phosphor, which partially converts the light into yellow. The yellow and blue photons together produce white light. The second method uses ultraviolet (UV) LEDs and RGB phosphors for the perception of white light. The third method uses RGB LEDs, which, with varying hues of red, green, and blue light output, have the capability of not only producing white light but also other colors.

According to the type of driving source, the white LED driver circuit can be divided either into voltage-driven or current-driven sources [96]. The LED circuit typically consists of a digital converter, a complementary metal oxide semiconductor (CMOS) transistor driver, which is a type of metal oxide semiconductor field effect transistor (MOSFET), implemented as a switching element, and the LED itself, as shown in Figure 3.3.



Figure 3.3: Configuration of a typical LED.

## 3.2.2 Receivers

In OCC, the receiver converts LED light signals into digital data. Receivers typically are the camera sensors found in smartphones, laptops, tablets, or CCTV cameras.

Cameras' shutter mechanism regulates the exposure of the pixels internally in the image sensor (IS). Image sensors are classified into two types based on their architecture: CCD and CMOS [120]. CCD sensors are physically larger in size since they have a proportionately larger analog-to-digital converter (ADC) than CMOS sensors. Due to this reason, CCD sensors are rarely used in smartphones. On the other hand, CMOS cameras can offer advantages such as low power consumption, a more compact IS, faster data readout, low cost, and high programmability.

A typical CMOS-based camera consists of an imaging lens, a color filter array (CFA), an image sensor, and an image processing unit (IPU) [121], [122], as shown in Figure 3.4.

The imaging lens is a precision optical component that projects the light from a source or a reflected object onto IS. The field of view (FOV) of the camera is determined by the lens' focal length and the sensor size, while the working distance indicates the optimum distance for focused image acquisition.

The IS, is typically a CMOS-based active pixel sensor in smartphones, which consists of a two-dimensional array of photodetectors that detect and incident light and convert

#### **Chapter 3** Theoretical Framework

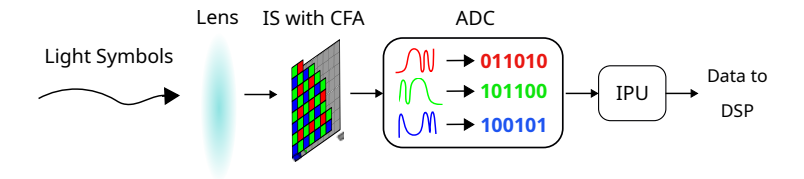


**Figure 3.4:** Configuration of a typical complementary metal-oxide semiconductor (CMOS)-based camera.

it into electrical signals. These image sensors use a CFA of a distinct pattern, most commonly the Bayer filter. The Bayer filter arranges pixels in a repeating  $2\times2$  block of one red, one blue, and two green filters, as the human eye is more sensitive to green light. Thus green pixels are prioritized in order to enhance image quality by capturing fine details with reduced noise.

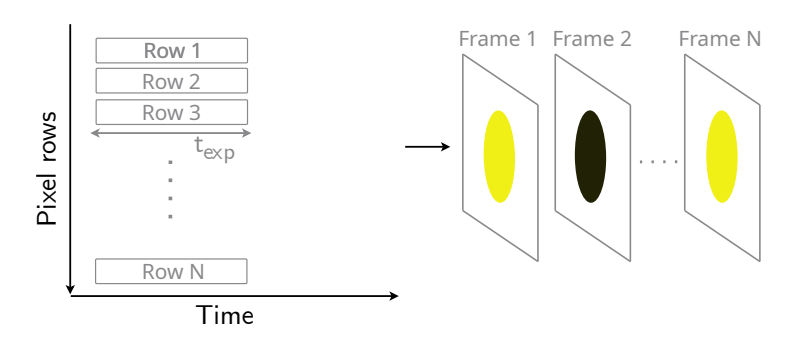
Each pixel of the IS captures only red, green, or blue color and forms raw analog signals which are then read and digitized by an analog-to-digital converter (ADC). The IPU, a digital signal processor, then builds a colored image by a demosaicing process (or deBayering), applies white balancing and color correction, and corrects optical imperfections. The final processed image can be stored and compressed, with additional processing for autofocus, auto-exposure, and camera control. In the OCC's context, the ability to demultiplex RGB signals enables wavelength-division multiplexing (WDM) with enhanced data throughput, without additional receivers.

There are two image acquisition methods for capturing a still image or video frames, global shutter (GS) and rolling shutter (RS) [3] [123]. Figure 3.5 shows the frame capturing process of an OOK transmitted signal (on-off states of an LED) captured by GS and RS camera's acquisition mechanism.

In GS cameras, all pixels of the IS begin and end exposure simultaneously, capturing the entire image at once. While this ensures high-quality image capture for multimedia applications, it limits OCC to detecting only a single state of the light source per frame. Since GS cameras sample the optical signal at a rate equal to their frame rate (typically 30–120 fps) the achievable receiver bandwidth remains low. As a result, OCC throughput is inherently constrained by the camera's frame rate, with the maximum achievable data rate limited by the Nyquist-Shannon theorem [124], meaning that the sampling rate of the image sensor, which is the frequency at which a row of pixels is sampled, must be at least twice the rate of the highest signal frequency.

In RS cameras [100] [124] [125], images are captured row by row, meaning different lines of pixels are exposed at different times to detect light intensity. This row-by-row scanning process is because modern camera sensors are not capable of reading all photodetectors in parallel but use electronic signals to activate and reset each row sequentially. The duration for which each row is exposed to light is known as the exposure time  $t_{\rm exp}$ . This sequential exposure causes fast-moving or big objects to become distorted, creating a motion blur. However, this property is advantageous for OCC, as it can record multiple light-source changes in a single frame. When the LED transmitter is modulated at a rate higher than the row sampling time but lower than the frame rate, distinct bands of intensity appear in the captured image. These bands

## Global shutter method



## Rolling shutter method

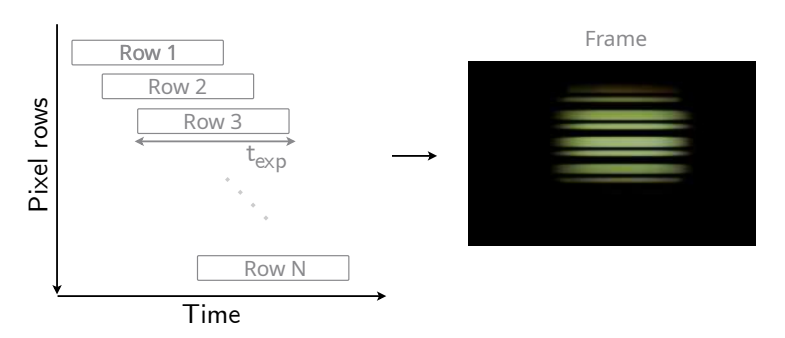


**Figure 3.5:** Frame capturing process by global shutter (GS) and rolling shutter (RS) camera of an on-off keying (OOK) transmitted signal.

are a representation of binary data and allow higher data rates than the camera's frame rate alone. By using this effect, OCC can achieve multi-kbps throughput.

CCD sensors inherently capture images via the GS, while most CMOS ISs' exposure method is based on RS. Nevertheless, RS sensors in hardware can perform as GS when used with low transmission data rate transmitters. This is because, at low rates, the signal changes slowly enough that the row-by-row capture of the RS sensor aligns with the transmitted signal and effectively captures the entire frame as if all pixels were exposed simultaneously.

The next chapter describes the methodology followed to address the mentioned objectives of the thesis.

This chapter outlines the methodology employed to achieve the objectives of this thesis, including the experimental setups, hardware implementations, and data processing techniques. First, it describes the experimental setups conducted, along with the transmitter and receiver hardware implemented. Then, it details the steps of the image processing techniques applied across all experimental setups, the implementation steps of the YOLO object detection algorithm, and the analysis of exercise data.

## 4.1 Experimental setups

To align with the objectives stated in this thesis, different experiments were conducted, to demonstrate the feasibility and performance of OCC-based communication and tracking in real-world scenarios.

First, the general objective (O1) is to implement OCC links using image sensors for optical communication in indoor and outdoor environments. To achieve this, experiments were conducted in both indoor and outdoor environments, as shown in Fig. 4.1, to test the feasibility of using commercial off-the-shelf cameras embedded in many devices such as smartphones, or commercial cameras (Raspberry Pi cameras) for the reception of signals emitted by wearable sensors using optical spectrum image sensors that implement image processing algorithms and wireless optical communication. The transmitter and receiver nodes in all experimental setups, utilize LED-based light sources and CMOS cameras, each incorporating different optical front-ends built from commercially available components.



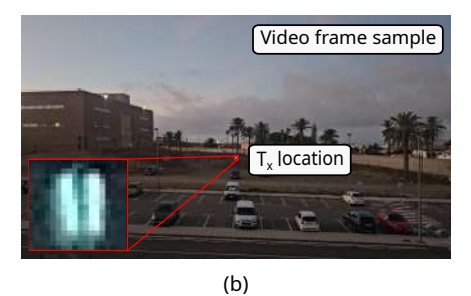


**Figure 4.1:** Examples of experimental setups implemented, with the wearable LED transmitter device and the smartphone camera receiver. (a) In an indoor environment, where the user engages in physical exercise on a stationary bicycle. (b) In an outdoor environment, where the user is standing and walking.

## Chapter 4 Methodology

To address the second objective (O2), which is to examine the impact of sensor positioning and channel conditions on data rate performance, the experimental setups examined various sensor-node configurations, including different transmitter placements (static, wearable), orientation (horizontally, vertically), and receiver positions (near-far distances, different viewing angles), as shown in Fig. 4.2. Measurements were taken at various distances, ranging from short-range (e.g., indoor room, 20 cm to 4 m) to long-range (e.g., outdoor 90–120 m), allowing for a comprehensive assessment of communication performance across different spatial conditions. In addition, it was analyzed how controlled lighting conditions (ambient light, dark room) and camera exposure settings influence data reception. The feasibility of multi-user OCC networks was also tested by assessing the ability of multiple wearable transmitters to transmit concurrently in the same environment, thus evaluating their interference on network performance and signal integrity.

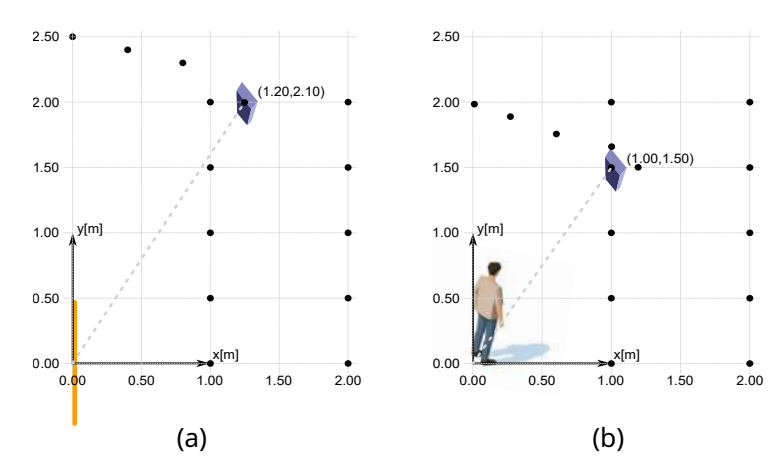


**Figure 4.2:** Examples of experimental setups implemented. The 2D coordinates of the room (in meters) represent the camera's capturing positions, always facing the center of the transmitter at (0.0, 0.0). (a) Laboratory experimental setup with a yellow line representing the transmitter. (b) Wearable experimental setup with a person wearing the transmitter on their T-shirt.

Finally, for the last objective (O3), deploying networks with multiple receivers and Al-based tracking, a multi-camera setup was implemented, where two Raspberry Pi cameras were positioned in a room to monitor and track multiple users, as shown in Fig. 4.3. This setup allowed for node recognition and movement tracking by evaluating different walking patterns (e.g., parallel, lemniscate, and random trajectories). The use of different RGB color channels for ID transmission further enabled Al-based recognition of users in a multi-sensor environment.

By analyzing different types of transmitters, camera configurations, and environments, these experimental setups provided a comprehensive evaluation of the capability of the OCC system, particularly in wearable communications, tracking, and multi-user identification applications.

All experiments were performed assuming LoS optical communication between LED-based transmitters and CMOS camera receivers Fig. 4.4. The optical channel was described using a simplified power model:  $P_{Rx} = a \cdot P_{Tx}$ , where  $a = R(\theta_{\text{out}}, \phi_{\text{out}}) \cdot A_{Rx}$  with  $R(\theta_{\text{out}}, \phi_{\text{out}})$  representing the angular radiation response of the LED and  $A_{Rx}$  the

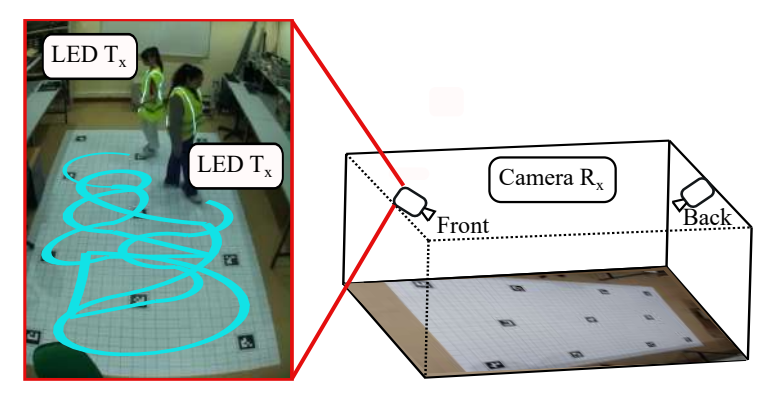


**Figure 4.3:** Example of experimental setups implemented with the yellow safety jacket with the LED strip worn by people walking in the room, captured by the cameras placed on the front and back walls of the room.

effective area of the camera receiver [119]. Instead of developing a detailed analytical or probabilistic channel model, the OCC link was experimentally evaluated under various conditions. The impact of external light sources was also considered through indoor and outdoor experiments, under varying ambient lighting environments.

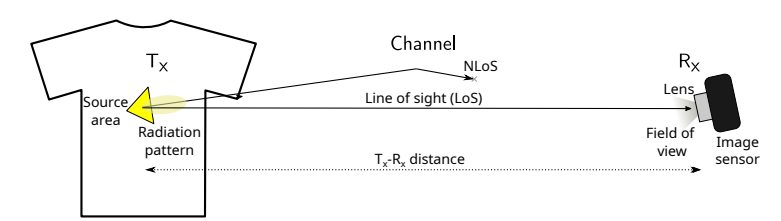


**Figure 4.4:** Line-of-sight (LoS) optical communication model between the LED transmitter and CMOS camera receiver.

## 4.1.1 Transmitter equipment

The experimental setups aimed to evaluate different configurations of an OCC system using wearable LED-based transmitters under various conditions. Across all setups, the system implemented consisted of digital signal processing hardware and optical front-ends.

The transmitters consisted of LED-based light sources, including a standard LED array, white and RGB LED strips, and LED-coupled side-emitting optical fiber, as depicted in Fig. 4.5. The LEDs were modulated using the non-return-to-zero on-off keying (NRZ-OOK) technique to encode data. This modulation exploits the switching digital outputs available in most MCUs, where the packet data is converted into a voltage signal that drives the LED directly. If the LED's current exceeds the MCU's maximum, a transistor connected to the power source must be implemented to drive the LED. The transmitters were powered by dedicated power sources and controlled via microcontrollers (Arduino Nano [126] or Seeeduino Xiao [127]), ensuring consistent signal transmission. The MCU generates a 6-bit data packet, repetitively, indicating the user's identification (ID). The light symbols produced by the LEDs were then

## Chapter 4 Methodology

transmitted through the free-space channel. The block diagram of the transmitting node is shown in Fig. 4.6.

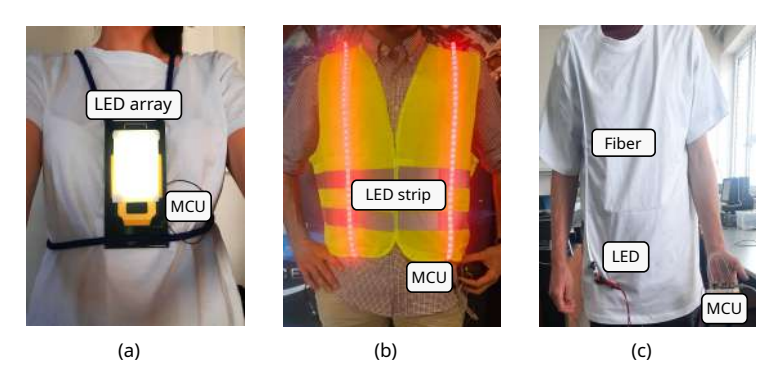


**Figure 4.5:** Wearable LED transmitter devices. (a) LED array. (b) LED strip. (c) LED-coupled side-emitting fiber.

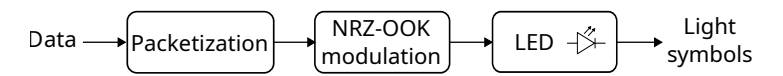


**Figure 4.6:** Block diagram of the transmitting node.

As detailed in Table 4.1, three kinds of transmitters were implemented. The LED array device [128] with dimensions  $11\times6.5\times3.5$  cm is compromised of 30 white LEDs, rechargeable batteries of 5 V, and a diffuser. Two types of LED strips were used, white and RGB, both with 10 mm width consisting of an array of surface-mounted device white LEDs, 5.0 mm by 5.0 mm size (commercially known as SMD 5050). The white LED strip was covered with a diffuser, and operating at two different voltage states, 9 and 12 V (i.e., 432 mW and 720 mW electrical power, 50 mA and 60 mA current, respectively). The side-emitting fiber ("Super Bright" by ZDEA) is made of polymethyl-methacrylate (PMMA) with a 3 mm outer diameter and with 1 m diffusion length. A white LED (LA CW20WP6 [129]) couples light to one end of the side-emitting fiber, and once the light is coupled, the side-emitting fiber becomes the data transmitter. The coupling LED operates at 3 V (i.e., 525 mW, 175 mA).

**Table 4.1:** Key parameters of the transmitter nodes.

$T_x$	LED array	LED strip	Side-emitting fiber
Light source	30 white LEDs $11\times6.5\times3.5~\mathrm{cm}$ 5V	SMD 5050 (white, RGB)	LA CW20WP6 (white)
Size		10 mm width	4 mm diameter
Power supply		9V, 12V	3V

White LEDs were mainly used for transmission. White color is a combination of the red, green, and blue channels. However, with the RGB LED strip, we also evaluated individual RGB colors (Red: 620–625nm, Green: 520–525nm, Blue: 465–470nm). Compared to white LEDs, RGB channels offer narrowband emission, which facilitates color-based modulation. The performance of each transmitter was evaluated in terms of achievable data rate. The white LED strip and the optical fiber give a data rate of

approximately 0.5 kbps. For the RGB LED strip, each channel reached 3.8 bps, and by transmitting distinct patterns simultaneously on all three channels, an overall achievable data rate of 11.4 bps. The RGB colors are easily detected by the image sensors and recognized by the image processing algorithm, as well as, they serve as visual indicators for people monitoring a surveillance system in high-risk environments providing insight into the situation of its users. For instance, red could indicate danger, green could represent safety, and blue could communicate additional information.

All transmitters used in the experimental setups were chosen based on their ability to emit diffuse light with wide radiation patterns without requiring strict alignment between the transmitter and the camera receiver.

## 4.1.2 Receiver equipment

The receiver equipment used across all experimental setups consisted of CMOS-based cameras, including smartphone cameras (Samsung A51 with image sensor Sony IMX582, Samsung S23 with image sensor S5KGN3) and Raspberry Pi HQ cameras with CCTV lenses (Sony IMX477 image sensors [130]). These cameras captured optical signals emitted by the LED-based transmitters under various conditions, using either the RS or the GS acquisition mechanisms, as explained in the previous Chapter.

The smartphone cameras recorded high-resolution images and videos ( $1920\times1080$  px,  $7680\times4320$  px,  $4000\times1800$  px) at frame rates of 60 fps and 30 fps in both indoor and outdoor environments, ensuring signal detection at varying distances (from short-range indoor setups to long-range outdoor scenarios up to 120 m). The Raspberry Pi cameras, set to a resolution of  $640\times480$  px, were placed in indoor environments to capture videos at 30 fps. Other parameters, such as exposure time and ISO varied depending on the specific experimental conditions. The exposure time refers to the time the camera is exposed to light and the ISO number refers to the amount of light the camera lets on the sensor. All the key parameters of the receiver nodes are detailed in Table 4.2.

**Table 4.2:** Key parameters of the receiver nodes.

$R_x$	Samsung A51	Samsung S23	Raspberry Pi
Image sensor (IS) Frame rate (fps)	Sony IMX582 30 fps	S5KGN3 30 fps, 60 fps	Sony IMX477 30 fps
Resolution	$1920 \times 1080 \text{ px} $ $4000 \times 1800 \text{ px}$	1920×1080 px 7680×4320 px	640×480 px

# 4.2 Image Processing

The image processing techniques applied across all experimental setups involved multiple stages to ensure accurate decoding of the transmitted optical signals. Different steps were followed depending on the image sensor's acquisition mechanism, GS or RS, as represented in Fig. 4.7.

The image processing techniques implemented in GS camera-based reception of data focused on the extraction and decoding of transmitted optical signals by analyzing pixel intensity and color information. GS cameras capture several states of the transmitter

## Chapter 4 Methodology

in a sequence of frames. Initially, video recordings were segmented into frames and a region of interest (ROI) was selected depending on the position of the transmitter in the frame. Then, the selected ROI was converted on grayscale, where the highest intensity pixel was selected to reconstruct the received signal. On the other hand, on color-based detection, the pixel values of the selected ROI were analyzed to indicate the dominant color in transmission. A binarization and normalization threshold of the mean intensity value was applied for analysis. Subsequently, for determining the correct decoded number of patterns, a cross-correlation method was applied to correlate the received signal with the predefined template of the transmitted ID pattern to ensure accuracy in the signal detection. Correlation peaks exceeding a 90% threshold were considered valid transmissions, ensuring reliable data extraction across multiple frames.

The image processing techniques implemented in RS camera-based data reception depended on template matching to accurately detect and decode the transmitted optical signals. Since RS cameras capture images row by row, the transmitted optical signal appears as horizontal intensity bands in an image frame. The recorded video was first segmented into frames, which then were converted to grayscale for intensity-based analysis. Simultaneously, a predefined template of the known transmission pattern was generated to perform a correlation-based search within each frame, similar to a 2D convolution process. This enabled the localization of the transmitted signal in the captured frame. Thresholding and binarization were then performed when the ROI with the highest correlation was found, to extract the transmitted data. The extracted signal was then normalized and analyzed to ensure accurate decoding.

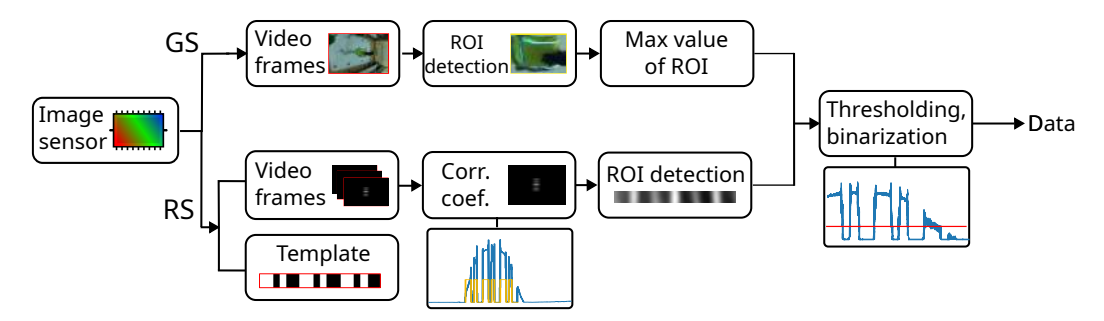


**Figure 4.7:** Block diagram of image processing based on the image sensor's acquisition mechanism.

# 4.3 Object detection

The ROI detection within the frames can be further facilitated by integrating Al-based techniques. For that reason, a YOLO object detection algorithm was implemented, as it represents the state-of-the-art in real-time object detection, particularly in scenarios requiring high speed and accuracy. Its open-source availability and widespread adoption also make it a practical and accessible solution. It was used for the processing of data captured in a multi-camera setup, where multiple users wearing yellow safety jackets with LED strip transmitters were walking in an indoor room, as shown in Fig. 4.3. The model followed a structured workflow as shown in the flow diagram in Fig. 4.8, which

included dataset preparation, model training, validation, testing, and deployment. The selection of YOLOv8 over its later versions, such as YOLOv9, YOLOv10, and YOLOv11, was due to its optimal balance between performance and resource efficiency. Although newer versions are improved, they have higher computational requirements and longer processing times. YOLOv8 was proved to be efficient and feasible in identifying and tracking LEDs.

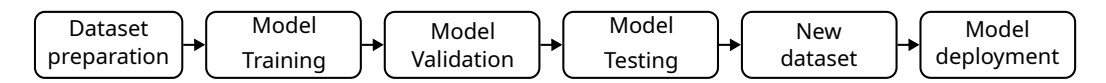


Figure 4.8: Flow diagram of the object detection algorithm.

Initially, the captured videos were converted into image frames, generating a dataset of 1,000 images that were deployed on the Roboflow platform [131] for training purposes. Each image was annotated manually, drawing bounding boxes around the target object, which in this case was a yellow safety jacket with an LED strip attached to it. 600 labeled images were used for the training of the model through 1,000 epochs, in which the YOLOv8 adjusted its parameters to minimize the difference between its predictions and ground-truth labels.

The validated model was tested on a separate set of 300 images that were not seen on training ensuring its ability to generalize on previously unseen data. Following that, a performance evaluation was carried out with a test set of 100 images for the precision, recall, and mean Average Precision calculation. The model performed a 99.8% precision, a 99.3% recall, and a 99.5% mAP, demonstrating high detection accuracy. The confusion matrix for the test set showed 100 true positives, 1 false positive, and 2 false negatives while no observation was made for the true negatives. The false positive detection could be due to duplicate detection.

From the testing results, the dataset was also enhanced to support more variable images and to correct any inconsistencies in the labeling to further strengthen the robustness of the model. The trained YOLOv8 model was then exported and used in the system to detect ROI and demonstrate effective tracking of the transmitter, as shown in Fig. 4.9.

# 4.4 Exercise analysis

The tracking process within the image frames could be confined to a reduced area in the image frame, refined by the  $T_x$ 's position in the frame. The user's position in the frame could be related to factors such as exercise intensity, age, or gender. The analysis of the characteristics of controlled exercise-induced movement, could offer valuable insights into their exercise intensity, age, and gender, uncover individual differences, and potentially identify chronic conditions or detect early signs of injuries.

For that reason, a person wearing an LED  $T_x$  device as shown in Fig. 4.1a. took part in a controlled exercise session on a stationary bicycle, with the camera  $R_x$  mounted on the bicycle. For the analysis of exercise data, the LED  $T_x$  was replaced with a smartphone, utilizing an accelerometer application to capture acceleration data throughout the session. Two types of measurements were conducted, corresponding to mild and intense

## Chapter 4 Methodology

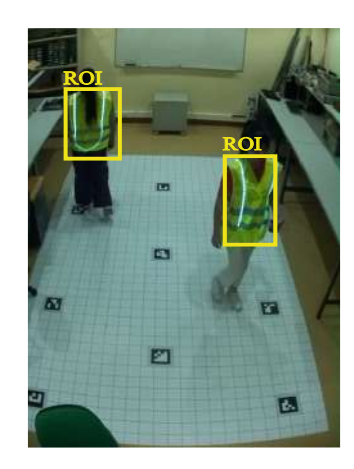


**Figure 4.9:** The two detected region of interest (ROI) corresponding to the location of the yellow safety jacket with the LED strip worn by two users, in one video frame sample, highlighted in yellow.

exercise routines. The 3D reference system used for these measurements is illustrated in Fig. 4.10.



**Figure 4.10:** 3D reference dimensions of the system, with the user engaging in physical exercise on a stationary bicycle.

To gain insight into exercise dynamics and to capture the exercise routine, two assumptions are required. First, it is assumed that the average position of the user  $\langle \vec{r}(t) \rangle$  during the workout corresponds to the initial position  $\vec{r}_0$  as expressed in 4.1. With this assumption, the analysis can be simplified by considering the average position as the starting point.

$$\langle \vec{r}(t) \rangle = \vec{r}_0 \tag{4.1}$$

Second, the analysis also accounts for errors due to the inertial measurement unit (IMU), and cumulative errors as described in 4.2, which may cause positional drift over time. Sensor inaccuracies, despite the controlled movement, can lead to cumulative

errors, which are accounted for in the analysis. In the equation,  $\vec{\mu}_N$  and  $\vec{\sigma}_N$  are the vectors of IMU drift and noise uncertainties, respectively.

$$\langle \vec{r}(t) \rangle \sim \mathcal{N}(\vec{r_0} + \vec{\mu}_N \cdot t, \vec{\sigma_N} \cdot t)$$
 (4.2)

By analyzing acceleration data,  $\vec{a}(t)$ , the user's position is determined in 4.3 through double integration, where the initial velocity,  $\vec{v}_0$ , is assumed to be  $\vec{0}$  at the start of the routine.

$$\vec{r}(t) = \int_0^t \int_0^t \vec{a}(t)dtdT = \int_0^t (\vec{v}(t) - \vec{v}_0) dt$$
 (4.3)

The velocity  $\vec{v}(t)$  at discrete time intervals  $j\Delta t$  in 4.4 is obtained by summing the acceleration components  $a_x(i)$  and  $a_y(i)$  over the time interval  $\Delta t$  along the x and y axes, respectively. The analysis is restricted to the XY plane, as it aligns with the camera's plane, making it sufficient for extracting relevant information in the sensing pathway of the integrated sensing and communication (ISAC)-enabled reception routines without requiring prior additional data.

$$\vec{v}(j\Delta t) = \Delta t \sum_{i=0}^{j} a_x(i\Delta t) \cdot \vec{n}_x + a_y(i\Delta t) \cdot \vec{n}_y$$
(4.4)

Likewise, the position  $\vec{r}$  in discrete time intervals  $k\Delta t$  in 4.5 is determined by summing the velocity components  $v_x(j)$  and  $v_y(j)$  over the time interval  $\Delta t$  along the x and y axes, respectively.

$$\vec{r}(k\Delta t) = \Delta t \sum_{j=0}^{k} v_x(j\Delta t) \cdot \vec{n}_x + v_y(j\Delta t) \cdot \vec{n}_y$$
(4.5)

Applying Equation 4.5, the drift characteristics of the IMU were examined using 25 seconds of calibrated acceleration data (with gravity removed). The drift pattern indicates that analyses should be conducted within a sliding window, and its duration should be limited to a few seconds to minimize disruptions caused by cumulative errors.

The expected position value can be determined using Equation 4.6, by substituting Equation 4.5 into Equation 4.4.

$$E[\vec{r}(k\Delta t)] = \Delta t^2 \sum_{i=0}^{k} \sum_{i=0}^{j} E[a_x(i\Delta t)] \cdot \vec{n}_x + E[a_y(i\Delta t)] \cdot \vec{n}_y$$
(4.6)

Applying a moving average with a window size of M results in Equation 4.7.

$$E_M[\vec{r}(k\Delta t)] = \frac{\Delta t^2}{M} \sum_{l=k-(M-1)}^{k} \sum_{j=0}^{l} \sum_{i=0}^{j} \vec{a}(i)$$
(4.7)

For analysis simplicity, several assumptions were made. The first assumption was that the reversion to the mean occurs within a given window, ensuring that the average position within the sliding window was fixed during the process. This assumption is statistically valid due to the controlled experiment (static cycling). The second

## Chapter 4 Methodology

assumption was that the sliding window size was determined by a frequency-domain analysis of deviations from the average. This analysis, mathematically represented in Equation 4.8, indicated that the majority of energy is concentrated in the first 47 Hz of the spectrum, which led to selecting a sliding window length M of 47.

$$R_z(\tau) = \mathcal{F}^{-1}(\mathcal{F}((a_x(t)) \cdot conj(\mathcal{F}(a_x(t))))) \tag{4.8}$$

The integration of the data obtained from the accelerometer sensor with the image processing algorithm is presented in the flow diagram in Fig.4.11.

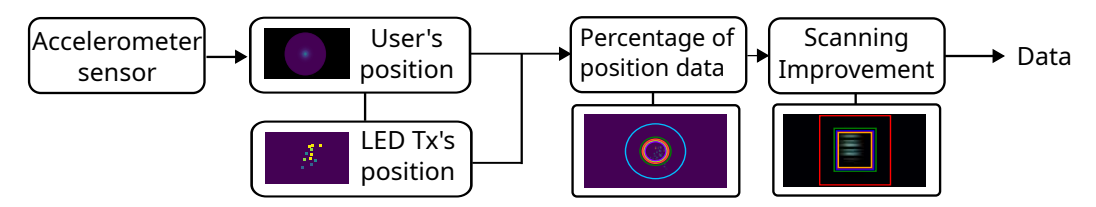


Figure 4.11: Flow diagram of the exercise analysis data.

First, the distribution of the user's position in pixels within one frame can be represented as a circle's radius corresponding to the frequency of the user's position. Then, these data, combined with the data obtained from the LED  $T_x$ , provide information about the percentage of the position data that can be considered. Thus, the tracking process can be confined to a smaller area on the image frame.

All the obtained results from the experimental setups are presented in the next chapter, in a compendium of publications.

This chapter presents all the articles published in high-impact journals, following the progression of the research, as a compendium. Each paper is outlined with its main topic, key contributions, objectives addressed, and the results obtained. At the end of the chapter, a summary of the key contributions of the methodology and findings of each article is presented.

# 5.1 Publication 1 (P1)

The article entitled "Optical Camera Communications in Healthcare: A Wearable LED Transmitter Evaluation during Indoor Physical Exercise" [132] evaluates an OCC system featuring a wearable LED-based transmitter for data transmission, user detection, and tracking during indoor physical exercise. The evaluation assumes a controlled user exercise session on a stationary bicycle. The wearable LEDs are modulated in intensity to transmit binary data, imperceptible to the human eye but detectable by a smartphone camera operating at a specific frequency. The camera tracks the user's movements and captures the transmitted data. The main innovation is that widely available commercial devices are employed for communication purposes, which paves the way for practical implementations of OCC in healthcare and beyond.

A key contribution of this research is the development of an image processing algorithm for accurate detection of the transmitted bits in video frames, even under user movement, through a correlation process. This enables higher reliability for data transmission and more robust performance over a range of intensities of exercises, mild and intense.

Beyond communication performance, this study also explores the integration of OCC in health and fitness applications. The analysis of the user's position within the frame could provide insights into exercise intensity, age, gender, and individual differences. This could contribute to monitoring physical activity and detecting early signs of chronic conditions or injuries. The proposed system has the potential for applications in environments, such as rehabilitation centers, gyms, and elderly care facilities, to monitor the activities of individuals with good health conditions or those who face health problems.

This study addresses O1 by demonstrating the feasibility of using off-the-shelf cameras for optical communication, without the need for additional specialized hardware. With the integration of image processing algorithms and OCC, the system decodes the transmitted bits from the wearable LED-based transmitter. In addition, this study supports O2 by evaluating the effects of sensor positioning and movement dynamics on OCC performance. The system examines data transmission in a controlled indoor environment, analyzing the effects of movement intensity, mild or intense, on communication reliability.

Finally, by analyzing the characteristics of controlled exercise-induced movement, the

## **Chapter 5** Experimental Results

 $T_x$ 's detection process is simplified, as the tracking process is confined to a smaller area within the image frame, achieving a reduction of 87.3% for mild exercise and 79.0% for intense exercise. Note, that this work is an extended version of a previous study [133] (see Chapter A), where the SNR had been calculated at 22 dB.





Article

# Optical Camera Communications in Healthcare: A Wearable LED Transmitter Evaluation during Indoor Physical Exercise †

Eleni Niarchou <sup>1,\*</sup> , Vicente Matus <sup>1</sup>, Jose Rabadan <sup>1</sup>, Victor Guerra <sup>2</sup> and Rafael Perez-Jimenez <sup>1</sup>

- Institute for Technological Development and Innovation in Communications (IDeTIC), University of Las Palmas de Gran Canaria, 35001 Las Palmas de Gran Canaria, Spain; vicente.matus@ulpgc.es (V.M.); jose.rabadan@ulpgc.es (J.R.); rafael.perez@ulpgc.es (R.P.-J.)
- Pi-Lighting, 1950 Sion, Switzerland; victor.guerra@pi-lighting.com
- \* Correspondence: eleni.niarchou@ulpgc.es
- <sup>†</sup> This paper is an extended version of our paper published in 17th International Conference on Telecommunications (ConTEL), Graz, Austria, 11–13 July 2023.

Abstract: This paper presents an experimental evaluation of a wearable light-emitting diode (LED) transmitter in an optical camera communications (OCC) system. The evaluation is conducted under conditions of controlled user movement during indoor physical exercise, encompassing both mild and intense exercise scenarios. We introduce an image processing algorithm designed to identify a template signal transmitted by the LED and detected within the image. To enhance this process, we utilize the dynamics of controlled exercise-induced motion to limit the tracking process to a smaller region within the image. We demonstrate the feasibility of detecting the transmitting source within the frames, and thus limit the tracking process to a smaller region within the image, achieving an reduction of 87.3% for mild exercise and 79.0% for intense exercise.

**Keywords:** optical camera communications (OCC); wearable devices; image processing; exercise analysis



Citation: Niarchou, E.; Matus, V.; Rabadan, J.; Guerra, V.; Perez-Jimenez, R. Optical Camera Communications in Healthcare: A Wearable LED Transmitter Evaluation during Indoor Physical Exercise. Sensors 2024, 24, 2766. https://doi.org/10.3390/ s24092766

Academic Editor: Yang Yue

Received: 29 March 2024 Revised: 20 April 2024 Accepted: 24 April 2024 Published: 26 April 2024



Copyright: © 2024 by the authors. Licensee MDPI, Basel, Switzerland. This article is an open access article distributed under the terms and conditions of the Creative Commons Attribution (CC BY) license (https://creativecommons.org/licenses/by/4.0/).

## 1. Introduction

Optical wireless communications (OWC) stand as a significant area of exploration in mobile communication, offering advantages such as cost effectiveness, high-speed capabilities, and reliable data transmission [1]. Already acknowledged as a complementary or sometimes viable alternative to radio-frequency (RF) technology, OWC includes promising technologies such as optical camera communications (OCC). OCC employs a light-emitting diode (LED) as the transmitter ( $T_x$ ), an image sensor (IS) (i.e., camera) as the receiver ( $R_x$ ), and light as as the signal communication carrier. This approach boasts several valuable attributes, including low cost, high security, low power consumption, and enhanced reliability. Importantly, it is devoid of electromagnetic interference, ensuring complete safety for human health [2]. The extensive deployment of smart devices, not only smartphones that have built-in complementary metal oxide semiconductor (CMOS) cameras and are all interconnected within the Internet, has paved the way for innovative applications of OCC and serves as a cornerstone for the development of OWC-based Internet of Things, termed optical IoT (OIoT) [3]. These applications include indoor positioning systems [4], underwater [5], localization [6], and healthcare applications [2].

Smart devices, encompassing smartphones, smartwatches, and smart clothing, are recognized as products that seamlessly incorporate wearable technologies to distinguish human activities [7]. Wearable devices, designed to be lightweight and compact, offer user convenience and integrate seamlessly into clothing or accessories or directly attached to the body (like glucose sensor patches) without disrupting daily activities. Equipped with sensors, processors, and communication capabilities, these devices aim to provide

specific functionalities, such as monitoring health and fitness metrics [8]. Wearable health-monitoring sensors have become ubiquitous in our daily lives [9,10], playing a crucial role in healthcare systems for real-time and continuous patient health monitoring [10]. They also serve as a cornerstone for the IoT [11]. Sensors measure parameters before the OCC system collects the data, forwarding them to the camera through integrated light-emitting diodes. With the emergence of 6G, the integration of wearables in healthcare is poised to expand, signaling an era of intelligent healthcare [12] characterized by enhanced sensing, processing, and communication capabilities.

To date, only a limited body of research has explored the integration of wearable sensors with LEDs as transmitters. For instance, in [13], medical sensors and infrared LEDs collaborate to transmit medical data for patient monitoring. Similarly, ref. [14] employs this combination for indoor health monitoring, taking into account patient mobility. Additionally, ref. [15] introduces an all-optical bidirectional wireless communication system that evaluates sensor mobility, variations in orientation, and placement on the body. Furthermore, ref. [16] investigates the performance of optical code-division multiple access in asynchronous mode, considering the impact of mobility and random transmitter orientations. Moreover, [17] explores optoelectric sensors monitoring cardiovascular vital signs.

The use of OWC technologies in healthcare tourism has been extensively studied in [18], including the use of this technology for monitoring elder or impaired people with special needs. The use of wearable devices, jointly with location techniques [19], allows detecting whether the user is immobile for long periods, has suffered a fall or a sudden change in vital signs, or is simply leaving a predefined safety zone, in which they can remain without requiring constant attention from their caregiver. For this cases IR emitters can be considered instead of the visible ones, to preserve user privacy in general-purpose environments such as hotels, without loss of generality in this proposal as near-IR can be detected by regular CMOS-Silicon based cameras [20].

In the field of OCC, few works have been done considering wearables as transmitters. In our previous research, we showcased a wearable LED array [21] and a fiber attached on T-shirt [22] as distributed transmitters. Recently, there has been notable development in various medical applications that focus on using wearable sensors to measure individuals' health conditions. For instance, in [2], a system has been implemented for real-time remote monitoring of a patient's heart rate and oxygen saturation data. Similarly, in [23], a system facilitates the transmission of multiple clinical data types, including electrocardiogram, photoplethysmogram, and respiration signals in a home-based rehabilitation system. In addition, OCC has demonstrated its adaptability by being combined with other technologies, giving rise to hybrid systems that leverage the strengths of each technology, thereby enhancing their robustness [24]. Specifically, in [25], OCC is integrated with Bluetooth Low Energy (BLE) to enable efficient, remote, and real-time transmission of a patient's electrocardiogram signal to a monitor. A similar combination is explored in [26] for real-time health monitoring, where data from body sensors is transmitted to a central gateway. In cases where node movement in OCC can disrupt the connection, BLE steps in to ensure continuous communication.

Analysis of human exercise routine data can provide valuable insights. For instance, in [27], a smart exercise bike was developed specifically for rehabilitation from Parkinson's disease. Another example is found in [28], where a camera-based monitoring system offers indications for cardiovascular health and optimizes training protocols. Additionally, ref. [29] introduces a video-based heart rate detection system to monitor people's heart rates during exercise. Moreover, ref. [30] introduces a monitoring system for elderly people is introduced, capable of autonomously identifying significant deviations in their presence pattern. Furthermore, in [31] the proposed system determines body posture and identifies the physical condition and health of the body. Moreover, ref. [32] presents a machine learning-based analysis of the typing pattern analysis detects depressive disorder. Similarly, ref. [33] explores the analysis of keyboard interactions recorded on an individual's smartphone

Sensors **2024**, 24, 2766 3 of 13

can offer valuable insights into the clinical status of multiple sclerosis. Lastly, ref. [34] investigates keystroke dynamics for the early detection of loneliness and the development of targeted interventions.

In this study, we conduct an experimental evaluation of an OCC system utilizing a wearable LED transmitter. The evaluation assumes controlled user movement during physical exercise in an indoor setting. The wearable LEDs are modulated in intensity to transmit binary data, imperceptible to the human eye but detectable by a smartphone camera operating at a specific frequency. The camera tracks the user's movements and captures the transmitted data.

Our focus is on addressing challenges related to transmitter detection and tracking [35]. To achieve this, we propose employing a template signal transmitted by the LED, denoted as  $T_x$ , and detected in the image through a correlation process. This information will serve a dual purpose aligned with the Integrated Sensing And Communication (ISAC) paradigm. The main hypothesis is that the user's position (i.e.,  $T_x$ 's detection) within the frame correlates with factors such as exercise intensity, age, gender, etc. This correlation may be even more profound, suggesting individual differences and the potential to detect chronic conditions or even early signs of injuries. Further exploration of this hypothesis will be conducted in subsequent phases of the research, utilizing the acquired data. To simplify the  $T_x$ 's detection process within the frame, we leverage the characteristics of controlled exercise-induced movement, confining the tracking process to a smaller area within the image.

Our envisioned system is designed to monitor the activities of individuals who are either in good health or those who face health problems. This monitoring can take place in various environments such as homes, gyms, ambulances, hospitals, and intensive care units [12,36]. Consequently, it has the potential to aid in rehabilitation, sports training, elderly care [37], early detection of musculoskeletal or cognitive diseases, and evaluations of falls and balance. The main innovation of this study revolves around employing widely accessible and commercially available wearable devices, including LEDs, and integrating them with smartphones for communication purposes.

The structure of the paper is outlined as follows. Section 2 describes the system designed, with the equipment employed in both the transmitting and receiving nodes and the experimental setup. Section 3 examines the methodology, including the image processing and the analysis of the user's exercise. Section 4 discusses the experimental results obtained. Ultimately, Section 5 presents the conclusions drawn from this work.

#### 2. System Design

In this section, we provide an overview of the equipment utilized in both transmitting and receiving nodes of the proposed system. Additionally, we provide a detailed description of the experimental setup. The block diagram of the proposed OCC link is shown in Figure 1.

The system utilized for the envisioned experiment included digital signal processing hardware and optical front-ends. The  $T_x$  consisted of a standard LED device linked to the digital output of a micro-controller unit (MCU) (Seeeduino Xiao [38]). The devise is comprised of 30 white LEDs, rechargeable batteries of 5 V, and a diffuser. The LED's transmitted illuminance at 0 cm measured with testo 545 lux meter, is 17,443 lux, while the received illuminance at 25 cm is 105 lux.

The proposed OCC system utilizes the non-return-to-zero on-off keying (NRZ-OOK) modulation technique for transmitting data wirelessly across a free-space channel. Employing the digital switching outputs of the micro-controller unit (MCU), the system facilitates NRZ-OOK modulation [39]. The  $T_{x}$  device is modified accordingly in order to drive the LEDs with a transistor powered directly from the battery terminals. The MCU generates a 6-bit data packet [110100] at a rate of 0.4 ms per bit, corresponding to a modulation frequency of 2.5 kHz per bit. This data packet is transformed into a voltage signal, directly driving the LEDs. To overcome the MCU's maximum current limit, a transistor is connected

Sensors **2024**, 24, 2766 4 of 13

to the power source for LED driving. To enhance link performance, a repeat-packet strategy is implemented.

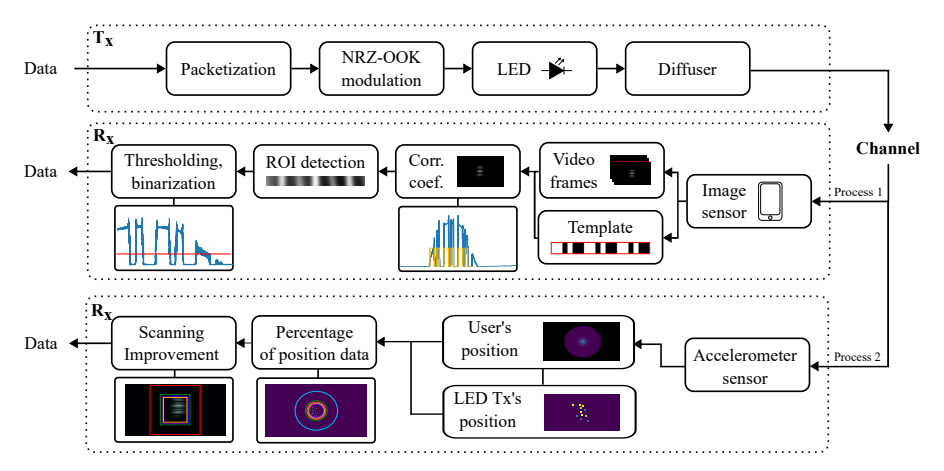


Figure 1. Block diagram of the transmitting and receiving node.

On the other hand, the  $R_x$  was a smartphone [40] camera which captures video in rolling shutter (RS) mode. The RS-based cameras can capture the image row-by-row of pixels, which means that different lines of the image array are exposed at various times to read the light intensity through the sensor enabling multiple states of LEDs (ON and OFF) can be obtained in a single frame [41]. The smartphone camera captures video from a distance of 20–30 cm. The smartphone camera captures a 30 fps frame-rate video, with exposure time of 83  $\mu$ s, and ISO 125 [42], using resolution (7680  $\times$  4320 px). The exposure time is the time the camera is exposed to light and the ISO number refers to to the amount of light the camera lets on the sensor. The most relevant parameters of the proposed system are summarized in Table 1. It is important to note that all measurements were performed under indoor ambient lighting conditions.

Module	Parameter	Value	
	Light source	LED array	
	Device dimensions	$11 \times 6.5 \times 3.5$ cm	
T	Power supply	5 V	
$T_x$	Microcontroller	Seeeduino XIAO (Shenzhen, China)	
	Illuminance	105 lux	
M 1 1 c	Modulation time	0.4 ms	
Modulation	Data packet size	6b/packet [110100]	
	Smartphone camera	Samsung Galaxy S23 (Suwon, Republic of Korea)	
	Image sensor	S5KGN3	
$R_x$	Exposure time	83 µs	
	Frame rate	30 fps	
	ISO	125	
	Resolution	$7680 \times 4320 \text{ px}$	
Channel	Link distance d	20–30 cm	

Sensors **2024**, 24, 2766 5 of 13

For the evaluation of the OCC system, the person wearing the  $T_x$  participated in a controlled exercise session on a stationary bicycle. The experimental setup featuring the wearable  $T_x$  and the  $R_x$  attached on the bicycle, is illustrated in Figure 2.

The recorded video undergoes offline processing, with the main objective being the detection and tracking of the  $T_x$ . To achieve this, we use a template signal emitted by the LED, which is then identified within the image through a correlation procedure, as shown in Process 1 in Figure 1. To simplify Process 1, we leverage the characteristics of controlled exercise-induced movement in Process 2, thereby limiting the tracking process to a smaller area within the image. Both processes will explained in the next section.

For the exercise scenario we replaced the LED  $T_x$ , with a smartphone, and employed an accelerometer application to measure acceleration data during the exercise. Two types of measurements were conducted, involving the user performing mild and intense exercise routines. Our reference system is depicted in Figure 2b.





**Figure 2.** Experimental setup with the wearable transmitter device and the smartphone camera receiver. (a) The user engages in physical exercise on a stationary bicycle. (b) 3D reference dimensions of the system.

#### 3. Methodology

In this section, we elaborate on the methodology employed for this experimental setup. Firstly, we analyze the image processing, along with demodulation and data acquisition. Following that, we provide a detailed analysis of exercise-related data within the context of our experimental setup.

#### 3.1. Image Processing

In the image processing procedure in Figure 1 (Process 1), the video is first segmented into frames, and a single frame is chosen while a template is generated. This template comprises three consecutive packets, each containing a sequence of [110100] bits. Due to the RS effect, the data rate of the OCC using a CMOS camera can be significantly increased [43].

Afterward, the image frames are converted to grayscale, facilitating the extraction of the pixel intensity profile. The correlation process involves sliding the template image over the frame, akin to a 2D convolution, to pinpoint the 2D position of the signal captured from the transmitting source. The blue lines within the inset of the  $R_x$  section of the block diagram represent the average row value, while the orange line depicts the template signal, and the red line illustrates the binarization threshold. In Figure 3, the region of interest (ROI) in the frame, where the correlation attains the maximum value, is highlighted. This process is carried out iteratively for all frames. The identified ROI is then used for data

Sensors **2024**, 24, 2766 6 of 13

decoding. Through the application of thresholding and binarization to the acquired data, the received signal is effectively decoded, as shown in Figure 4.

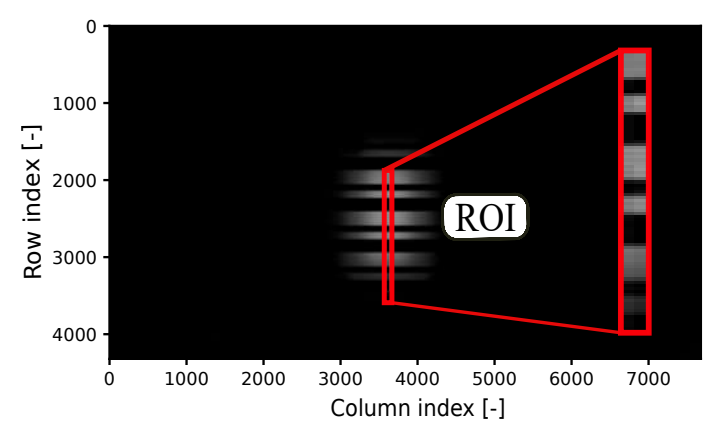


**Figure 3.** Frame showing values obtained from the correlation coefficient between a random frame and the template. The region of interest (ROI) is highlighted in red.

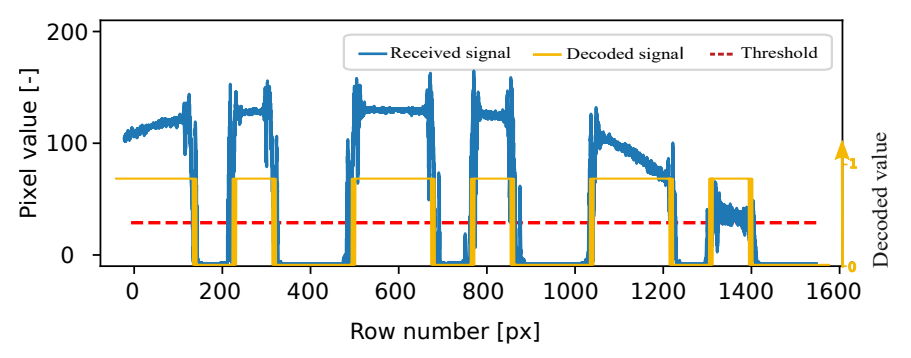


Figure 4. Received grayscale signal, decoded signal, and threshold.

#### 3.2. Exercise Analysis

For the exercise scenario mentioned above, our aim is to gain insight into the dynamics of the exercise and capture the exercise routine. To achieve this, we make two assumptions. Firstly, it is assumed that the individual's average position  $\langle \vec{r}(t) \rangle$  during the workout corresponds to the initial position  $\vec{r}_0$  as shown in Equation (1), simplifying the analysis by considering the average position as the starting point.

$$\langle \vec{r}(t) \rangle = \vec{r}_0 \tag{1}$$

Secondly, the analysis acknowledges the presence of inertial measurement unit (IMU) error and accounts for cumulative errors in Equation (2) that may cause a drift in position data over time. Despite controlled movement, factors such as sensor inaccuracies can introduce cumulative errors, which are considered in the analysis.

$$\langle \vec{r}(t) \rangle \sim \mathcal{N}(\vec{r}_0 + \vec{\mu}_N \cdot t, \vec{\sigma_N} \cdot t)$$
 (2)

where  $\vec{\mu}_N$  and  $\vec{\sigma}_N$  are the vectors derived from the IMU's uncertainties with respect to drift and noise, respectively. Analyzing the acceleration data  $\vec{a}(t)$ , we obtain the position of the user in Equation (3) by double integrating the acceleration, where  $\vec{v}_0$  is the initial velocity (assumed in  $\vec{0}$  at the beginning of the routine).

Sensors **2024**, 24, 2766 7 of 13

$$\vec{r}(t) = \int_0^t \int_0^t \vec{a}(t)dtdT = \int_0^t (\vec{v}(t) - \vec{v}_0) dt$$
 (3)

The velocity  $\vec{v}(t)$  at discrete time intervals  $j\Delta t$  in Equation (4) is a sum of acceleration  $a_x(i)$  and  $a_y(i)$  with the time interval  $\Delta t$  along the x and y directions, respectively. We focus on the XY plane since it is the camera's plane and no additional information is needed a paior for extracting information in the sensing pathway of the ISAC-enabled reception routines.

$$\vec{v}(j\Delta t) = \Delta t \sum_{i=0}^{j} a_x(i\Delta t) \cdot \vec{n}_x + a_y(i\Delta t) \cdot \vec{n}_y \tag{4}$$

Similarly, the position  $\vec{r}$  at discrete time intervals  $k\Delta t$  in Equation (5) is a sum of velocity  $v_x(j)$  and  $v_y(j)$  with the time interval  $\Delta t$  along the x and y directions, respectively.

$$\vec{r}(k\Delta t) = \Delta t \sum_{j=0}^{k} v_x(j\Delta t) \cdot \vec{n}_x + v_y(j\Delta t) \cdot \vec{n}_y$$
 (5)

Using Equation (5), the drift behavior of the IMU was analyzed after capturing 25 s of calibrated acceleration data (removing gravity). This behavior can be observed in Figure 5, suggesting that any analysis should be carried out within a sliding window. In addition, the duration of that window should be lower than a few seconds to avoid any disruption due to cumulative errors.

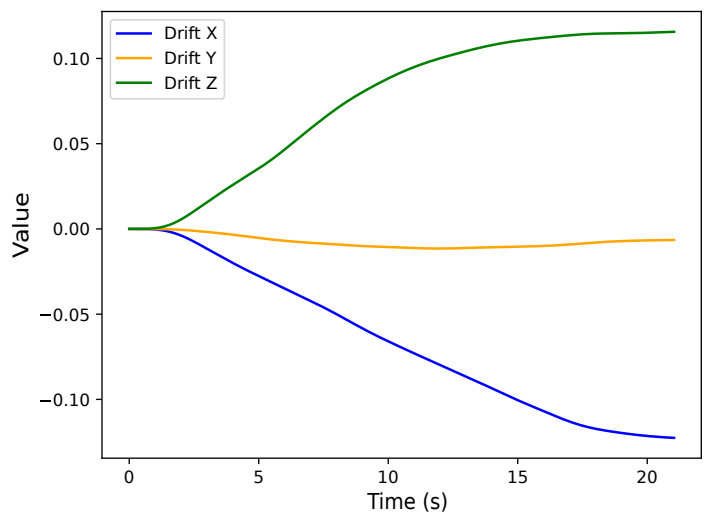


**Figure 5.** Drift in position data in 3D direction in axis x, y and z.

The expected value of the position can be calculated as shown in Equation (6), introducing Equation (5) into Equation (4)

$$E[\vec{r}(k\Delta t)] = \Delta t^2 \sum_{i=0}^{k} \sum_{i=0}^{j} E[a_x(i\Delta t)] \cdot \vec{n}_x + E[a_y(i\Delta t)] \cdot \vec{n}_y$$
 (6)

Using a moving average of the window size *M*, it yields Equation (7).

$$E_{M}[\vec{r}(k\Delta t)] = \frac{\Delta t^{2}}{M} \sum_{l=k-(M-1)}^{k} \sum_{j=0}^{l} \sum_{i=0}^{j} \vec{a}(i)$$
 (7)

Some additional assumptions have been made in order to simplify the process. Firstly, reverse to the mean is considered to happen within a given window. Thereby, the averaged

Sensors **2024**, 24, 2766 8 of 13

position inside that sliding window will be conserved during all the process. This statement holds statistically given the nature of the experimental situation (static cycling). In addition, it has been assumed that it is possible to define the size of the sliding window based on a frequency-domain analysis of the deviation with respect to the average. This analysis, depicted in Figure 6 and mathematically described in Equation (8), suggested that most of the energy is concentrated in the first 47 Hz of the spectrum. This leads to a sliding window length M of 47.

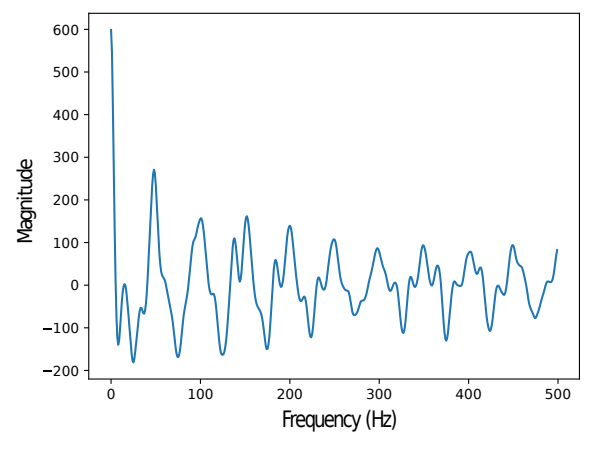


Figure 6. Frequency-domain analysis of the deviation in the XY plane. Data obtained from the IMU.

$$R_z(\tau) = \mathcal{F}^{-1}(\mathcal{F}((a_x(t)) \cdot conj(\mathcal{F}(a_x(t)))))$$
(8)

Following the above calculations and the Process 2 in Figure 1, we determined the frequency of the user's position in pixels within one frame for both mild and intense exercise scenarios. The results are presented in the following section.

#### 4. Results

In this section, we provide a summary of the outcomes derived from applying the image processing algorithm to the video frames obtained, as well as from the analysis of the user's exercise, during the previously described experiment.

The frequency of the user's position in pixels within one frame for both mild and intense exercise scenarios is illustrated in Figure 7a and Figure 7b, respectively. Consequently, the user's position in pixels within one frame can be depicted as the circle's radius in Figure 8a for mild exercise and in Figure 8b for intense exercise.

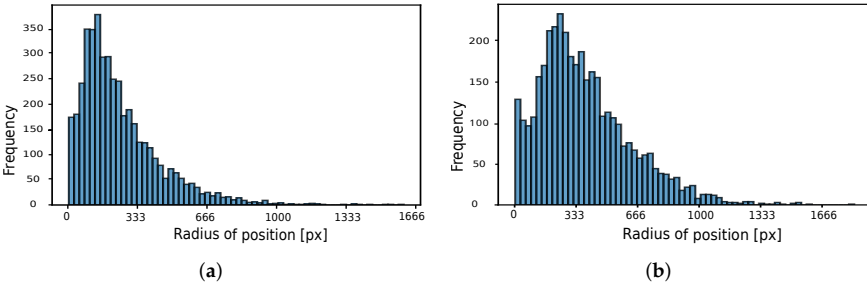


**Figure 7.** Histograms representing the frequency of a user's position in pixels within a single frame. Each bin corresponding to the frequency of one position. (a) Mild exercise. (b) Intense exercise.

Sensors **2024**, 24, 2766 9 of 13

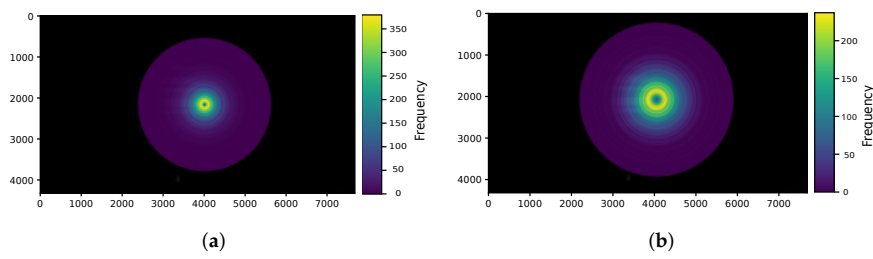


**Figure 8.** Rings representing the distribution of user's position within a single frame. Each circle's radius corresponding to the frequency of the user's position. (a) Mild exercise. (b) Intense exercise.

Then, these data, combined with the data obtained from the LED  $T_x$ , provide information about the percentage of the position data we can consider. Considering only the center of the LED  $T_x$  from previous measurements, we determined the frequency of the center of the LED  $T_x$  within one frame, represented by the dots in Figure 9a for mild exercise and in Figure 9b for intense exercise. In the same figures, the circles represent the percentage of position data (obtained from the accelerometer), spanning from 100% down to 95%.

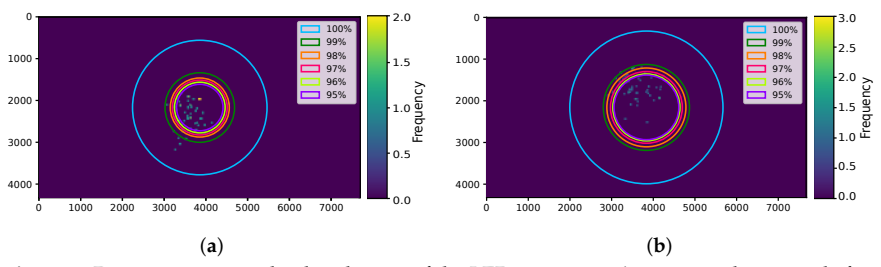


**Figure 9.** Dots representing the distribution of the LED transmitter's center within a single frame. Each dot corresponding to the frequency of the LED transmitter's center. The circles representing the percentage of the position data. (a) Mild exercise. (b) Intense exercise.

From the image processing on the video frames captured with the LED  $T_x$ , we successfully identify the ROI and decode the received signal in all frames, despite the user's movement within the frame.

By combining these data with the data obtained from the accelerometer, we aim to improve the process of ROI identification by reducing the scanning area in the frame. All the relevant results are presented in Table 2 for mild exercise and in Table 3 for intense exercise.

**Table 2.** Mild exercise. Percentage of position data considered, their corresponding radius in pixels, data included and lost from the LED transmitter and the percentage of reduction of the scanning area in the frame.

Position Data	Radius [px]	Data Included	Data Lost	Reduction
100%	1609	100%	0%	52.9%
99%	832	97%	3%	82.6%
98%	706	92%	8%	86.1%
97%	656	85%	15%	87.3%
96%	606	82%	18%	88.6%
95%	556	65%	35%	89.7%

Sensors **2024**, 24, 2766

**Table 3.** Intense exercise. Percentage of position data considered, their corresponding radius in pixels, data included and lost from the LED transmitter and the percentage of reduction of the scanning area in the frame.

Position Data	Radius [px]	Data Included	Data Lost	Reduction
100%	1841	100%	0%	41.2%
99%	1036	98%	2%	76.2%
98%	950	86%	14%	79.0%
97%	864	74%	26%	81.7%
96%	807	64%	36%	83.4%
95%	778	62%	38%	84.2%

The first columns of the tables display the percentage of position data considered along with their corresponding radius in pixels in one frame, as illustrated in Figure 9. Subsequently, the third and fourth columns present the percentage of data included within the radius of the LED  $T_x$ , as well as the percentage of data lost. Finally, the last column summarizes the percentage of reduction of the scanning area in the frame, depicted in Figure 10. In general, during intense exercise, the  $T_x$ 's wider range within the frame leads to an expansion of the scanning area.

It is evident that when all position-related data are considered, we do not lose any LED position in the frame, resulting in a reduction in the scanning area by 52.9% for mild exercise and 41.2% for intense exercise. On the contrary, when only 95% of the position data are considered, 35% and 38% of the data are lost for mild and intense exercise, respectively, despite the significant reduction in the scanning area, reaching 89.7% and 84.2%, respectively. By imposing a limitation on including 85% of the LED data to achieve a good accuracy in our system, we observe a reduction of 87.3% for mild exercise and 79.0% for intense exercise.

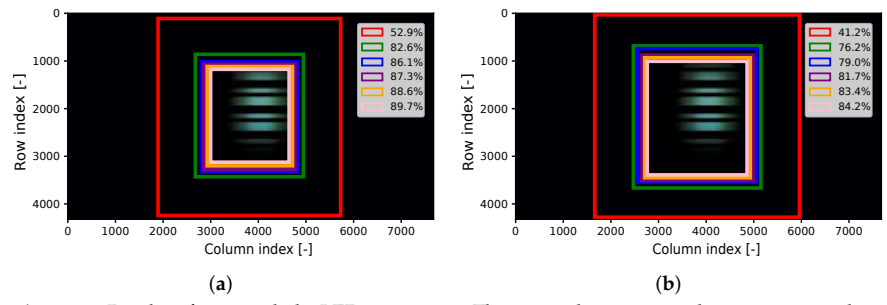


**Figure 10.** Random frame with the LED transmitter. The rectangles represent the percentage reduction of the scanning area in the frame. (a) Mild exercise. (b) Intense exercise.

## 5. Conclusions

In this paper, we experimentally evaluate an OCC system utilizing a wearable LED transmitter. Evaluation is carried out under controlled user movement during physical exercise in an indoor setting. We demonstrate the feasibility of detecting the transmitting source within the frames. Finally, by analyzing the characteristics of controlled exercise-induced movement, we confine the tracking process to a smaller area within the image.

Our system is intended to oversee the activities of individuals, whether they are healthy or facing health issues, at sports training, elderly care, or rehabilitation. The obtained results highlight the significance of our system, as detecting the user's position within the frame could offer valuable insights into their exercise intensity, age, gender, and uncover individual differences. Additionally, it has the potential to identify chronic conditions or detect early signs of injuries.

Although the proposed system has numerous advantages, there are various challenges that need further research to improve the effectiveness of the monitoring system. Primarily,

Sensors **2024**, 24, 2766

there is a need to improve the hardware design of the wearable device to be light in weight, compact, user-friendly, waterproof and effortlessly incorporated into clothing or accessories, all without causing disruptions to user's regular activities. Online video monitoring of individuals or multiple users in care units, gyms, or homes presents an additional challenge. However, it could offer people a sense of safety while engaging in their daily activities, knowing that they are being supervised in real time. Considerations for eye sensitivity with regard to light intensity must also be taken into account, especially in healthcare environments.

Future research will explore the relationship of the user's position within the frame with factors such as exercise intensity, age, or gender. This exploration will involve comprehensive data analysis to uncover potential correlations and implications for personalized health monitoring. Additionally, we will investigate the efficacy of different transmitter technologies, including LED strips and fiber optics, to determine their suitability and performance in various scenarios. Moreover, understanding the influence of user movement on data transmission and reception will be a central point, as it can significantly impact the system's reliability and accuracy. Furthermore, we plan to extend our experimental setup to encompass longer distances, enabling the evaluation of the system's performance and robustness across larger spatial domains. This expansion will open up new possibilities for remote monitoring applications, promoting advancements in healthcare and beyond.

**Author Contributions:** Conceptualization, E.N., V.M., V.G. and J.R.; Funding acquisition, R.P.-J.; Investigation, E.N.; Methodology, E.N., V.M. and J.R.; Project administration, J.R.; Software, E.N.; Supervision, V.M., J.R. and R.P.-J.; Validation, V.G.; Writing—original draft, E.N.; Writing—review and editing, V.M. and V.G. All authors have read and agreed to the published version of the manuscript.

**Funding:** This study has been supported by the OCCAM project (PID2020-114561RB-100) and SUCCESS (TED2021-130049B-C21) of the Agencia Estatal de Investigación (AEI, Spanish Research Agency). E. Niarchou enjoys a FPI grant (PRE2021-100311) also funded by AEI. Additional support has been provided through the Catalina Ruiz Grant (APCR2022010014) from the Agencia Canaria de Investigación, Innovación y Sociedad de la Información (ACIISI) under the European Social Fund.

Institutional Review Board Statement: Not applicable.

Informed Consent Statement: Not applicable.

**Data Availability Statement:** The data presented in this study are available on request from the corresponding author.

**Conflicts of Interest:** The authors declare no conflict of interest. The funding sponsors had no role in the design of the study; in the collection, analyses, or interpretation of data; in the writing of the manuscript, and in the decision to publish the results.

#### References

- Uysal, M.; Capsoni, C.; Boucouvalas, A.; Udvary, E. Optical Wireless Communications—An Emerging Technology; Springer: Cham, Switzerland, 2017. [CrossRef]
- Ahmed, M.F.; Hasan, M.K.; Shahjalal, M.; Alam, M.M.; Jang, Y.M. Design and implementation of an occ-based real-time heart rate and pulse-oxygen saturation monitoring system. *IEEE Access* 2020, 8, 198740–198747. [CrossRef]
- Teli, S.R.; Zvanovec, S.; Ghassemlooy, Z. Optical Internet of Things within 5G: Applications and Challenges. In Proceedings of the 2018 IEEE International Conference on Internet of Things and Intelligence System (IOTAIS), Bali, Indonesia, 1–3 November 2018; pp. 40–45. [CrossRef]
- Lin, B.; Ghassemlooy, Z.; Lin, C.; Tang, X.; Li, Y.; Zhang, S. An Indoor Visible Light Positioning System Based on Optical Camera Communications. IEEE Photonics Technol. Lett. 2017, 29, 579–582. [CrossRef]
- Majlesein, B. Towards Sustainable IoUT Networks: Enhancing Self-Powered and Camera-Based Underwater Optical Wireless Communication Systems. Ph.D. Thesis, Universidad of de Las Palmas de Gran Canaria, Las Palmas de Gran Canaria, Spain, 2023.
- Chavez-Burbano, P.; Guerra, V.; Rabadan, J.; Jurado-Verdu, C.; Perez-Jimenez, R. Novel Indoor Localization System Using Optical Camera Communication. In Proceedings of the 2018 11th International Symposium on Communication Systems, Networks & Digital Signal Processing (CSNDSP), Budapest, Hungary, 18–20 July 2018; pp. 1–5. [CrossRef]
- Wang, Y.; Cang, S.; Yu, H. A survey on wearable sensor modality centred human activity recognition in health care. Expert Syst. Appl. 2019, 137, 167–190. [CrossRef]

Sensors 2024, 24, 2766 12 of 13

- 8. Majumder, S.; Mondal, T.; Deen, M.J. Wearable sensors for remote health monitoring. Sensors 2017, 17, 130. [CrossRef] [PubMed]
- Heo, J.S.; Hossain, M.F.; Kim, I. Challenges in design and fabrication of flexible/stretchable carbon-and textile-based wearable sensors for health monitoring: A critical review. Sensors 2020, 20, 3927. [CrossRef]
- Nasiri, S.; Khosravani, M.R. Progress and challenges in fabrication of wearable sensors for health monitoring. Sens. Actuators Phys. 2020, 312, 112105. [CrossRef]
- 11. De Fazio, R.; De Vittorio, M.; Visconti, P. Innovative IoT solutions and wearable sensing systems for monitoring human biophysical parameters: A review. *Electronics* **2021**, *10*, 1660. [CrossRef]
- 12. Kharche, S.; Kharche, J. 6G Intelligent Healthcare Framework: A Review on Role of Technologies, Challenges and Future Directions. J. Mob. Multimed. 2023, 19, 603–644. [CrossRef]
- Adiono, T.; Armansyah, R.F.; Nolika, S.S.; Ikram, F.D.; Putra, R.V.W.; Salman, A.H. Visible light communication system for wearable patient monitoring device. In Proceedings of the 2016 IEEE Region 10 Conference (TENCON), Singapore, 1–4 November 2016; pp. 1969–1972. [CrossRef]
- Le Bas, C.; Hoang, T.B.; Sahuguede, S.; Julien-Vergonjanne, A. Lighting fixture communicating in infrared and visible for indoor health monitoring. In Proceedings of the 2017 IEEE 19th International Conference on e-Health Networking, Applications and Services (Healthcom), Dalian, China, 12–15 October 2017; pp. 1–6. [CrossRef]
- Hoang, T.B.; Sahuguede, S.; Julien-Vergonjanne, A. Optical wireless network design for off-body-sensor based monitoring. Wirel. Commun. Mob. Comput. 2019, 2019, 5473923. [CrossRef]
- Hasan, M.J.; Khalighi, M.A.; García-Márquez, J.; Béchadergue, B. Performance analysis of Optical-CDMA for uplink transmission in medical extra-WBANs. IEEE Access 2020, 8, 171672–171685. [CrossRef]
- Chen, S.; Qi, J.; Fan, S.; Qiao, Z.; Yeo, J.C.; Lim, C.T. Flexible wearable sensors for cardiovascular health monitoring. Adv. Healthc. Mater. 2021, 10, 2100116. [CrossRef] [PubMed]
- Aguiar-Castillo, L.; Guerra, V.; Rufo, J.; Rabadan, J.; Perez-Jimenez, R. Survey on optical wireless communications-based services applied to the tourism industry: Potentials and challenges. Sensors 2021, 21, 6282. [CrossRef]
- 19. Rabadan, J.; Guerra, V.; Rodríguez, R.; Rufo, J.; Luna-Rivera, M.; Perez-Jimenez, R. Hybrid visible light and ultrasound-based sensor for distance estimation. *Sensors* **2017**, *17*, 330. [CrossRef]
- Riurean, S.; Antipova, T.; Rocha, Á.; Leba, M.; Ionica, A. VLC, OCC, IR and LiFi reliable optical wireless technologies to be embedded in medical facilities and medical devices. J. Med. Syst. 2019, 43, 308. [CrossRef] [PubMed]
- Niarchou, E.; Matus, V.; Rabadan, J.; Guerra, V.; Perez-Jimenez, R. Experimental Evaluation of LED-Based Wearable Transmitter for Optical Camera Communications Systems. In Proceedings of the 2023 17th International Conference on Telecommunications (ConTEL), Graz, Austria, 11–13 July 2023; pp. 1–5.
- Eöllős-Jarošíková, K.; Neuman, V.; Niarchou, E.; Gomez-Cardenes, O.; Zvánovec, S.; Perez-Jimenez, R.; Komanec, M. Pilot Experiments of Side-Emitting Fiber-Based Optical Camera Communication for Wearable Applications. In Proceedings of the 2023 South American Conference On Visible Light Communications (SACVLC), Santiago, Chile, 8–10 November 2023; pp. 65–69.
- Rachim, V.P.; An, J.; Quan, P.N.; Chung, W.Y. A novel smartphone camera-LED communication for clinical signal transmission in mHealth-rehabilitation system. In Proceedings of the 2017 39th Annual International Conference of the IEEE Engineering in Medicine and Biology Society (EMBC), Jeju Island, Republic of Korea, 11–15 July 2017; pp. 3437–3440.
- 24. Teli, S.R.; Chvojka, P.; Vítek, S.; Zvanovec, S.; Perez-Jimenez, R.; Ghassemlooy, Z. A SIMO Hybrid Visible-Light Communication System for Optical IoT. *IEEE Internet Things J.* 2022, *9*, 3548–3558. [CrossRef]
- Hasan, M.K.; Shahjalal, M.; Chowdhury, M.Z.; Jang, Y.M. Real-time healthcare data transmission for remote patient monitoring in patch-based hybrid OCC/BLE networks. Sensors 2019, 19, 1208. [CrossRef] [PubMed]
- Hasan, M.K.; Shahjalal, M.; Chowdhury, M.; Jang, Y.M. Access Point Selection in Hybrid OCC/RF eHealth Architecture for Real-Time Remote Patient Monitoring. In Proceedings of the 2018 International Conference on Information and Communication Technology Convergence (ICTC), Jeju Island, Republic of Korea, 17–19 October 2018. [CrossRef]
- Mohammadi-Abdar, H.; Ridgel, A.L.; Discenzo, F.M.; Phillips, R.S.; Walter, B.L.; Loparo, K.A. Test and Validation of a Smart Exercise Bike for Motor Rehabilitation in Individuals With Parkinson's Disease. *IEEE Trans. Neural Syst. Rehabil. Eng.* 2016, 24, 1254–1264. [CrossRef]
- Tan, C.; Xiao, C.; Wang, W. Camera-based Cardiovascular Screening based on Heart Rate and Its Variability In Pre- and Post-Exercise Conditions. In Proceedings of the 2023 45th Annual International Conference of the IEEE Engineering in Medicine & Biology Society (EMBC), Sydney, Australia, 24–27 July 2023; pp. 1–5. [CrossRef]
- 29. Xie, K.; Fu, C.H.; Liang, H.; Hong, H.; Zhu, X. Non-contact Heart Rate Monitoring for Intensive Exercise Based on Singular Spectrum Analysis. In Proceedings of the 2019 IEEE Conference on Multimedia Information Processing and Retrieval (MIPR), San Jose, CA, USA, 28–30 March 2019; pp. 228–233. [CrossRef]
- Mertens, M.; Debard, G.; Davis, J.; Devriendt, E.; Milisen, K.; Tournoy, J.; Croonenborghs, T.; Vanrumste, B. Motion Sensor-Based Detection of Outlier Days Supporting Continuous Health Assessment for Single Older Adults. Sensors 2021, 21, 6080. [CrossRef] [PubMed]
- 31. Huang, L.; Liu, G. Functional motion detection based on artificial intelligence. J. Supercomput. 2022, 78, 4290–4329. [CrossRef]
- Mastoras, R.E.; Iakovakis, D.; Hadjidimitriou, S.; Charisis, V.; Kassie, S.; Alsaadi, T.; Khandoker, A.; Hadjileontiadis, L.J. Touchscreen typing pattern analysis for remote detection of the depressive tendency. Sci. Rep. 2019, 9, 13414. [CrossRef]

Sensors **2024**, 24, 2766

 Hoeijmakers, A.; Licitra, G.; Meijer, K.; Lam, K.H.; Molenaar, P.; Strijbis, E.; Killestein, J. Disease severity classification using passively collected smartphone-based keystroke dynamics within multiple sclerosis. Sci. Rep. 2023, 13, 1871. [CrossRef] [PubMed]

- Lim, S.; Kim, C.; Cho, B.H.; Choi, S.H.; Lee, H.; Jang, D.P. Investigation of daily patterns for smartphone keystroke dynamics based on loneliness and social isolation. *Biomed. Eng. Lett.* 2024, 14, 235–243. [CrossRef] [PubMed]
- 35. Mederos-Barrera, A.; Jurado-Verdu, C.; Guerra, V.; Rabadan, J.; Perez-Jimenez, R. Design and experimental characterization of a discovery and tracking system for optical camera communications. *Sensors* **2021**, 21, 2925. [CrossRef] [PubMed]
- Chowdhury, M.Z.; Hossan, M.T.; Shahjalal, M.; Hasan, M.K.; Jang, Y.M. A New 5G eHealth Architecture Based on Optical Camera Communication: An Overview, Prospects, and Applications. IEEE Consum. Electron. Mag. 2020, 9, 23–33. [CrossRef]
- 37. Stavropoulos, T.G.; Papastergiou, A.; Mpaltadoros, L.; Nikolopoulos, S.; Kompatsiaris, I. IoT wearable sensors and devices in elderly care: A literature review. *Sensors* **2020**, *20*, 2826. [CrossRef]
- 38. Atmel. XIAO SAMD21, 32 bit 48 MHz microcontroller(SAMD21G18) with 256 KB Flash, 32 KB SRAM, Datasheet; Atmel: San Jose, CA, USA, 2016.
- 39. Matus, V.; Guerra, V.; Jurado-Verdu, C.; Zvanovec, S.; Perez-Jimenez, R. Wireless sensor networks using sub-pixel optical camera communications: Advances in experimental channel evaluation. Sensors 2021, 21, 2739. [CrossRef]
- Samsung. Samsung Galaxy S23. 2023. Available online: https://www.samsung.com/us/smartphones/galaxy-s23/buy/galaxy-s23-256gb-unlocked-sm-s911uzkexaa/ (accessed on 9 February 2014).
- Le, T.; Le, N.T.; Jang, Y.M. Performance of rolling shutter and global shutter camera in optical camera communications. In Proceedings of the 2015 International Conference on Information and Communication Technology Convergence (ICTC), Jeju Island, Republic of Korea, 28–30 October 2015; IEEE: Piscataway, NJ, USA, 2015; pp. 124–128.
- 42. *ISO* 2720:1974; General Purpose Photographic Exposure Meters (Photoelectric Type)—Guide to Product Specification. International Organization for Standardization (ISO): Geneva, Switzerland, 1974. Available online: https://www.iso.org/standard/7690.html (accessed on 23 April 2024).
- 43. Chow, C.W.; Chen, C.Y.; Chen, S.H. Enhancement of Signal Performance in LED Visible Light Communications Using Mobile Phone Camera. *IEEE Photonics J.* **2015**, *7*, 7903607. [CrossRef]

**Disclaimer/Publisher's Note:** The statements, opinions and data contained in all publications are solely those of the individual author(s) and contributor(s) and not of MDPI and/or the editor(s). MDPI and/or the editor(s) disclaim responsibility for any injury to people or property resulting from any ideas, methods, instructions or products referred to in the content.

# 5.2 Publication 2 (P2)

The work in the article entitled "Experimental evaluation of wearable LED strip and side-emitting fiber for optical camera communications systems" [134], presents an experimental evaluation of two types of LED-based distributed transmitters, namely an LED strip and an LED-coupled side-emitting optical fiber, in both laboratory and wearable OCC systems. The system performance of both wearable transmitters was evaluated and compared in terms of success of reception (SoR), SNR, power consumption, and heat emission.

A key contribution is that widely accessible and commercially available components, including LEDs, side-emitting fiber, and smartphones were employed for communication purposes, showing the practical feasibility of the proposed system. In addition, two different offline image processing techniques were developed, each dedicated to the different nature of each transmitter (shape and illumination decay along the fiber length).

This study addresses O1 through the utilization of commercially available components for optical communication and through the design of different image processes. It also supports O2 through the evaluation of the effect of node positioning and channel conditions, that is, transmitter-camera placement and light conditions, on data transmission performance.

All the results are discussed in detail in the article. The best value of SoR with regard to the transmitter placement relative to the camera receiver position occurs when the camera faces directly the  $T_x$  from a close distance of 1 m. In the laboratory setup, the LED strips maintained a consistently high SoR of almost 100%, while the side-emitting fiber showed higher variation. In the wearable setup, the values of SoR were lower due to the shorter  $T_x$  length. However, with the processing method developed for fibers, fibers had improved results, in both setups, emphasizing its necessity.

In both laboratory and wearable experiments, the LED strip showed consistent SNR values around 21–22 dB under ambient light and improved performance in dark conditions (up to 27.4 dB). The side-emitting fiber exhibited a wider SNR range, from 28.6 down to 13.3 dB in the laboratory and from 42.7 to 19.3 dB in wearable setups, with higher values in dark conditions. Also, the theoretical BER versus SNR was calculated  $10^{-11}$  considering the minimum measured SNR at 16 dB and proven to be below  $3.8 \times 10^{-3}$ , the forward error correction (FEC) limit.

Power consumption was measured at 432 mW and 720 mW, for the two operating voltage stages of the LED strips, and 525 mW for the side-emitting optical fiber. Regarding the heat emission, it can be concluded that neither transmitter had significant overheating, as their temperatures remain close to room temperature (except for the LED holder).

The evaluation of two distinct wearable OCC technologies demonstrates their effectiveness in accurately detecting transmitted bits while considering transmitter placement relative to the camera receiver.

Further evaluation of side-emitting fibers as distributed wearable transmitters in OCC is presented in [135] (see Chapter B).

# Experimental evaluation of wearable LED strip and side-emitting fiber for optical camera communications systems

**Abstract:** This paper presents an experimental evaluation of two types of light-emitting diode (LED)-based distributed transmitters, namely an LED strip and an LED-coupled side-emitting optical fiber, in both laboratory and wearable optical camera communication (OCC) systems. We study the system performance in terms of success of reception (SoR) with regard to the transmission distance. The best value of SoR is achieved when the camera is facing directly to the transmitter ( $T_x$ ) from a close distance of 1 m. Additionally, we compare the power consumption, the signal-to-noise ratio performance (SNR) and all the obtained values under optimal conditions are better than the forward error correction (FEC) limit in OCC systems.

© 2024 Optica Publishing Group under the terms of the Optica Open Access Publishing Agreement

#### 1. Introduction

The widespread presence of smartphones equipped with cutting-edge cameras has prompted wider possibilities within optical wireless communications (OWC), particularly within the framework IEEE 802.15.7a [1]. This approach is known as optical camera communications (OCC) and employs a light-emitting diode (LED) as the transmitter ( $T_x$ ), an image sensor (i.e., camera) as the receiver ( $R_x$ ), and light as signal carrier.

OCC overcomes some of the limitations of Bluetooth and other existing radio frequency (RF)-based technologies [2], such as security and interference. A notable advantage lies in the fact that OCC does not incur additional hardware costs for the receiver as smartphones have been integrated with an embedded complementary metal oxide semiconductor (CMOS) camera in rolling shutter (RS) mode [3]. New generation smartphones can capture high-resolution photos and videos, with an average viewpoint resolution of 360×800 px [4], which means an actual resolution of 1080×2400 px and a recording speed of 30 frames per second (fps) or more, which is more than adequate for low-speed applications [5]. Moreover, the transmitter side can be implemented with a simple LED circuit, which has comparably lower complexity than the full Bluetooth circuitry.

Smart devices, including smartphones, smartwatches, and smart clothes, are viewed as products that integrate wearable technologies for recognizing human activities [6]. Wearable devices can be worn on the body, often designed to be lightweight and compact, offering convenience for users and seamless integration into clothing or accessories without disrupting their daily activities. These devices typically come equipped with sensors, processors, and communication capabilities, aiming to provide specific functionalities, such as tracking health and fitness metrics

#521967 https://doi.org/10.1364/OE.521967 Journal © 2024 Received 22 Feb 2024; revised 23 Apr 2024; accepted 11 May 2024; published 27 Jun 2024

<sup>&</sup>lt;sup>1</sup>Institute for Technological Development and Innovation in Communications, University of Las Palmas de Gran Canaria, Las Palmas de Gran Canaria 35001, Spain

<sup>&</sup>lt;sup>2</sup> Department of Electromagnetic Field, Faculty of Electrical Engineering, Czech Technical University in Prague, Prague 16627, Czech Republic

<sup>†</sup>These authors contributed equally to this work.

 $<sup>^</sup>st$ eleni.niarchou@ulpgc.es

Research Article

Vol. 32, No. 14/1 Jul 2024/ Optics Express 25092

Optics EXPRESS

[7]. Wearable health-monitoring sensors have become a part of our daily life [8,9] and represent a headstone for the Internet of Things (IoT) [10]. Sensors can measure parameters before the OCC system collects those data and forwards them to the camera from integrated light-emitting diodes. With the advent of 6G, the integration of wearables in healthcare is set to expand, paving the way for smart healthcare [11] in terms of sensing, processing, and communication.

To date, only a limited number of studies have explored the integration of wearable sensors in conjunction with LEDs as transmitters. For instance, in [12], medical sensors and infrared LEDs transmit medical data for patient monitoring. Similarly, in [13], this combination is used for indoor health monitoring, accounting for patient mobility. Additionally, in [14], an all-optical bidirectional wireless communication system assesses sensor mobility, variations in orientation, and placement on the body. Furthermore, in [15], the authors delve into the performance of optical code-division multiple access in asynchronous mode, considering the impact of mobility and random transmitter orientations. Moreover, in [16], optoelectric sensors monitor cardiovascular vital signs.

Recently, side-emitting optical fibers have been introduced as distributed transmitters for OCC [17,18]. Side-emitting fibers differ from conventional optical fibers by gradually emitting light along the side-emitting fiber length [19]. To achieve this glow-stick-like effect, the side-emitting fibers are modified by implementing scattering particles or voids into the side-emitting fiber core or cladding [20,21]. Side-emitting fibers are characterized by the so-called diffusion length, which is a side-emitting fiber length over which 90 % of the coupled power is emitted [22]. When using side-emitting fibers in OCC, a single LED is used to couple data into one end of the side-emitting fiber. The side-emitting fiber then acts as a distributed transmitter. Data is then captured by the RS camera, as in conventional OCC.

In the field of wearables, LED strips and LED-coupled side-emitting fibers represent two approaches to distributed transmitters. Both approaches have their advantages and drawbacks. Side-emitting optical fibers offer advantages such as 360° radiation pattern in contrast to 120° of LED strips. On the other hand, LED strips provide constant brightness in contrast to side-emitting fibers. LED strips are composed of multiple LEDs, offering flexibility in LED control, i.e., different spatial transmitting properties. Conversely, LED-coupled side-emitting fibers require only a single LED for their operation, allowing small and compact wearable solutions. Both types of distributed transmitters allow mechanical flexibility, while fiber-based transmitters in the future can be involved within textiles, multiple LEDs then could allow different shapes, etc. Apart from wearables, LED strips, and side-emitting fibers find applications in IoT, interior design [23], shopping centers, aircraft, fashion, health, safety, geolocation [24], promoting active lifestyles [25], and playing a role in industrial robotics [26]. In [27], the authors show the impact of a user moving with a camera receiver within cells at 20 cm/s speed.

In this work, we experimentally evaluate the above-mentioned types of LED-based distributed transmitters in laboratory and wearable OCC systems. We employ both solutions based on widely accessible and commercially available components, including LEDs, side-emitting fibers, and smartphones. The system performance of both wearable transmitters is evaluated and compared in terms of the success of reception, signal-to-noise ratio, and power consumption.

The structure of the paper is organized as follows. Section 2 provides details of the OCC system design and the experimental setup. Section 3 specifically focuses on the image processing techniques applied in the study. Section 4 is then dedicated to the discussion of the results obtained from the experiments with both transmitters. Lastly, Section 5 presents the main conclusions.

#### 2. OCC system design and experimental setup

We consider two types of transmitters. The first transmitter is a 10 mm wide LED strip with a diffuser, consisting of an array of surface-mounted device white LEDs, 5.0 mm by 5.0 mm

Research Article

Vol. 32, No. 14/1 Jul 2024/ Optics Express 25093

Optics EXPRESS

size (commercially known as SMD 5050), operating at two different voltage states, 9 and 12 V (i.e.,  $432 \,\mathrm{mW}$  and  $720 \,\mathrm{mW}$  electrical power,  $50 \,\mathrm{mA}$  and  $60 \,\mathrm{mA}$  current, respectively). This power supplies both the LED strip and the control circuit. The second transmitter is a side-emitting optical fiber. The side-emitting fiber ("Super Bright" by ZDEA) is made of polymethyl-methacrylate (PMMA) with a 3 mm outer diameter and with 1 m diffusion length, meaning that  $90 \,\%$  of the coupled power will be emitted from the fiber over the first 1 m side-emitting fiber length. An LED couples light to one end of the side-emitting fiber, and once the light is coupled, the side-emitting fiber becomes the data transmitter. The coupling LED operates at  $3 \,\mathrm{V}$  (i.e.,  $525 \,\mathrm{mW}$ ,  $175 \,\mathrm{mA}$ ). Both  $T_x$ s are connected to the digital output of a micro-controller unit (MCU).

The proposed OCC system uses the non-return-to-zero on-off keying (NRZ-OOK) modulation technique [28] for data transmission over a free-space wireless channel of up to 2.5 m distance, which resembles a typical indoor scenario. However, the system can be extended even for longer distances (tens or hundreds of meters) [29]. We carry out experimental analysis both in ambient light and dark conditions. The system uses the digital switching outputs of the MCU to facilitate the NRZ-OOK modulation. The micro-controller generates a 6-bit data packet [001011] at 0.4 ms per bit, which corresponds to a modulation frequency of 2.5 kHz per bit. The data packet is converted into a voltage signal that directly drives the LED. Since the current of the LEDs in the LED strip, exceeds the maximum limit of the MCU, a transistor is connected to the power source to drive the LEDs. To enhance the link performance, a repeat-packet strategy is employed. For the LED strip experiments, the MCU is a Seeeduino Xiao [30], powered by the power supply unit, and for the LED-coupled side-emitting fiber experiments, the MCU is an Arduino Nano [31], powered by a laptop.

The receiver is a smartphone camera of Samsung A51 [32], which offers frame capture in pro mode, using  $4000 \times 1800$  px resolution in rolling shutter mode. The OCC link scenario is depicted in Fig. 1. In OCC, the image is captured row-by-row using an RS camera. The RS camera exposes different lines of the image array at various times to read the light intensity through the sensor, enabling capturing multiple states of LEDs (ON and OFF) within a single frame [33]. The exposure time values of the camera (i.e., the duration of time over which a camera sensor line is exposed to light) are summarized in Table 1.

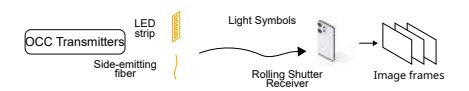


Fig. 1. Optical camera communications link scenario.

	•		
Experiment	Transmitter	Environment	$t_{\rm exp}  (\mu {\rm s})$
	Strip (9 V)	ambient light	250
Laboratory	Strip (12 V)	ambient light	250
	Side-emitting fiber	dark room	500
	Strip (9 V)	ambient light	170
	Strip (9 V)	dark room	170
Wearable	Strip (12 V)	ambient light	170
wearable	Strip (12 V)	dark room	170
	Side-emitting fiber	ambient light	500
	Side-emitting fiber	dark room	500

Table 1. Exposure times of the camera.

The systems implemented for the proposed laboratory experiments are shown in Fig. 2, where both transmitters (1 m length) are placed horizontally. In the wearable experiments, a  $50\,\mathrm{cm}$  length transmitter is vertically attached to the front side of a T-shirt, with direction from waist to shoulder, as shown in Fig. 3.

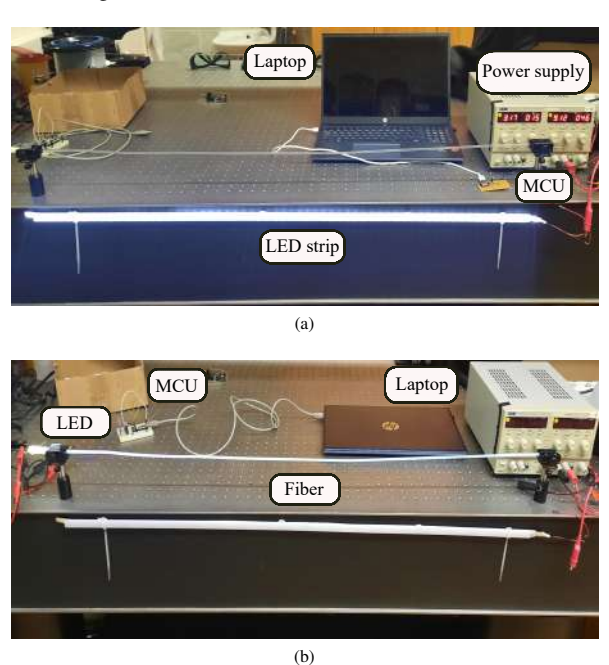


Fig. 2. Laboratory experimental setup. (a) LED strip. (b) LED-coupled side-emitting fiber.



 $\textbf{Fig. 3.} \ \ We arable \ experimental \ setup. \ (a) \ LED \ strip. \ (b) \ LED - coupled \ side-emitting \ fiber.$ 

Research Article

Vol. 32, No. 14/1 Jul 2024/ Optics Express 25095

#### Optics EXPRESS

The measurements are illustrated in Fig. 4, with x and y representing the 2D coordinates of the room (in meters). The smartphone camera captures multiple frames of  $T_x$  from various distances, always focusing on the center of  $T_x$  at  $(0.0,\,0.0)$ . As the orientation of the  $T_x$ s is different in laboratory and wearable setups, each measurement tests different constraints by placing the camera accordingly. In the laboratory setup, we move the camera in the same plane where the  $T_x$  is placed, meaning we capture alongside the  $T_x$ . In wearable setup we move the camera in the plane that is perpendicular to the person wearing the  $T_x$ , meaning we capture images around the person. The most relevant parameters of the system are summarized in Table 2.

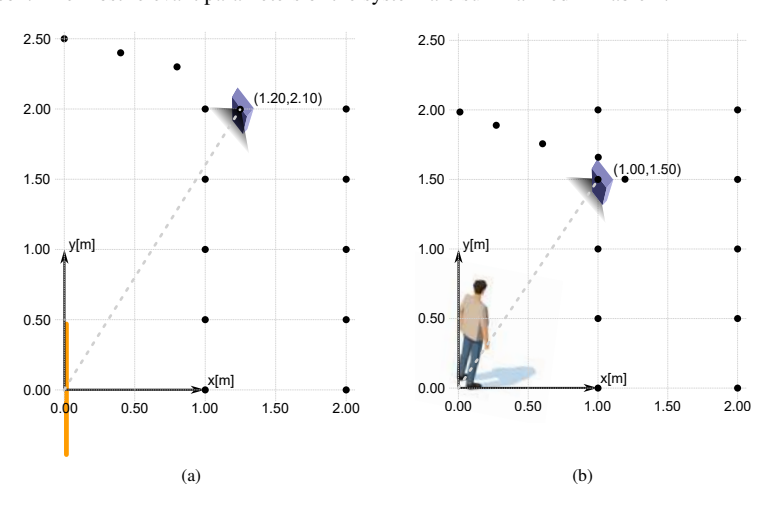


**Fig. 4.** The 2D coordinates of the room (in meters) represent the camera's capturing positions, always facing the center of the transmitter at (0.0, 0.0). (a) Laboratory experimental setup with a yellow line representing the  $T_x$ . (b) Wearable experimental setup with a person wearing the  $T_x$  on their T-shirt.

Table 2. Parameters of the system and their values.

Module	Sub-module	Parameter	Value
		LED	SMD 5050, white
	LED strip	Width	10 mm
		Microcontroller	Seeeduino XIAO
		Diameter	4 mm
$T_X$	Side-emitting fiber	LED	LA CW20WP6, white
	Side-clifting fiber	Material	PMMA
		Microcontroller	Arduino Nano
	Modulation	Modulation frequency	2.5 kHz
	Wodulation	Data packet size	6b/packet [001011]
		Smartphone model	Samsung Galaxy A51
$R_x$	Camera	Image sensor	Sony IMX582
		Resolution	4000×1800 px



#### 3. Image processing

We used two different offline image processing techniques (see Fig. 5). Method 1 was developed especially for strip LED arrays. It uses for data recovery a template signal transmitted by the LED transmitter and detected within the image through a correlation process to find region of interest

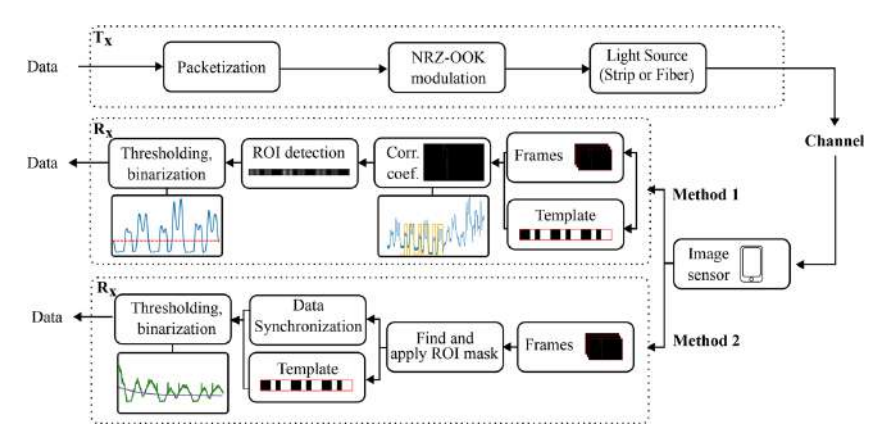
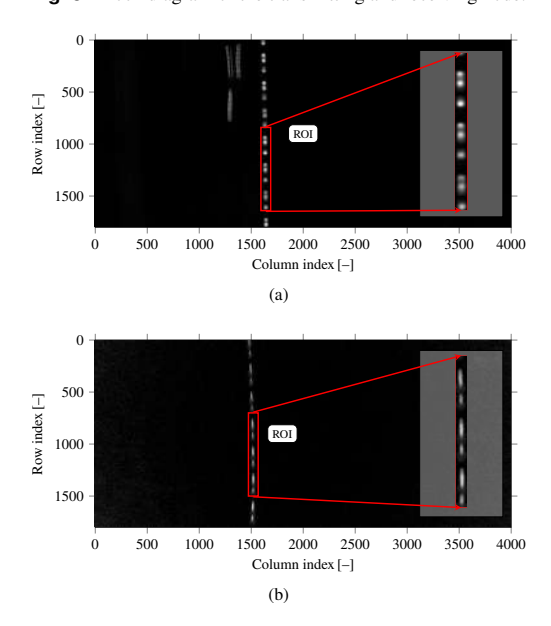


Fig. 5. Block diagram of the transmitting and receiving node.



**Fig. 6.** Frame showing values obtained from the correlation coefficient between a random frame and the template. The region of interest (ROI) is highlighted. (a) LED strip. (b) LED-coupled side-emitting fiber. In both of the displayed images in this figure the contrast was increased to better show the transmitting data to the reader.

Research Article

Vol. 32, No. 14/1 Jul 2024/ Optics Express 25097

Optics EXPRESS

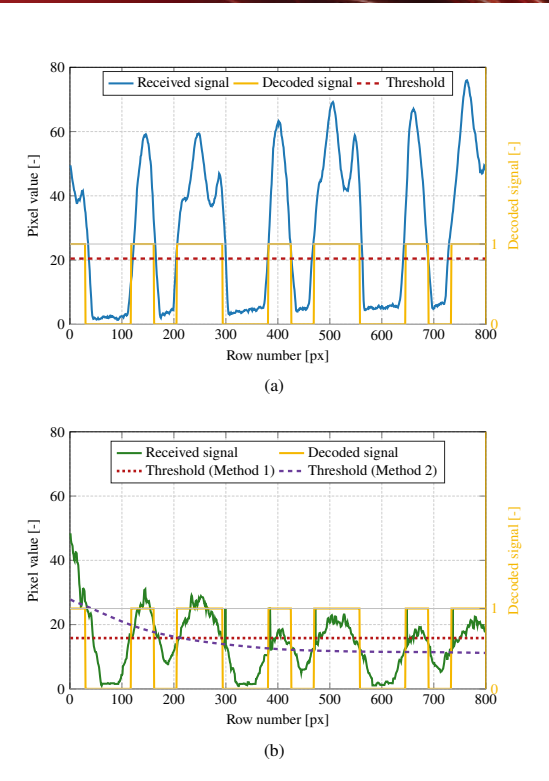


**Fig. 7.** Received grayscale signal, Decoded signal, and Thresholds for (a) LED strip and (b) side-emitting fiber (Method 1 and Method 2).

(ROI), while within Method 2, the ROI mask is determined by using the intensity information of the image.

In Method 1, one frame is selected while a template is generated, consisting of three consecutive packets, each with a sequence of [001011] bits. Image frames are then converted to grayscale, enabling retrieval of the pixels' intensity profile. The correlation process involves sliding the template image over the frame (similar to 2D convolution) to identify the 2D position of the signal captured from the transmitting source [34]. Figure 5 depicts a block diagram with  $T_x$  and  $R_x$  parts. The blue lines in inset within the  $R_x$  part of Fig. 5 represent the average row value, while the yellow line depicts the template signal, and the red line show binarization threshold. The ROI in the frame, where the correlation has the maximum value, is highlighted in Fig. 6. This process is repeated for all frames. The identified ROI is then utilized for data decoding. By applying thresholding and binarization to the acquired data, the received signal is efficiently decoded, as depicted in Fig. 7(a).

In Method 2, the mask is thereofore applied to the captured image using multiplication. From this image, a 1D data array with an intensity profile is generated. In this intensity profile, data synchronization is performed using the generated template. The synchronized data is binarized after thresholding. In Fig. 7(b), the binarization threshold is marked. Since the amount of light emitted from a side-emitting fiber decreases with increasing distance from the coupled light source (i.e., the LED) along the fiber, it is more suitable to use a moving average of intensity profile as the threshold instead of a constant threshold, which was used in Method 1. The

method for adapting the threshold value employed moving average based on the illumination level alongside the captured fiber. The same process is replicated for every frame. Efficient decoding of the received signal is achieved by employing the adaptive thresholding and binarization on the acquired data.

#### 4. Results

In this section, we show the performance of both transmitters in terms of signal-to-noise ratio (SNR) and success of reception (SoR). Additionally, we measured the thermal radiation emanating from the transmitters using an infrared camera (by Teledyne FLIR).

The captured thermal images are depicted in Fig. 8 for the LED strip and in Fig. 9 for the side-emitting fiber. On both transmitters, the maximum thermal radiation is emitted at the starting point of the LED strip and at the LED holder for the side-emitting fiber, measuring  $25.7^{\circ}$  C and  $31.3^{\circ}$  C, respectively.

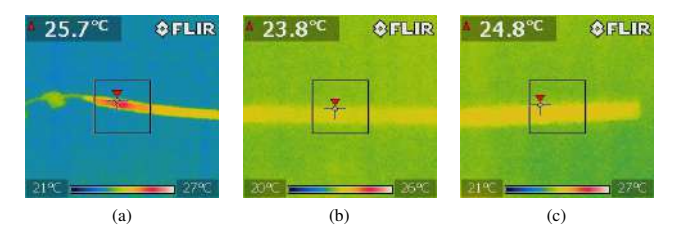


**Fig. 8.** Heat emanating from the entire length of the LED strip. (a) At the starting point. (b) In the middle section. (c) At the end.

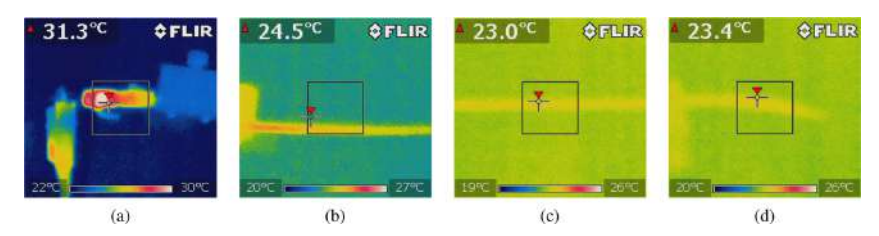


**Fig. 9.** Heat emanating from the entire length of the side-emitting fiber. (a) At the LED holder. (b) At the starting point. (c) In the middle section. (d) At the end.

Based on measurements from the infrared camera, it can be inferred that there is no excessive overheating in any parts of both transmitters. The temperature of the transmitters was approximately at room temperature. However, the LED holder for side-emitting fiber could benefit from better heat-dissipation material.

To estimate the SNR, we captured frames using a direct connection of  $T_x$  to the power supply (i.e., the LEDs are driven only by a DC signal) at 2 m distance. Afterward, the frames were processed to align the  $T_x$  among the frames. Then, the image processing code calculated the average intensity of pixels for each row, representing the signal's mean value. The SNR was calculated as

 $SNR_{dB} = 10 \log_{10} \left( \frac{\mu^2}{\sigma^2} \right), \tag{1}$ 



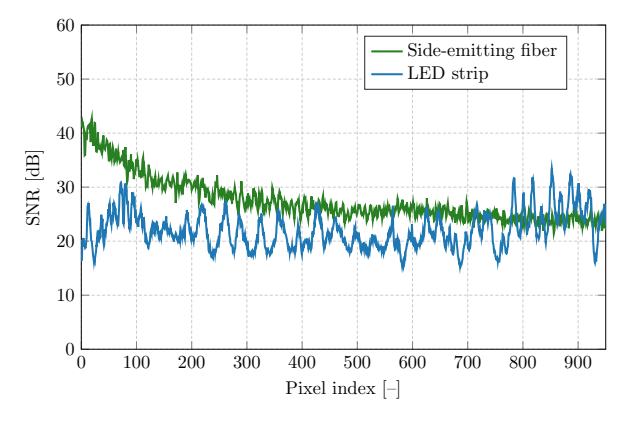
the ratio of the mean value of the signal  $\mu$ , to the standard deviation  $\sigma$ , assuming that the aggregated noise distribution can be modeled as additive white Gaussian noise (AWGN). The SNR values for each experimental setup are summarized in Table 3.

	Table 6. Olgital to	noise ratio (Sitil) vi	aides.
Experiment	Transmitter	Environment	SNR [dB]
	Strip (9 V)	ambient light	21.1
Laboratory	Strip (12 V)	ambient light	22.0
	Fiber	ambient light	28.6 down to 13.3
Wearable	Strip (9 V)	ambient light	21.9
	Strip (9 V)	dark room	23.8
	Strip (12 V)	ambient light	21.9
	Strip (12 V)	dark room	27.4
	Fiber	ambient light	42.7 down to 19.3
	Fiber	dark room	42.9 down to 20.2

Table 3. Signal to noise ratio (SNR) values

In the laboratory experiment, the SNR is almost the same for the LED strip at 9 and  $12\,V$  (21.1 and  $22.0\,dB$ , respectively), while the side-emitting fiber exhibited a range from  $28.6\,down$  to  $13.3\,dB$  under ambient light conditions. Similarly, in the wearable experiment, the SNR is equally good for the LED strip at 9 and  $12\,V$  under ambient light conditions (21.9 dB) and higher in dark conditions (23.8 and 27.4 dB, respectively). The side-emitting fiber exhibited a broader range from  $42.7\,down$  to  $19.3\,dB$  under ambient light and  $42.9\,down$  to  $20.2\,dB$  in dark conditions.

Figure 10 illustrates the SNR plots for the LED strip  $(12\,V)$  and the LED-coupled side-emitting fiber in ambient light conditions for the wearable experiment. The peaks in the plot of the LED strip correlate with the positions of the individual LEDs on the strip, whereas the gradual decrease in the LED-coupled side-emitting fiber plot of the same figure occurs mainly due to a fundamental property of side-emitting fiber: the power decrease along its length as a proportional amount of power has already been emitted from the fiber.



**Fig. 10.** Average signal-to-noise ratio (SNR) of the LED strip  $(12\,V)$  and side-emitting fiber in ambient light conditions for the wearable experiment.

A general assumption about the communication link performance in OCC systems is that the bit error rate (BER) should be below  $3.8 \times 10^{-3}$ , the forward error correction (FEC) limit [35].

Research Article

Vol. 32, No. 14/1 Jul 2024/ Optics Express 25100

Optics EXPRESS

In the case of an OOK codification, assuming a Gaussian noise distribution environment, the relation of the BER and the SNR is expressed as BER =  $Q(\sqrt{\text{SNR}})$  [36]. From this equation, the minimum SNR needed to ensure the required BER can be calculated; in this case, the SNR value is 12.2 dB. As can be seen from the experimental SNR results for all the measurement cases, the predicted system performance under optimal conditions is better than the FEC limit. Figure 11 shows the theoretical BER plot versus SNR, calculated from BER =  $Q(\sqrt{\text{SNR}})$ , considering the minimum measured SNR at 16 dB (from Fig. 10). The resulting BER for all cases is below  $10^{-11}$ , which ensures high system performance in both LED strip and side-emitting fiber schemes.

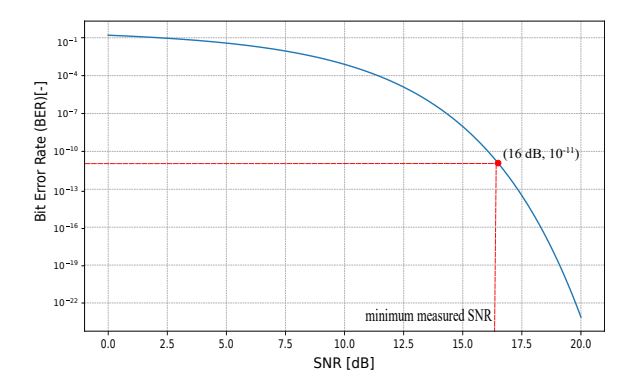


Fig. 11. Theoretical BER =  $Q(\sqrt{\text{SNR}})$  with highlighted the minimum measured SNR 16dB.

Next, we analyzed the quality of the captured data in terms of the SoR, which is defined as the ratio of correctly decoded bits to the total number of transmitted bits [17]. Note, that the SoR is calculated from the correlation results in a dataset of 10 frames, equating to a total of 180 bits that we compare to the transmitted template. It is worth noting that the number of frames, in this case, was taken according to the experimental procedure, while in a real system, it would be a video recording of 30 frames per second, giving approximately 0.5 kbps. We considered that the detection of the template failed when we received less than 2 complete packets per frame. Consequently, the value of any dataset below 66.6% is considered as 'no detection'.

The calculated SoR is depicted in Table 4 and Table 5 for the laboratory and wearable experimental setup, respectively. Note that the LED strip was measured under ambient light conditions in both experimental setups, while the LED-coupled side-emitting fiber measurements were conducted in darkness.

From the obtained values, we can conclude that the LED strip  $(12\,V)$  generally results in higher SoR than the LED strip  $(9\,V)$  and comparable SoR with the LED-coupled side-emitting fiber considering Method 2.

Regarding the laboratory experimental setup, the SoR of the LED strips is consistently high, close to  $100\,\%$ . The LED-coupled side-emitting fiber using Method 1 exhibits variable and relatively lower SoR, spanning from approximately  $72.2\,\%$  to  $98.8\,\%$ . Once using the alternative image processing method (Method 2) produces improved results for the LED-coupled side-emitting fiber, rendering it comparable to the LED strip ( $12\,V$ ) outcomes.

Regarding the SoR values of the wearable experimental setup, we observe a decrease compared to the laboratory setup due to the reduced  $T_x$  length, which is caused by the limited amount of space on a T-shirt (100 cm transmitter length in laboratory setup vs. 50 cm in wearable setup). The LED strip (12 V) achieves SoR exceeding 88.8 %, while the LED strip (9 V) SoR exceeding 81.1 %. Based on Method 1, the LED-coupled side-emitting fiber demonstrates more SoR

Research Article

Vol. 32, No. 14/1 Jul 2024 / Optics Express 25101

Optics EXPRESS

Table 4. Success of reception (SoR) in the laboratory experimental setup.

x [m]	y [m]	Strip (9 V)	Strip (12 V)	Fiber (Method 1)	Fiber (Method 2)
0.0	2.5	<66.6 %	-	<66.6 %	78.3 %
0.4	2.4	89.8 %	-	86.6 %	96.7 %
0.8	2.3	96.2 %	-	75.8 %	97.5 %
1.2	2.1	98.3 %	-	90.0 %	99.1 %
	0.0	100 %	100 %	98.8 %	100 %
	0.5	100 %	100 %	72.7 %	100 %
1.0	1.0	100 %	100 %	79.4 %	100 %
	1.5	99.4 %	99.4 %	72.2 %	100 %
	2.0	93.8 %	93.3 %	72.8 %	96.9 %
	0.0	100 %	100 %	95.5 %	100 %
	0.5	100 %	100 %	87.5 %	99.3 %
2.0	1.0	100 %	100 %	80.5 %	99.4 %
	1.5	100 %	100 %	86.6 %	98.8 %
	2.0	90.5 %	94.4 %	90.0 %	97.7 %

Table 5. Success of reception (SoR) in the wearable experimental setup.

x [m]	y [m]	Strip (9 V)	Strip (12 V)	Fiber (Method 1)	Fiber (Method 2)
0.0	2.0	86.1 %	91.6 %	82.2 %	<66.6 %
0.3	1.9	90.0 %	97.7 %	90.0 %	90.0 %
0.6	1.8	81.6 %	96.6 %	92.2 %	98.3 %
1.2	1.5	91.6%	98.8 %	88.2 %	87.7 %
	0.0	100 %	100 %	85.0 %	100 %
	0.5	99.4 %	100 %	91.1 %	100 %
1.0	1.0	100 %	100 %	80.5 %	100 %
	1.5	99.4 %	100 %	93.3 %	98.3 %
	1.7	99.0%	98.3 %	92.2 %	98.8 %
	2.0	89.4 %	92.7 %	94.1 %	98.3 %
	0.0	95.5 %	95.0 %	78.8 %	100 %
	0.5	87.7 %	91.6 %	91.6 %	100 %
2.0	1.0	81.1 %	88.8 %	90.0 %	100 %
	1.5	99.1 %	99.1 %	87.5 %	100 %
	2.0	94.1 %	93.3 %	89.8 %	93.5 %

fluctuations than the LED strip (12 V), ranging from approximately 78.8 % to 94.1 %. Conversely, with Method 2, the side-emitting fiber exhibits even superior performance compared to the LED strips. This result underscores the requirement of using Method 2 for side-emitting fibers in wearable OCC scenarios as they fundamentally differ in transmitter shape (not being a perfect line source and having illumination decay along the fiber length).

We noticed that the detection of the template failed at (0.0, 2.5) capturing position in the laboratory experimental setup (with Method 1), but not in the wearable, and this can be attributed to the visibility of the  $T_x$ 's side. As mentioned earlier, in each setup (laboratory vs. wearable) a different position between the  $T_x$  and camera was tested. In general, in both experimental setups,

Research Article

Vol. 32, No. 14/1 Jul 2024/ Optics Express 25102

Optics EXPRESS

the best SoR is achieved at (1.0, 0.0) capturing position, when the camera and the  $T_x$  are aligned and in close distance.

#### 5. Conclusion

In this paper, we experimentally evaluate two types of LED-based distributed transmitters, the LED strip and the LED-coupled side-emitting optical fiber, in both laboratory and wearable OCC systems. Evaluation encompasses power consumption (432 mW and 720 mW for the LED strip, and 525 mW for the side-emitting optical fiber), the success of reception, and the signal-to-noise ratio. The primary contribution of this research lies in the demonstration of two different technologies for wearable OCC both allowing for accurately detecting transmitted bits and showing critical aspects for the LED strip and side-emitting fiber placement and camera receiver position.

In conclusion, we identify some practical considerations that impact the performance of our system. Initially, the reduced power of illumination stems from the side-emitting fiber operating at a lower voltage. Furthermore, the side-emitting fiber's diameter of 4 mm is significantly smaller than the 1 cm diameter of the LED strip, resulting in a reduced illuminating area. On the other hand, the smaller diameter of the side-emitting fiber is more flexible, tolerating more movement in wearable applications. An additional aspect impacting practicality is the fact that the LED strip is more distributed electrically, whereas the side-emitting fiber only requires circuitry at one end, allowing for a more compact design.

The proposed setup was tested using standard devices, which makes it applicable for widespread use. Our future research will encompass the implementation of a wearable device seamlessly integrated into clothing and combined with sensors to transmit real health data. Additionally, we plan to integrate wavelength division multiplexing techniques, where the template can act as a beacon for transmitting data across multiple light wavelengths. Furthermore, we will experiment a wearable setting with user in motion. Lastly, employing the latest smartphone versions capable of capturing video with reduced exposure time and higher frame rates. The global shutter capturing mechanism of smartphones enables simultaneous video streaming and data acquisition, which could enable lower power consumption transmitters to operate over longer distances.

Funding. Agencia Canaria de Investigación, Innovación y Sociedad de la Información (APCR2022010014); NEWFO-CUS COST action (CA19111); České Vysoké Učení Technické v Praze (SGS23/168/OHK3/3T/13); Agencia Estatal de Investigación (TED2021-130049B-C21, PID2020-114561RB-100).

**Acknowledgment.** The authors also thank for his technical support, Mr. Daniel Dousek from Czech Technical University.

**Disclosures.** The authors declare no conflicts of interest.

**Data availability.** Data underlying the results presented in this paper are not publicly available at this time but may be obtained from the authors upon reasonable request.

#### References

- 1. "IEEE standards association," https://standards.ieee.org/ieee/802.15.7a/10367/. Accessed: 2023-09-15.
- M. Z. Chowdhury, M. T. Hossan, M. Shahjalal, et al., "A new 5G ehealth architecture based on optical camera communication: An overview, prospects, and applications," IEEE Consumer Electron. Mag. 9(6), 23–33 (2020).
- N.-T. Le and Y. M. Jang, "Performance evaluation of MIMO optical camera communications based rolling shutter image sensor," in 2016 Eighth International Conference on Ubiquitous and Future Networks (ICUFN), (2016), pp. 140–144.
- 4. "Statcounter," https://gs.statcounter.com/screen-resolution-stats/mobile/worldwide. Accessed: 2023-09-15.
- R.-A. Dobre, R.-O. Preda, and R.-A. Badea, "Robust occ system optimized for low-frame-rate receivers," Sensors 22(16), 5938 (2022).
- Y. Wang, S. Cang, and H. Yu, "A survey on wearable sensor modality centred human activity recognition in health care," Expert Syst. with Appl. 137, 167–190 (2019).
- S. Majumder, T. Mondal, and M. J. Deen, "Wearable sensors for remote health monitoring," Sensors 17(12), 130 (2017).

Research Article

Vol. 32, No. 14/1 Jul 2024 / Optics Express 25103

#### Optics EXPRESS

- J. S. Heo, M. F. Hossain, and I. Kim, "Challenges in design and fabrication of flexible/stretchable carbon-and textile-based wearable sensors for health monitoring: A critical review," Sensors 20(14), 3927 (2020).
- S. Nasiri and M. R. Khosravani, "Progress and challenges in fabrication of wearable sensors for health monitoring," Sensors Actuators A: Phys. 312, 112105 (2020).
- R. De Fazio, M. De Vittorio, and P. Visconti, "Innovative IoT solutions and wearable sensing systems for monitoring human biophysical parameters: a review," Electronics 10(14), 1660 (2021).
- S. Kharche and J. Kharche, "6G intelligent healthcare framework: A review on role of technologies, challenges and future directions." Journal of Mobile Multimedia 19, 603–644 (2023).
- T. Adiono, R. F. Armansyah, S. S. Nolika, et al., "Visible light communication system for wearable patient monitoring device," in 2016 IEEE Region 10 Conference (TENCON), (2016), pp. 1969–1972.
- C. Le Bas, T. B. Hoang, S. Sahuguede, et al., "Lighting fixture communicating in infrared and visible for indoor health monitoring," in 2017 IEEE 19th International Conference on e-Health Networking, Applications and Services (Healthcom), (2017), pp. 1–6.
- T. B. Hoang, S. Sahuguede, and A. Julien-Vergonjanne, "Optical wireless network design for off-body-sensor based monitoring," Wirel. Commun. Mob. Comput. 2019, 1–13 (2019).
- M. J. Hasan, M. A. Khalighi, J. García-Márquez, et al., "Performance analysis of Optical-CDMA for uplink transmission in medical extra-WBANs," IEEE Access 8, 171672–171685 (2020).
- S. Chen, J. Qi, S. Fan, et al., "Flexible wearable sensors for cardiovascular health monitoring," Adv. Healthcare Mater. 10(17), 2100116 (2021).
- S. R. Teli, K. Eollosova, S. Zvanovec, et al., "Optical camera communications link using an LED-coupled illuminating optical fiber," Opt. Lett. 46(11), 2622–2625 (2021).
- K. Eöllos-Jarošíková, V. Neuman, C. M. Jurado-Verdú, et al., "Long-distance indoor optical camera communication using side-emitting fibers as distributed transmitters," Opt. Express 31(16), 26980 (2023).
- A. Reupert, J. Schröder, and L. Wondraczek, "Radiation from side-emitting optical fibers and fiber fabrics: Radiometric model and experimental validation," Adv. Photonics Res. 3(4), 2100104 (2022).
- S. L. Logunov, K. W. Bennett, E. J. Fewkes, et al., "Silica nano-structured fiber for illumination," J. Lightwave Technol. 37(22), 5667–5673 (2019).
- M. Lanzarini-Lopes, S. Garcia-Segura, K. Hristovski, et al., "Particle-modified polymeric cladding on glass optical fibers enhances radial light scattering," J. Opt. Soc. Am. B 36(6), 1623 (2019).
- W. S. Klubben, S. L. Logunov, E. J. Fewkes, et al., "Novel light diffusing fiber for use in medical applications," in SPIE Proceedings, I. Gannot, ed. (SPIE, 2016).
- B. Selm, E. A. Gürel, M. Rothmaier, et al., "Polymeric optical fiber fabrics for illumination and sensorial applications in textiles," J. Intell. Mater. Syst. Struct. 21(11), 1061–1071 (2010).
- V. Georlette, F. Piras, C. Jurado-Verdu, et al., "Content triggering system using tricolor led strips and optical camera communication in rolling shutter mode," in 2021 Third South American Colloquium on Visible Light Communications (SACVLC), (2021), pp. 01–06.
- F. Cocconcelli, G. Matrella, N. Mora, et al., "IoT smart flooring supporting active and healthy lifestyles," Sensors 23(6), 3162 (2023).
- M. Domonkos, Z. Dombi, and J. Botzheim, "Led strip based robot movement intention signs for human-robot interactions," in 2020 IEEE 20th International Symposium on Computational Intelligence and Informatics (CINTI), (IEEE, 2020), pp. 121–126.
- J. He, K. Yu, Z. Huang, et al., "Multi-column matrices selection combined with k-means scheme for mobile occ system with multi-leds," IEEE Photonics Technol. Lett. 33(12), 623–626 (2021).
- V. Matus, V. Guerra, C. Jurado-Verdu, et al., "Wireless sensor networks using sub-pixel optical camera communications: Advances in experimental channel evaluation," Sensors 21(8), 2739 (2021).
- V. Matus, V. Guerra, C. Jurado-Verdu, et al., "Demonstration of a sub-pixel outdoor optical camera communication link," IEEE Latin Am. Trans. 19(10), 1798–1805 (2021).
- 30. Atmel, "XIAO SAMD21, 32-bit 48MHz microcontroller (SAMD21G18) with 256KB flash, 32KB SRAM," Datasheet (2016).
- 31. A. Nano, "ATmega328 16 MHz, 2KB SRAM, 32KB flash, 1KB EEPROM," Datasheet (2023).
- Samsung, "Samsung galaxy A51 Dual SIM (4GB/128GB)," https://www.samsung.com/gr/smartphones/galaxy-a/galaxy-a51-blue-128gb-sm-a515fzbveue/ (2021). Accessed: [2023-10-02].
- T. Le, N.-T. Le, and Y. M. Jang, "Performance of rolling shutter and global shutter camera in optical camera communications," in 2015 International Conference on Information and Communication Technology Convergence (ICTC), (IEEE, 2015), pp. 124–128.
- C. Jurado-Verdu, V. Matus, J. Rabadan, et al., "Correlation-based receiver for optical camera communications," Opt. Express 27(14), 19150–19155 (2019).
- P. Luo, M. Zhang, Z. Ghassemlooy, et al., "Undersampled-based modulation schemes for optical camera communications," IEEE Commun. Mag. 56(2), 204–212 (2018).
- M. Gismalla, M. Abdullah, W. A. Mabrouk, et al., "Data rate and ber analysis for optical attocells configuration model in visible light communication," in 2019 International Conference on Information Science and Communication Technology (ICISCT), (2019), pp. 1–6.

## 5.3 Publication 3 (P3)

The last publication entitled "CNN-Based Human Detection and Identification in Indoor Optical Camera Communication Systems Using a Wearable LED Strip" [136] is a proof of concept for an indoor OCC system that utilizes a deep learning network to detect, track, and identify humans wearing a yellow safety jacket with RGB LED strips. The RGB LED strips utilize various colors (red, green, blue), each color serves as an indicator of the user's status. The same wearable transmitter has also been evaluated in an outdoor setting with a link distance of 90 to 120 m, in the conference version of this publication [26] (see Chapter A).

Apart from repurposing commercial devices such as RGB LED strips and cameras, commonly installed in many buildings, for communication and monitoring functionalities, which address O1, this work makes several key contributions to the field of OCC. The most important contribution is that it introduces a deep learning-based detection and identification system using the YOLO version 8 object detection algorithm, which is a CNN-based model, to track wearable LED transmitters in challenging scenarios, including low visibility, user mobility, and multiple users, addressing O3 by enabling Al-based tracking and identification of multiple users. Finally, it evaluates the system in an indoor room, testing both static and dynamic conditions to evaluate the efficiency of the system in detecting, tracking, and identifying users. This addresses O2 by assessing the impact of sensor positioning and movement dynamics on communication performance.

In this context, mobility refers to the two experimental setups: static and walking. In the static setup, the yellow safety jacket with the LED strip was placed on a chair in the center of the room. For the walking setup, one person walked in a lemniscate pattern, whereas two users followed parallel, lemniscate, or random patterns to evaluate detection accuracy during movement. Environmental conditions included ambient light and dark room scenarios to evaluate the system's performance under different lighting conditions. A fully empirical approach was used, and no probabilistic models were employed in this study.

The experimental evaluation demonstrates the system's potential for practical implementation in high-risk environments, such as mining, factories, construction, and healthcare facilities. The results indicate that the system achieved up to 100% SoR for static experimental setups, whereas for a walking experimental setup with a single user, the system maintained a high SoR of 96.2%. On the contrary, when tested with two users, the system failed to effectively detect and track them, revealing the limitations that must be improved to support multiple users.

In conclusion, the results demonstrate the feasibility of using OCC with deep learning in human detection and identification, particularly in hazardous environments where real-time monitoring is essential.



IET Optoelectronics





ORIGINAL RESEARCH OPEN ACCESS

## CNN-Based Human Detection and Identification in Indoor Optical Camera Communication Systems Using a Wearable LED Strip

<sup>1</sup>IDETIC, Universidad de Las Palmas de Gran Canaria, Las Palmas de Gran Canaria, Spain | <sup>2</sup>Instituto de Telecomunicações, Universidade de Aveiro, Aveiro, Portugal | <sup>3</sup>Pi-Lighting, Valais, Switzerland

Correspondence: Eleni Niarchou (eleni.niarchou@ulpgc.es)

Received: 7 November 2024 | Revised: 10 March 2025 | Accepted: 30 April 2025

Handling Editor: Wasiu O. Popoola

Funding: This work has received support from the OCCAM project (PID2020-114561RB-100) and SUCCESS (TED2021-130049B-C21) funded by the Agencia Estatal de Investigación (AEI, Spanish Research Government) and from the European Union COST Action NEWFOCUS (CA19111). This work was supported by the European Union's Horizon Europe Programme in the frame of Marie Sklodowska-Curie Actions Doctoral Networks (MSCA-DN) project OWINGG (Optical and wireless sensors networks for 6G scenarios) under Agreement No. 101119624. E. Niarchou enjoys a FPI Grant (PRE2021-100311) also funded by AEI. V. Matus enjoys a Grant Catalina Ruiz (APCR2022010014) from the Agencia Canaria de Investigación, Innovación y Sociedad de la Información (ACIISI) through the European Social Fund.

Keywords: cameras | image sensors | LED lamps | object detection | optical communication | optical tracking

#### ABSTRACT

In this paper, we present a proof of concept for an indoor optical camera communication (OCC) system utilising a deep learning network to detect and identify humans wearing light-emitting diode (LED) strips. Specifically, we propose using the You Only Look Once (YOLO) version 8 object detection algorithm, which is built on convolutional neural networks (CNNs), to identify wearable LED transmitters in challenging scenarios such as low visibility, mobility and multiple users, followed by image processing to effectively decode the transmitted data. The red-green-blue (RGB) LED strip's colours (red, green, blue and white) serve as indicators of the user's status. By combining communication and monitoring functionalities, the LEDs facilitate not only the transmission of user data but also accurate detection, tracking and identification within the environment. This demonstrates the feasibility of utilising widely available devices like LED strips and cameras, commonly found in many buildings, with potential applications in high-risk environments where monitoring individuals' physical conditions is crucial. The obtained results indicate our system's effectiveness, as it achieved up to 100% success of reception (SoR) in a static experimental setup, 96.2% in a walking experimental setup with one user and showed no effectiveness with two users.

#### 1 | Introduction

Cameras are now an integral part of our daily lives, embedded in smartphones and utilised as surveillance tools in public infrastructure. They offer various functionalities within optical camera communications (OCC), which have been extensively explored in the field of optical wireless communications (OWC), particularly under the IEEE 802.15.7a standard [1]. Specifically, OCC employs a light-emitting diode (LED) as the transmitter  $(T_x)$ , an image sensor (IS) (i.e., camera) as the receiver  $(R_x)$  and

This paper is an extended version of our paper published in the 14th International Symposium on Communication Systems, Networks and Digital Signal Processing (CSNDSP) Rome, Italy, 17–19 July 2024.

This is an open access article under the terms of the Creative Commons Attribution License, which permits use, distribution and reproduction in any medium, provided the original work is properly cited.

© 2025 The Author(s). IET Optoelectronics published by John Wiley & Sons Ltd on behalf of The Institution of Engineering and Technology.

light as the communication medium. The functionalities of cameras stem from their ability to capture details beyond the capabilities of the human eye [2], making them valuable for communication, localisation and motion detection within indoor and outdoor Internet of Things (IoT) environments [3]. However, they lack the human ability to detect, recognise and track objects within images or videos.

Identifying objects in an image and tracking them throughout a video sequence has been a key challenge in computer vision, driving extensive research over the past several decades [4]. Consequently, human activity recognition in surveillance systems has emerged as a significant area of research, with a wide range of practical applications such as monitoring elderly care, tracking rehabilitation activity, sports analysis and detection of security intrusions [5, 6]. To overcome these limitations, computer vision serves as a complementary technology in image processing, and convolutional neural networks (CNNs) have proven highly effective for deep learning-based computer vision tasks [7]. Among these, the You Only Look Once (YOLO) algorithm, which is built on CNNs, is recognised as a state-of-the-art architecture for real-time tracking.

Currently, the YOLO architecture consists of 11 versions, ranging from YOLOv1 to YOLOv11. Each version brings advancements to meet different challenges in object detection. For instance, in ref. [8], YOLO version 2 has been proposed for realtime human detection, whereas YOLO version 5 has been considered in ref. [4] for LED detection and data decoding within a MIMO C-OOK (Multiple-Input Multiple-Output Camera On-Off Keying) scheme. This implementation aimed to enhance data transmission rates and reduce bit error rates (BER) in challenging environments characterised by long-range communication and mobility impacts. YOLOv8 has been proposed in ref. [9] for use in a real-time OCC system under high mobility conditions and in ref. [10] for real-time health monitoring and indoor location tracking within the Internet of Medical Things (IoMT). YOLOv9 has been used for vehicle detection within aerial urban transportation images in ref. [11]. YOLOv10 has been evaluated in ref. [12] for real-time pedestrian detection in autonomous vehicles. The latest version YOLOv11 has been used for miner detection in underground coal mines in ref. [13].

Wearable devices have become ubiquitous in modern life, appearing as smartphones, smartwatches or integrated into clothing. In our previous research, we demonstrated the feasibility of using wearable LEDs as transmitters in both indoor and outdoor OCC systems. In ref. [14], a wearable LED array was tested in an indoor environment, whereas in ref. [15], the evaluation was carried out under controlled user movement during physical exercise. Additionally, in ref. [16], two types of LED-based distributed transmitters, an LED strip and an LED-coupled side-emitting optical fibre attached on T-shirt, were evaluated in terms of success of reception and the signal-to-noise ratio performance (SNR). Moreover, in ref. [17], we demonstrated an outdoor OCC system using a strip of redgreen-blue (RGB) LEDs on a yellow safety jacket to transmit user identification data.

In this work, we propose an OCC system utilising a deep learning network. Specifically, we demonstrate the feasibility of employing widely available devices, such as LED strips and cameras, commonly installed in many buildings, for communication and monitoring in indoor environments. Furthermore, we propose using the YOLOv8 object detection model, developed by Ultralytics, to identify the yellow safety jacket with the wearable LED strip in challenging scenarios involving low visibility, mobility and more than one user. The LED strip displays different colours (red, green, blue and white) each representing the user's status. Red indicates danger, green represents safety, whereas blue and white communicate additional information. The colour transmission of the LEDs also encodes data related to user identification (ID).

Our system has potential applications in high-risk environments where it is essential to monitor the physical condition of individuals in professions such as mining, factory and construction. Moreover, this technology is also relevant in settings such as rehabilitation centres and elderly care facilities, where health and fitness data collected by wearable sensors can be transmitted via LEDs to existing surveillance cameras in the room, enabling real-time alerts to those monitoring an individual's condition.

The paper is structured as follows. Section 2 outlines the design of the OCC system along with the object detection algorithm and image processing. Section 3 describes the experimental methodology. Section 4 presents the results, and Section V concludes the study.

#### 2 | Proposed System

In this section, we describe the proposed system with the equipment used in the experimental setup, focusing on both the transmitting and receiving nodes. Specifically, we utilise a wearable LED  $T_x$  and camera  $R_x$  in an indoor environment to transmit the user's ID and status through colour transmission. In addition, our system incorporates an object detection algorithm to identify the wearable LED transmitters and then employs image processing to effectively decode transmitted data. A block diagram of the OCC link, showing the transmitter and receiver, is presented in Figure 1, whereas key parameters are detailed in Table 1. The components used for the experimental setup were selected based on their commercial availability, cost-effectiveness and energy efficiency.

#### 2.1 | System Description

The transmitting node consisted of a 10 mm-wide strip of RGB LEDs (commercially known as SMD 5050), attached to the front and back of a yellow safety jacket worn by the user, as shown in Figure 2. A yellow safety jacket was chosen because high-visibility safety garments are typically bright (yellow or orange) in real-world applications. Although the dominant yellow colour of the vest may influence light reflection, image-forming optics ensure that different angles of departure from

2 of 8

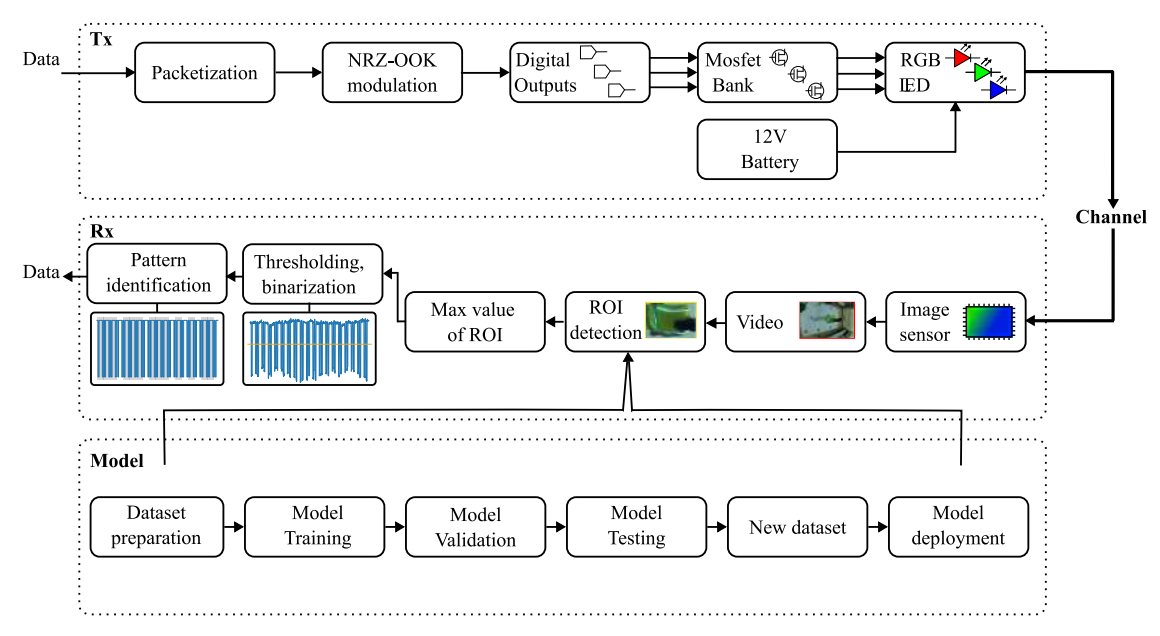


FIGURE 1 | Block diagram of the transmitting and receiving node.

TABLE 1 | Experiment key parameters.

Module	Parameter	Value
$T_{\chi}$	Light source	RGB LED strip (SMD 5050)
	Power supply	12 V
	Microcontroller	Arduino Nano
	Illuminance	7603 lux
Modulation	Modulation frequency	3.8 Hz
	Data pattern	[110100], [101110]
$R_{x}$	Camera	Raspberry Pi
	Image sensor	Sony IMX477
	White balance	0
	Analogue gain	8 dB
	Frame rate	30 fps
	Exposure time	$133 \mu s$
	Resolution	640 × 480 px

the LED strip arrive at different pixels, minimising its impact of line-of-sight (LOS) interference between rays. The LEDs were connected to the digital outputs of a microcontroller (Arduino Nano [18]) via a transistor-based switching circuit (mosfet bank). Both the LED strip and the circuit were powered by a 12-V battery. The transmitted illuminance of the RGB LEDs at 0 cm measured with testo 545 lux metre is 7603 lux.

The circuitry modulated the RGB channels to emit a repetitive beacon signal, utilising nonreturn-to-zero on-off keying (NRZ-OOK) modulation—which is the simplest modulation for



FIGURE 2 | The wearable transmitter device.

OCC—with pulse sequences [110100] or [101110] at a frequency of 3.8 Hz and a data rate of 3.8 bps for each RGB channel and an overall achievable data rate of 11.4 bps if all channels transmitted different patterns simultaneously. We primarily used the white colour for transmission, which is a combination of the red, green and blue channels, and evaluated each colour separately. RGB colours are easily detected by the image sensors and recognised by the image processing algorithm, and they serve as visual indicators for the people monitoring the surveillance system in high-risk environments for the situation of its users.

In the receiving node, two Raspberry Pi cameras [19] with Sony IMX477 image sensors capture 30 s videos at a frame rate of 30 fps with a resolution of  $640 \times 480$  px, an exposure

time of 133  $\mu$ s, white balance set to 0 and an analogue gain of 8 dB. Although many OCC systems use the rolling shutter (RS) image acquisition method, where images are captured row by row [20], this experimental setup leverages the global shutter (GS) capability of the camera. The GS allows simultaneous communication during video capture, as all pixels in the image sensor are exposed to light simultaneously and changes are detected per frame, enabling efficient data acquisition for low transmission data rates. The GS image acquisition method was preferred over the RS because of the dual purpose of our system—communication and surveil lance—and considerations such as link range and transmitter motion

#### 2.2 | Object Detection

In the context of OCC systems, detecting LEDs in challenging scenarios such as mobility, low visibility and multiple users remains a significant challenge. To address this, we propose the use of the YOLOv8 model, which has demonstrated feasibility and effectiveness in identifying and tracking LEDs or its optimal balance of performance and resource efficiency. Although newer versions such as YOLOv9, YOLOv10 and YOLOv11 offer advancements, they also demand increased computational resources and longer processing times compared to YOLOv8 of equivalent size. The proposed methodology efficiently identifies the region of interest (ROI) within videos, thereby enhancing overall system performance.

Object detection using YOLOv8 involved several key steps, from dataset preparation to model deployment. First, the captured videos were converted to image frames and uploaded as a dataset of 1000 images in the Roboflow platform training environment [21]. The images were labelled by marking the objects of interest (the jacket with the LED strip) with bounding boxes. The model was then trained using 600 labelled images with the number of training epochs set to 1000. During training, YOLOv8 learnt to detect objects by optimising its parameters to minimise the difference between its predictions and ground-truth labels. After training, the model was validated on a separate dataset of 300 images, which were not used during training, to evaluate its ability to generalise to unseen data, ensuring accuracy and reliability. Following validation, the model was tested on a test dataset of 100 images to assess its performance in real-world scenarios, using metrics such as precision, recall and mean Average Precision (mAP). The model achieved 99.8% precision, 99.3% recall and 99.5% mAP. The confusion matrix, calculated on the test set, is represented as

100 represents true positives, 1 represents false positives, 2 represents false negatives and 0 represents true negatives. Ideally, all results should be true positives, indicating that there should be no true negatives. The occurrence of false positives is attributed to double detection events. Based on the test results, a new dataset was created to include more diverse images or correct labelling issues, further improving the model's robustness. Finally, the trained model was exported for deployment.

#### 2.3 | Image Processing

Once the YOLOv8 model is trained, it is applied locally to all captured videos, automatically detecting the ROI in every frame, which in this case is the jacket with the LED strip worn by the users, as presented in Figure 3. For each frame, the model identifies and tracks the jacket with the LED strip with high precision. Following detection, the image processing algorithm is employed to analyse the content within the ROI detected.

The detected ROI is converted to greyscale and the pixel with the highest intensity (max value) is identified. The pixel values with the highest intensity extracted from all frame samples represent the received signal and are displayed in Figure 4a with the threshold applied on the mean value of the received signal for binarisation. After binarisation, the signal is normalised to create a buffer for further analysis, which is then used for cross-correlation with a template signal of the transmitted pattern. This correlation process identifies the alignment between the received and template signals. The algorithm computes correlation coefficients at various offsets, and the peaks in these results indicate strong similarities, suggesting successful pattern detection. Regions with correlation values exceeding 90% are considered detected patterns. Frame samples in which this pattern is successfully identified are highlighted in Figure 4b. The 900 frame samples correspond to a transmission period of 30 s, during which a total of 18 patterns were transmitted.

Variations in the received signal can be attributed to different types of noise in image sensors, including thermal, shot and flicker noise, which affect signal accuracy and consistency [22]. However, in scenarios where the  $T_x$  is mobile, such as in Figure 4a, the variations in the received signal are primarily due to the user's movement relative to the camera, which constantly changes the transmission angle of the LEDs relative to the camera, despite their fixed emission pattern of  $120^\circ$ .

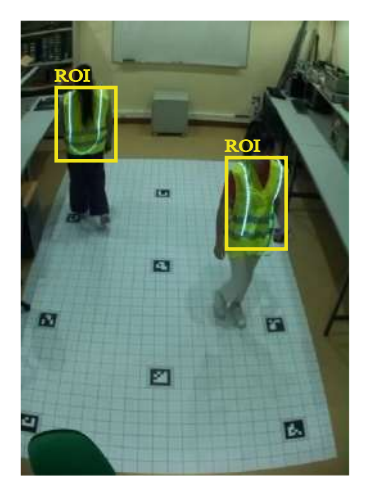


**FIGURE 3** | The two detected region of interest (ROI) corresponding to the location of the yellow safety jacket with the LED strip worn by two users, in one video frame sample, are highlighted in yellow.

4 of 8

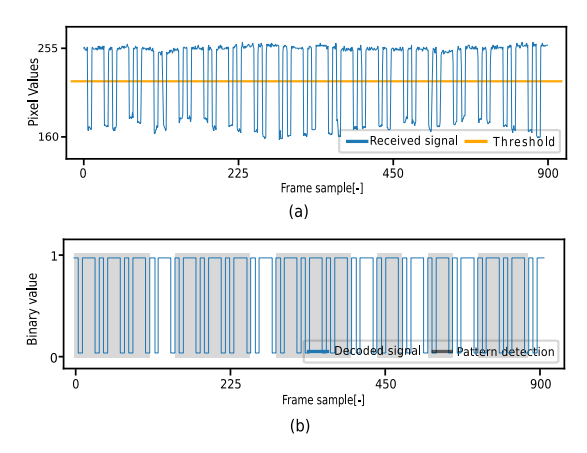


FIGURE 4 | Received signal plots. (a) The pixel values of the detected regions of interest (ROIs) with the highest intensity in greyscale, representing the white colour, extracted from all frame samples with the threshold at the mean value. (b) Binary values of white colour, extracted from all frame samples, with highlighted frames where the pattern is detected.

#### 3 | Methodology

In this section, we elaborate on the methodology employed for the experimental setup. The system was evaluated under different mobility and environmental conditions, with several users, to assess its performance.

Our measurements were taken in an indoor environment with floor dimensions  $4 \times 2.5$  m. Two Raspberry Pi cameras were placed on the front and back walls of the room to capture the interior with the wearable LED  $T_x$  from different angles.

Regarding mobility, two experimental setups, static and walking, were tested. In the static setup, the yellow safety jacket with the LED strip was placed on a chair in the centre of the room, as seen in Figure 5. In addition, to increase the complexity of the system, two users participated in walking scenarios, transmitting different identification patterns [110100] and [101110]. For the walking experimental setup, one person walked in a lemniscate pattern Figure 6a, whereas two people walked in parallel Figure 6b, lemniscate Figure 6c or random patterns Figure 6d to evaluate detection accuracy during movement.

Finally, two environmental conditions, ambient light and dark room, were tested to evaluate the system's performance under different lighting conditions. For ID transmission, we used different colours (white, red, green and blue), with each representing the user's status. White colour was primarily used for transmission in both experimental setups, combining all the RGB channels. However, in the static experimental setup, each colour channel was also evaluated separately.

#### 4 | Results

In this section, we show the performance of the system under various environmental conditions, mobility scenarios and with

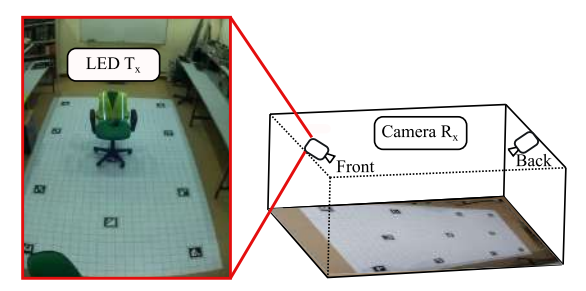


FIGURE 5 | Static experimental setup with the yellow safety jacket with the LED strip was placed on a chair in the centre of the room with dimensions 4 × 2.5 m, and the cameras were placed on the front and back walls of the room.

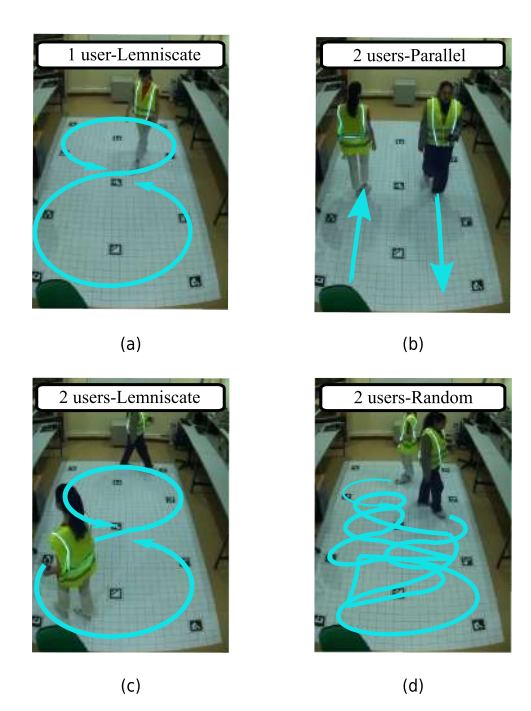


FIGURE 6 | Walking experimental setup with the yellow safety jacket with the LED strip worn by people walking in the room, in different walking patterns. (a) One user walking in a lemniscate pattern. (b) Two users walking in a parallel pattern. (c) Two users walking in a lemniscate pattern. (d) Two users walking in a random pattern.

different users. The results from the two experimental setups demonstrate the efficiency of our system, measured as the success of reception (SoR) [16] of pattern identifications. SoR is defined as the ratio of correctly decoded patterns to the total number of transmitted patterns, which in this case is 18, in a transmission period of 30 s.

Figure 7 shows the SoR of pattern identifications under different lighting conditions for each  $T_x$  ID (101110 and 110100) in the static setup, captured by the front wall camera. Similarly, Figure 8 presents the data from the back wall camera. Figure 9 displays the SoR of pattern identifications for each  $T_x$  ID in the

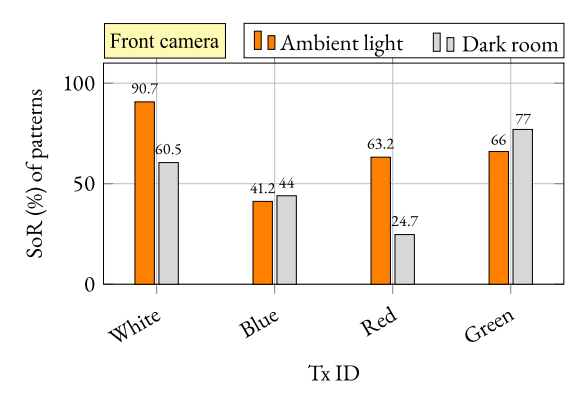


FIGURE 7 | Success of reception (SoR) of pattern identifications under different light conditions for each transmitted ID (101110, 110100) in white, blue, red and green colour transmission, captured by the front camera in the static experimental setup.

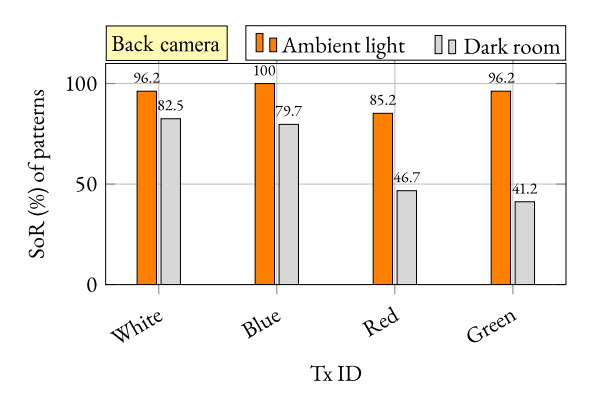


FIGURE 8 | Success of reception (SoR) of pattern identifications under different light conditions for each transmitted ID (101110, 110100) in white, blue, red and green colour transmission, captured by the back camera in the static experimental setup.

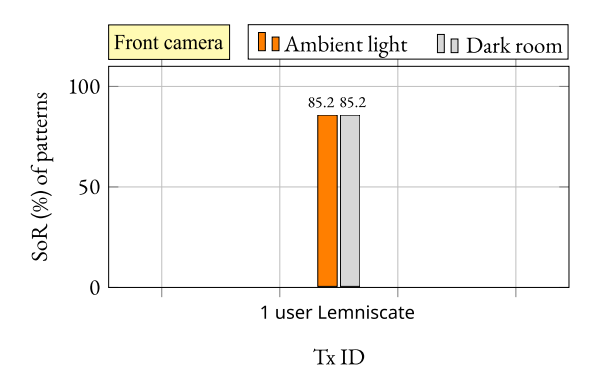


FIGURE 9 | Success of reception (SoR) of pattern identifications under different light conditions for each transmitted ID (101110, 110100), captured by the front camera in the walking experimental setup.

walking setup under various lighting conditions, again captured by the front wall camera. Likewise, Figure 10 provides the corresponding data from the back wall camera.

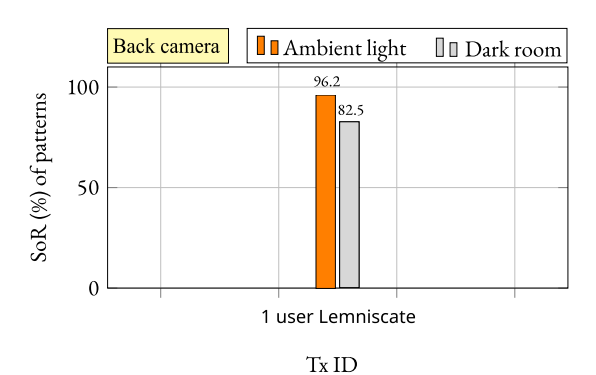


FIGURE 10 | Success of reception (SoR) of pattern identifications under different light conditions for each transmitted ID (101110, 110100), captured by the back camera in the walking experimental setup.

In terms of mobility, it is evident that the static experimental setup performed better than the walking setup, achieving even 100% SoR of pattern identifications, which corresponds to the total number of transmitted patterns.

In the walking measurements, our system accurately detects and tracks a single user walking in a lemniscate pattern within the room, achieving a high number of pattern identifications (96.2%). The one-user case can serve as a reference point for our system. However, in the case of two users, the system failed to detect, track or identify the users.

Regarding the environmental conditions, the system performed better under ambient light, as the object detection algorithm was able to detect and track the transmitting source more accurately in the video frames. The dark room conditions proved to be the worst-case scenario in almost all cases.

In terms of the different colour transmissions (blue, red and green), the system achieved a lower SoR compared to white. Although the object detection algorithm was trained using frames from all experimental setups, as the walking experimental setups (e.g., one user lemniscate and two users in parallel, lemniscate, random patterns) were conducted using white colour transmission, the dataset contains a higher proportion of white-coloured frames compared to other colours. This imbalance in the dataset causes lower SoR values for colour transmissions compared to white.

Overall, the system performed effectively, showing promise for use in real-world applications. Although the current model effectively detects and tracks the wearable object using YOLOv8, it only extracts the pixel with the maximum intensity, corresponding to the LED signal. This approach limits the amount of information captured from the LED pattern, as many additional pixels containing relevant data are not utilised. Although the front and back cameras share identical hardware (i.e., the same image sensors), variations in SoR are observed due to certain physical parameters (e.g., lens focus) that could have been installed with different configurations. These differences can also be attributed to the model's basic object detection method, which lacks advanced image processing techniques for detecting and tracking the LED within the detected object. By focusing

6 of 8

only on the maximum value of the ROI, we are unable to effectively minimise noise, which could be addressed by tracking multiple pixels containing LED information.

#### 5 | Conclusion

This work presents an OCC system that uses deep learning. It uses commercial devices such as LED strips and cameras for indoor communication and monitoring. The YOLOv8 object detection model is employed to identify the yellow safety jacket with the wearable LED strip even in difficult conditions, such as low visibility and user movement. The LED strips use different colours (red, green, blue and white), with each colour encoding user identification data. The results obtained indicate that our system has potential applications in environments with high risks, where monitoring individuals' physical conditions is of vital importance. Our system achieved up to 100% SoR in the static experimental setup, 96.2% in the walking experimental setup with one user, but proved ineffective with two users.

However, for the system's implementation in a real-world scenario, there are still some challenges to be addressed. As noted in the results in the previous section, the system failed to detect and track multiple users in the video frames. This can be improved with the acquisition and training of a bigger dataset that ensures the system's performance in complex environments. Regarding the lower system's performance in dark room conditions compared to ambient light, this can be improved during the signal modulation stage using an NRZ-OOK modulation scheme with two nonzero power levels to avoid completely dark transmission, which is not highly relevant since people typically do not walk in complete darkness. Although our study evaluated the system's performance under ambient light and dark room conditions, the impact of external light sources or reflections on detection accuracy was not specifically analysed because we have LOS communication, ensuring seamless reception. Future work could investigate how factors, such as glare, shadows and varying illumination levels affect the performance to enhance robustness in real-world environments. Regarding the low SoR in different colour transmissions, future work could include more experimental setups with colour transmissions. This would allow the system to be trained on more frames with colour transmissions, enabling a fairer comparison with white. Regarding the difference in SoR between the front and back wall cameras, combining their captured data could enhance the overall performance of the system. Additionally, enhancing detection capabilities by integrating advanced image processing techniques and tracking all pixels containing LED information would also improve the SoR. Moreover, integrating the simultaneous localisation and mapping (SLAM) method with YOLO could improve real-time performance and localisation accuracy, particularly in dynamic and complex environments, which would further enhance the system's overall reliability and performance in real-world applications. Future work could also explore the integration of other CNN models while continuously using the updated YOLO versions to assess their impact on system performance.

Furthermore, to ensure reliable functionality across various environments, both indoors and outdoors, transmitting nodes must be waterproof and equipped with extended battery life. On the receiving side, the primary challenge involves managing real-time data decoding and user monitoring. This includes identifying multiple users from live video streams, filtering out ambient lighting interference and continuously tracking users' movements. Overcoming these challenges will require the development of advanced computer vision models as well as cloud-based architectures to handle the complexity of processing and analysing the incoming data simultaneously.

#### **Author Contributions**

Eleni Niarchou: conceptualization, data curation, formal analysis, investigation, methodology, software, validation, visualization, writing – original draft. Atiya Fatima Usmani: investigation, methodology, writing – original draft. Vicente Matus: conceptualization, formal analysis, investigation, methodology, software, supervision, writing – original draft. Jose Rabadan: funding acquisition, methodology, project administration, resources, supervision, writing – review and editing. Victor Guerra: formal analysis, investigation, methodology, supervision, writing – review and editing. Luis Nero Alves: funding acquisition, project administration, resources, supervision, writing – review and editing. Rafael Perez-Jimenez: funding acquisition, project administration, resources, supervision, writing – review and editing.

#### Acknowledgements

This work has received support from the OCCAM project (PID2020-114561RB-100) and SUCCESS (TED2021-130049B-C21) funded by the Agencia Estatal de Investigación (AEI, Spanish Research Government), and from the European Union COST Action NEWFOCUS (CA19111). This work was supported by the European Union's Horizon Europe Programme in the frame of Marie Sklodowska-Curie Actions Doctoral Networks (MSCA-DN) project OWIN6G (Optical and wireless sensors networks for 6G scenarios) under Agreement No. 101119624. E. Niarchou enjoys a FPI Grant (PRE2021-100311) also funded by AEI. V. Matus enjoys a Grant Catalina Ruiz (APCR2022010014) from the Agencia Canaria de Investigación, Innovación y Sociedad de la Información (ACIISI) through the European Social Fund.

#### **Conflicts of Interest**

The authors declare no conflicts of interest.

#### Data Availability Statement

The data that support the findings of this study are available from the corresponding author upon reasonable request.

#### References

- IEEE Standards Association. Accessed, 09 26, 2024, https://standards.ieee.org/ieee/802.15.7a/10367/.
- W. A. Cahyadi, Y. H. Chung, Z. Ghassemlooy, and N. B. Hassan, Optical Camera Communications: Principles, Modulations, Potential and Challenges, (Vol. 9(9), 1339 2020), https://www.mdpi.com/2079-9292/9/9/1339Electronics.
- 3. S. R. Teli, S. Zvanovec, and Z. Ghassemlooy, "Optical Internet of Things Within 5G: Applications and Challenges," in 2018 IEEE International Conference on Internet of Things and Intelligence System (IOTAIS) (IEEE, 2018), 40–45.
- V. L. Nguyen, D. H. Tran, H. Nguyen, and Y. M. Jang, "An Experimental Demonstration of MIMO C-OOK Scheme Based on Deep Learning for Optical Camera Communication System," *Applied Sciences* 12, no. 14 (2022): 6935, https://doi.org/10.3390/app12146935.

- 5. M. Nallasivam and V. Senniappan, "Moving Human Target Detection and Tracking in Video Frames," *Studies in Informatics and Control* 30, no. 1 (2021): 119–129, https://doi.org/10.24846/v30i1y202111.
- D. K. Vishwakarma and T. Singh, "A Visual Cognizance Based Multi-Resolution Descriptor for Human Action Recognition Using Key Pose," International Journal of Electronics and Communications 107 (2019): 157– 169, https://www.sciencedirect.com/science/article/pii/S143484111 9303942AEU.
- 7. X. Zhao, L. Wang, Y. Zhang, X. Han, M. Deveci, and M. Parmar, "A Review of Convolutional Neural Networks in Computer Vision," *Artificial Intelligence Review* 57, no. 4 (2024): 99, https://doi.org/10.1007/s10462-024-10721-6.
- 8. H. H. Nguyen, T. N. Ta, N. C. Nguyen, V. T. Bui, H. M. Pham, and D. M. Nguyen, "YOLO-Based Real-Time Human Detection for Smart Video Surveillance at the Edge," in 2020 IEEE 8th International Conference on Communications and Electronics (ICCE) (IEEE, 2021), 439–444.
- 9. O. S. Sitanggang, V. L. Nguyen, H. Nguyen, R. F. Pamungkas, M. M. Faridh, and Y. M. Jang, "Design and Implementation of a 2D MIMO OCC System Based on Deep Learning," *Sensors* 23, no. 17 (2023): 7637, https://doi.org/10.3390/s23177637.
- 10. H. Herfandi, O. S. Sitanggang, M. R. A. Nasution, H. Nguyen, and Y. M. Jang, "Real-Time Patient Indoor Health Monitoring and Location Tracking With Optical Camera Communications on the Internet of Medical Things," *Applied Sciences* 14, no. 3 (2024): 1153, https://doi.org/10.3390/app14031153.
- 11. M. Bakirci and I. Bayraktar, "YOLOv9-Enabled Vehicle Detection for Urban Security and Forensics Applications," in 2024 12th International Symposium on Digital Forensics and Security (ISDFS) (IEEE, 2024), 1–6.
- 12. Y. Li, W. Leong, and H. Zhang, "YOLOv10-Based Real-Time Pedestrian Detection for Autonomous Vehicles," in 2024 IEEE 8th International Conference on Signal and Image Processing Applications (ICSIPA) (IEEE, 2024), 1–6.
- 13. Y. Li, H. Yan, D. Li, and H. Wang, Robust Miner Detection in Challenging Underground Environments: An Improved YOLOv11 Approach, (Vol. 14(24), 11700, 2024), https://www.mdpi.com/2076-3417/14/24/11700AppliedSciences.
- 14. E. Niarchou, V. Matus, J. Rabadan, V. Guerra, and R. Perez-Jimenez, "Experimental Evaluation of LED-Based Wearable Transmitter for Optical Camera Communications Systems," in 2023 17th International Conference on Telecommunications (ConTEL) (IEEE, 2023), 1–5.
- 15. E. Niarchou, V. Matus, J. Rabadan, V. Guerra, and R. Perez-Jimenez, "Optical Camera Communications in Healthcare: A Wearable LED Transmitter Evaluation During Indoor Physical Exercise," *Sensors* 24, no. 9 (2024): 2766, https://doi.org/10.3390/s24092766.
- 16. E. Niarchou, K. Eollos-Jarosikova, V. Matus, et al., "Experimental Evaluation of Wearable LED Strip and Side-Emitting Fiber for Optical Camera Communications Systems," *Optics Express* 32, no. 14 (2024): 25091–25103, https://doi.org/10.1364/oe.521967.
- E. Niarchou, V. Matus, R. Perez-Jimenez, J. Rabadan, and V. Guerra, "Experimental Evaluation of Wearable LED Strip for Outdoor Optical Camera Communications Systems," in 2024 14th International Symposium on Communication Systems, Networks and Digital Signal Processing (CSNDSP) (IEEE, 2024), 621–625.
- 18. Arduino\* Nano, *ATmega328 16 MHz., 2KB SRAM, 32KB Flash, 1KB EEPROM* (Datasheet, 2023), https://docs.arduino.cc/resources/datasheets/A000005-datasheet.pdf.
- 19. SONY-semicon, IMX477-AACK Diagonal 7.853 mm (Type 1/2.3) 12.3 Mega-Pixel CMOS Image Sensor (Datasheet, 2018), https://www.sonysemicon.com/files/62/pdf/p-13\_IMX477-AACK\_Flyer.pdf.

- T. Le, N.-T. Le, and Y. M. Jang, "Performance of Rolling Shutter and Global Shutter Camera in Optical Camera Communications," in 2015 International Conference on Information and Communication Technology Convergence (ICTC), 2015), 124–128.
- 21. Roboflow. Accessed, 09 20, 2024, https://roboflow.com/.
- 22. N. Bani Hassan, "MIMO Visible Light Communications With Camera-Based Receiver for Intelligent Transport Systems," Copyright Database copyright ProQuest LLC; ProQuest does not claim copyright in the individual underlying works; Última actualización 2024-07-18, PhD Thesis (2019), https://www.proquest.com/dissertations-theses/mimovisible-light-communications-with-camera/docview/2322017666/se-2.

8 of 8

## 5.4 Summary

This chapter presents a comprehensive evaluation of the three publications that contribute to the applications of OCC to wearable sensor networks. A summary of system design, data processing methods, and evaluation metrics considered in each work, as well as the most important findings, is presented in Table 5.1.

The first publication (P1) explores an OCC system consisting of a stationary bike, a portable LED array  $T_x$ , and a smartphone camera  $R_x$ , to track user movement during indoor physical exercise. A correlation-based ROI detection is evaluated using the correlation coefficient, and exercise analysis is evaluated using the position frequency distribution data obtained from the IMU, achieving a significant reduction in the tracking process.

The second study (P2) compares two types of wearable LED-based transmitters: an LED strip and an LED-coupled side-emitting optical fiber. This study evaluates their performance in laboratory and wearable settings in terms of SoR, SNR, theoretical BER, power consumption, and heat emission. Two processing methods are employed: correlation-based ROI detection, evaluated using the correlation coefficient, and mask-based ROI detection, evaluated using an ROI mask. The findings show that the LED strip achieves high SoR, while the SoR for side-emitting fiber is high with the use of the mask-based image processing method.

The last paper (P3) utilizes deep learning techniques in the OCC system with the YOLOv8 object detection model to detect, track, and identify humans wearing yellow safety jackets with the wearable LED strip. This work proves the feasibility of tracking humans under difficult conditions, including low visibility and mobility. The system is tested according to SoR in terms of communication performance and according to validation metrics for YOLOv8, including precision, recall, and mAP. The system achieves high SoR in static and single-user walking experiments but fails to detect multiple users simultaneously.

**Table 5.1:** Summary of the key contributions on methodology and findings of compendium articles.

	System Design	Processing	<b>Evaluation Metrics</b>	Findings
	Stationary bike	ROI detection	Corr. coef	Tracking process reduction:
P1	LED array Tx	(corrbased)	Exercise intensity	87.3% (mild),
	Smartphone Rx	Exercise analysis	Position freq. distribution	79.0% (intense)
	Laboratory, Wearable setups	ROI detection (corrbased)	Corr. coef., ROI mask	Best SoR: 100% Tx-Rx at 1m
P2	White LED strip Tx		SoR (corrbased)	LED strip: SoR 100%, Fiber (corrbased): SoR 72.2%-98.8% (lab), 78.8%-94.1% (wearable)
	Side-emitting Fiber Tx		SNR	LED strip: SNR up to 42.7dB, Fiber: 21.0-27.4dB
	Smartphone Rx	ROI detection (mask-based)	SoR (mask-based)	Fiber (mask-based): Improved SoR
P2			Theor. BER	BER: 10 <sup>-11</sup>
			Power consumption	Power: 432-720mW (LED strip), 525mW (Fiber)
			Achievable data rate	0.5kbps
			Heat emission	User-friendly
	Static, Walking	Object detection	SoR	SoR: 100% (static), 96.2% (1 user walking), fail(2 users walking)
P3	RGB LED strip Tx	ROI detection	Validation metrics	YOLO metrics: Precision 99.8%, Recall 99.3%, mAP 99.5%
	Raspberry pi Rx	(YOLO-based)	Data rate	3.8 bps/channel, achievable: 11.4 bps

This chapter outlines the key contributions of this thesis in the application of OCC systems to wearable sensor networks. The first section presents an overview of the achievements in line with the thesis objectives, supported by the experimental results. The second section discusses the potential new research works that emerge from the findings of this research.

## **Conclusions**

This doctoral thesis, titled "Contribution to the application of Optical Camera Communication to Wearable Sensor Networks", is focused on the development and experimental evaluation of wearable LED-based transmitters in indoor and outdoor OCC links. The research was structured around three main objectives that aimed to demonstrate the feasibility of implementing optical communication links based on cameras using image sensors in the optical spectrum, by combining image processing algorithms and wireless optical communication, to examine the impact of channel conditions related to the position and configuration of the sensor nodes on data rate performance, and to deploy networks with multiple receivers and apply node recognition and tracking algorithms based on artificial intelligence techniques.

The three publications [132], [134], [136] in the compendium of this thesis presented in the previous chapter, addressed the above-mentioned objectives through the implementation of several OCC systems with wearable LED transmitters. Across the three works, various OCC implementations were explored, including a wearable LED transmitter for exercise monitoring, LED-based distributed transmitters for wearable OCC, and deep learning-based detection of LED-equipped safety wearables.

The first article demonstrates the feasibility of detecting a user's position within the frame during indoor physical exercise, using a wearable LED transmitter. In this work, commercial devices were employed as transmitters showing the system's potential for widespread use, and an image processing algorithm was designed to identify a template signal transmitted by the LED and detected within the image. By evaluating controlled exercise-induced movement, the tracking process is confined to a smaller region in the image frame, improving efficiency and achieving a reduction of 87.3% for mild exercise and 79.0% for intense exercise. The system has potential applications in sports training, elderly care, and rehabilitation, and provides feedback on exercise intensity, individual differences, and early detection of chronic disease or injury.

The second study compares two types of LED-based distributed transmitters, the LED strip and the LED-coupled side-emitting optical fiber, under laboratory and wearable OCC systems, in their power consumption, SoR, SNR, and heat emission. The findings show some key differences between the two technologies. The LED strip has a larger illuminated area, while the side-emitting fiber has greater flexibility for wearable applications. Practical considerations are also related to the reduced power

#### **Chapter 6** Conclusions and Future Works

of illumination resulting from the side-emitting fiber operating at lower voltage, and the electrical distribution which impacts performance and practicality. The LED strip showed consistent SoR ( 100%) and SNR ranging from 21.0 to 27.4 dB, indicating stable performance. The side-emitting optical fiber reached higher peak SNR values (up to 42.7 dB) but exhibited greater variation in SoR (from 72.2% to 98.8 %), especially under wearable configurations (from 78.8% to 94.1 %). Power consumption ranged from 432–720 mW for the LED strip and 525 mW for the fiber. Furthermore, BER was estimated at  $10^{-11}$ , which is well below the FEC limit of  $3.8\times10^{-3}$ , confirming the reliability of data transmission.

The last work integrates deep learning and OCC, using YOLOv8 object detection in monitoring people with safety jackets with RGB LED strips in challenging conditions, such as in low visibility and mobility. The system achieves 100% reception efficiency for static measurements and 96.2% for single-user walking scenarios, although it is challenged in multi-user detection, revealing the need for further optimization. The utilization of color-coded LED strips for user identification suggests promising applications in risk-prone environments (e.g., mines, factories, construction sites, health care facilities) in which real-time monitoring is essential. The YOLOv8 model also achieved 99.8% precision, 99.3% recall, and 99.5% mAP in detecting wearable LED transmitters, demonstrating high accuracy in object identification.

In summary, during the exercise of this thesis, contributions have been achieved in the following areas:

- making the system available for widespread use, as in all experimental OCC setups in this research, commercial devices employed as transmitters (i.e., LED array, LED strip, LED-coupled side-emitting optical fiber) and receivers (i.e., smartphones, Raspberry Pi cameras),
- developing an image processing algorithm for accurately detecting transmitted bits within frames, despite the user's movement,
- detecting the user's position within the frame, offering valuable insights into the user's exercise intensity, and could potentially identify chronic conditions or detect early signs of injuries,
- analyzing critical aspects for the transmitter placement in relationship with the camera receiver position,
- making the system applicable in high-risk environments, where real-time monitoring of users' physical conditions is critical, with the integration of deep learning into OCC systems, enabling indoor communication and monitoring, even under challenging conditions such as low visibility, user movement, and multiple users.

The scalability of OCC systems in terms of the number of users that can be detected within a single image frame depends on the camera's capture method, the experimental setup, and the camera-transmitter distance. In RS capture during a physical exercise scenario, where the camera is positioned at 20–30 cm, the estimated number of users that fit within the image frame is limited to one due to the close-up nature of the setup. In contrast, in indoor experiments using the wearable LED strip and fiber, where the

maximum camera distance reaches 2.8 m, the system could detect approximately three users in the image frame.

With GS capture in a room setup, where the maximum distance is 4 m, the image frame could fit four to five walking users, although it failed in detecting two, with appropriate modifications (as mentioned in the following subsection). Finally, in an outdoor experiment conducted at 90-120 m, user scalability is theoretically calculated based on the walking area in pixels of the user within the image frame, and the size of the user's ROI, the system could theoretically detect up to 255 users, assuming perfectly distributed spacing across the area.

Existing wearable health monitoring devices, such as smartwatches, fitness bands, and ECG sensors, use RF-based communication technologies such as Bluetooth and Wi-Fi, which are power-consuming and susceptible to electromagnetic interference, which can be a major issue in medical settings where signal integrity is essential. Similarly, modern IoT devices and wearable sensors depend on short-range wireless protocols such as BLE, Zigbee, and NFC, but they struggle to scale in crowded environments. A major industry gap exists in providing a low-power, interference-free, and scalable communication alternative for wearable health monitoring and real-time tracking applications. In high-risk workplaces such as mines, construction sites, and industrial facilities, tracking workers in real time requires energy-efficient and interference-free communication solutions to ensure safety and reliability. By focusing on real-time user tracking, multiuser scalability, motion-resilient communication, and safety applications, this research has the potential to close critical gaps in healthcare, IoT, smart spaces, road safety, and industrial environments, making these technologies more effective and accessible.

## **Future research**

The aforementioned contributions open up several future research lines on the application of OCC in wearable sensor networks. Based on the scope of the results of this thesis, the author envisions the following new research works.

## Wearable and Hardware Design.

- Improvements in the design of the wearable device and power efficiency. Future research will focus on the hardware design of the wearable device to enhance its integration within clothing or accessories. The devices have to be compact in size, lightweight, waterproof, user-friendly, and equipped with extended battery life, allowing them to be worn long-term, under any environmental condition. Eye safety should also be taken into consideration, especially for medical-related applications, where issues like flickering in the light source have to be eliminated to prevent migraines and headaches. Data security will also be a concern to safeguard sensitive user information using user authentication processes.
- Exploring flexible hardware electronics as LED transmitters for OCC. Using printed electronics or 3D printing onto textiles as transmitters for OCC can offer a compact, cost-effective, and scalable solution. These custom-designed transmitters could improve the extent of practical applications in wearable and embedded OCC systems.

Integration of different health sensors (glucose monitors, fingertip pulse oximeter, temperature sensors) that operate simultaneously into wearable OCC-based communication systems. Future experiments would explore the feasibility of health monitoring in real-world scenarios to assess the practicality and effectiveness of OCC-integrated health wearables. Additionally, different transmitters utilizing SDMA modulation will be incorporated to enable efficient multi-sensor data transmission.

## Modulation and Signal Processing.

- Exploration of different signal modulation techniques. Wavelength Division Multiplexing (WDM) will be explored to transmit data over multiple light wavelengths and receive them with multispectral cameras [137], increasing the system's data rate and efficiency. For instance, if each one of the RGB channels of the LED transmitter transmits different patterns at the same time, the achievable data rate can be increased by three times. Additionally, improved signal modulation techniques, such as PAM modulation with two power levels, will ensure consistent performance even in low-light conditions.
- Digital signal processing (DSP) improvements. The application of AI algorithms for decoding will optimize signal detection and eliminate noise, ensuring more robust communication. Additionally, digitally generated data will be utilized to train the AI models.
- Hybrid schemes of OCC integrated with RF networks (5G or 6G) could guarantee the system's performance by supporting high data rates over a few kilometers and operating under non-line-of-sight (NLoS) conditions.

## Camera and Sensor Technology.

- Engaging the latest camera technology. The use of the newest cameras, capable of capturing high-resolution videos with reduced exposure time and higher frame rates, will support the operation of low-power transmitters over longer distances, providing enhanced efficiency.
- Combination of cameras operating in different capture modes. GS mode surveillance cameras can be combined with RS mode cameras in the same setup for ROI detection, for both surveillance and communication at the same time.
- Engaging event cameras as receiving and sensing devices. Event (or neuromorphic) cameras are biologically inspired sensors that have transformed visual data acquisition by replicating the neural structure of the human eye. Unlike traditional cameras, they operate asynchronously, detecting changes in scene illumination at the pixel level. This enables them to capture high-precision temporal information with minimal latency, usually in the microsecond range, allowing for higher modulation speeds and improving the system's data transmission rate. Since event cameras only capture pixel-level changes, they are motion-resilient, making them ideal for wearable OCC systems. Unlike conventional cameras that process entire frames, event cameras transmit only pixel-level events, reducing data bandwidth

and computational load, thus making real-time processing more efficient. Furthermore, their unique sensing mechanism not only enhances data communication but also enables advanced sensing capabilities, such as motion tracking and environmental awareness, further expanding their potential applications. These cameras have already been tested in OCC in [138].

## Al and Image Processing.

Real-time user monitoring and tracking with data decoding. Since in all
the experimental setups conducted for this thesis, the data decoding stages
were performed over offline video or image captures, implementing online
processing of video streams, will make OCC in wearable sensor networks
more practical, offering a sense of security in high-risk environments or
multi-user environments such as mines, factories or care units.

Cloud-based architectures with advanced computer vision models will be implemented for processing live video streams, identifying and separating signals from multiple users, filtering out ambient light interference, and for continuous tracking of user movements. Moreover, combining data from multiple cameras will further improve the system's performance, as the different perspectives can increase the reliability of the system and address challenges related to occlusions or overlapping signals in multi-user settings. All these capabilities can be integrated into a smartphone app, enabling real-time monitoring, data processing, and visualization on a user-friendly platform.

- Development of advanced image processing techniques. During the exercise
  of this thesis, we developed image processing techniques, dedicated to
  different LED transmitter shapes. However, advanced image processing
  techniques could enable accurate extraction of transmitted data from video
  streams by isolating pixels that contain LED information, and subtracting
  the background, even in challenging environments such as low visibility or
  user movement.
- Training algorithms enhancements. Expanding the training of the integrated AI algorithms (i.e., YOLO) with a broader range of data, including more frames in low-visibility conditions, with multiple users, and with different color transmissions, will improve the robustness and versatility of the system. Moreover, refining the ROI to focus only on the LED transmitter region in the frame, will reduce the processing time and will improve the overall performance of the system. Also, exploring other CNN models, or using always the updated YOLO versions, will help assess their impact on system performance and identify ways of improvement in detection accuracy and efficiency.

## Personalization and Insights.

 Further analysis in user dynamics and personalized insights. Since only the relationship between the user's position in the image frame and the user's exercise intensity was analyzed, future research will further explore factors such as age, gender, or fitness profile with experimentation with different users. This analysis could uncover valuable information on early detection of chronic conditions, early injury prevention, or personalized health monitoring.

Figure 6.1 illustrates some wearable design ideas for OCC systems, showing how LED transmitters can be seamlessly embedded into everyday clothing and accessories for enhanced usability and functionality.



Figure 6.1: Images generated by AI to visualize possible wearable designs.

# **Bibliography**

- [1] IEEE Standard Association, IEEE draft standard for local and metropolitan area networks part 15.7: Short-range optical wireless communications amendment 1: Higher speed, longer range optical camera communication (OCC), IEEE Std 802.15.7a. [Online]. Available: https://standards.ieee.org/ieee/802.15.7a/10367/ (see page 1).
- [2] M. Uysal, C. Capsoni, A. Boucouvalas, and E. Udvary, Optical Wireless Communications An Emerging Technology. Jan. 2017, ISBN: 978-3-319-30200-3. DOI: 10.1007/978-3-319-30201-0 (see pages 1, 9, 17, 22).
- [3] W. A. Cahyadi, Y. H. Chung, Z. Ghassemlooy, and N. B. Hassan, Optical camera communications: Principles, modulations, potential and challenges, Electronics, vol. 9:no. 9, ISSN: 2079-9292. DOI: 10.3390/electronics9091339. [Online]. Available: https://www.mdpi.com/2079-9292/9/9/1339 (see pages 1, 9, 13, 24).
- [4] S. R. Teli, S. Zvanovec, and Z. Ghassemlooy, Optical Internet of Things within 5G: Applications and challenges, in 2018 IEEE International Conference on Internet of Things and Intelligence System (IOTAIS), 2018, 40–45. DOI: 10.1109/IOTAIS.2018.8600894 (see pages 1, 9).
- [5] N. Saha, M. S. Ifthekhar, N. T. Le, and Y. M. Jang, Survey on optical camera communications: Challenges and opportunities, IET Optoelectronics, vol. 9:no. 5, 172–183. DOI: 10.1049/iet-opt.2014.0151. [Online]. Available: https://doi.org/10.1049/iet-opt.2014.0151 (see page 1).
- [6] J. Luna-Rivera, J. Rabadan, J. Rufo, V. Guerra, D. Moreno, and R. Perez-Jimenez, Color space-based autoencoder for optical camera communications, Expert Systems with Applications, vol. 245, 123101, ISSN: 0957-4174. DOI: https://doi.org/10.1016/j.eswa.2023.123101. [Online]. Available: https://www.sciencedirect.com/science/article/pii/S0957417423036059 (see page 1).
- [7] Statista, https://www.statista.com/statistics/1172711/forecast-of-digital-camera-sales-volume/, Accessed: 2024-12-05 (see page 1).
- [8] K. Yang, Wireless sensor networks. Springer, 2014 (see page 1).
- [9] L. E. Linderman, H. Jo, and B. F. Spencer, Low-latency data acquisition hardware for real-time wireless sensor applications, *IEEE Sensors Journal*, vol. 15:no. 3, 1800–1809. DOI: 10.1109/JSEN.2014.2366932 (see page 1).
- [10] B. Prabhu, M. Pradeep, and E. Gajendran, Military applications of wireless sensor network system, Military Applications of Wireless Sensor Network System (January 25, 2017). A Multidisciplinary Journal of Scientific Research & Education, vol. 2, 12 (see page 2).
- [11] V. Matus, V. Guerra, C. Jurado-Verdu, S. Zvanovec, J. Rabadan, and R. Perez-Jimenez, Design and implementation of an optical camera communication system for wireless sensor networking in farming fields, in 2021 IEEE 32nd Annual International Symposium on Personal, Indoor and Mobile Radio Communications (PIMRC), IEEE, 2021, 1–6 (see page 2).
- [12] V. Sharma, R. Beniwal, and V. Kumar, Multi-level trust-based secure and optimal IoT-WSN routing for environmental monitoring applications, The Journal of Supercomputing, vol. 80:no. 8, 11338–11381, ISSN: 1573-0484. DOI: 10.1007/s11227-023-05875-z. [Online]. Available: https://doi.org/10.1007/s11227-023-05875-z (see page 2).
- [13] P. C. Reddy, S. Latha, G. Kumar, and Y. Sucharitha, Multi-agent lot-based system for intelligent vehicle traffic management using wireless sensor networks, Recent Advances in Electrical & Electronic Engineering (Formerly Recent Patents on Electrical & Electronic Engineering), vol. 16. DOI: 10.2174/2352096516666230719114956 (see page 2).

- [14] S. Tarannum and S. Farheen, Wireless sensor networks for healthcare monitoring: A review, in *Inventive Computation Technologies*, S. Smys, R. Bestak, and Á. Rocha, Eds., Cham: Springer International Publishing, 2020, 669–676, ISBN: 978-3-030-33846-6 (see page 2).
- [15] Y. Wang, S. Cang, and H. Yu, A survey on wearable sensor modality centred human activity recognition in health care, Expert Systems with Applications, vol. 137, 167–190 (see page 2).
- [16] P. Šolic, R. Colella, G. Grassi, T. Perković, C. G. Leo, A. Čulić, V. Pleština, S. Sabina, and L. Catarinucci, Circuit design, realization, and test of a bluetooth low energy wireless sensor with on-board computation for remote healthcare monitoring, *IEEE Journal of Radio Frequency Identification*, vol. 8, 105–113. DOI: 10.1109/JRFID.2024.3363074 (see page 2).
- [17] R. Perez-Jimenez, J. Rufo, C. Quintana, J. Rabadan, and F. J. Lopez-Hernandez, **Visible light** communication systems for passenger in-flight data networking, in 2011 IEEE International Conference on Consumer Electronics (ICCE), 2011, 445–446. DOI: 10.1109/ICCE.2011.5722675 (see page 3).
- [18] R. Perez-Jimenez, J. Rabadan, V. Guerra, L. Aguiar, and J. Rufo, Fundamentals of indoor vlp: Providing autonomous mobility for visually impaired people, in 2017 International Conference and Workshop on Bioinspired Intelligence (IWOBI), 2017, 1–6. DOI: 10.1109/IWOBI.2017.7985542 (see page 3).
- [19] V. Matus Icaza, Contribution to the experimental channel evaluation of optical camera communication for wireless sensor networks, Ph.D. dissertation, 2021 (see page 3).
- [20] A. Mederos-Barrera, C. Jurado-Verdu, V. Guerra, J. Rabadan, and R. Perez-Jimenez, Design and experimental characterization of a discovery and tracking system for optical camera communications, Sensors, vol. 21:no. 9, ISSN: 1424-8220. DOI: 10.3390/s21092925. [Online]. Available: https://www.mdpi.com/1424-8220/21/9/2925 (see pages 3, 13).
- [21] P. Chavez-Burbano, V. Guerra, J. Rabadan, and R. Perez-Jimenez, **Optical camera communication system for three-dimensional indoor localization**, *Optik*, vol. 192, 162870, ISSN: 0030-4026. DOI: https://doi.org/10.1016/j.ijleo.2019.05.076. [Online]. Available: https://www.sciencedirect.com/science/article/pii/S0030402619307284 (see page 3).
- [22] P. Chavez-Burbano, V. Guerra, J. Rabadan, and R. Perez-Jimenez, **Optical camera communication for smart cities**, in 2017 IEEE/CIC International Conference on Communications in China (ICCC Workshops), 2017, 1–4. DOI: 10.1109/ICCChinaW.2017.8355271 (see page 3).
- [23] D. Moreno, J. Rufo, V. Guerra, J. Rabadan, and R. Perez-Jimenez, **Optical multispectral camera communications using LED spectral emission variations**, *IEEE Photonics Technology Letters*, vol. 33:no. 12, 591–594. DOI: 10.1109/LPT.2021.3078842 (see page 3).
- [24] V. Guerra, J. Rabadan, R. Perez-Jimenez, and J. Rufo, **Effect of absorbing and non-diffracting particles in UWOC links**, *IET Optoelectronics*, vol. 11:no. 5, 176–179. DOI: https://doi.org/10.1049/iet-opt.2016.0131. eprint: https://ietresearch.onlinelibrary.wiley.com/doi/pdf/10.1049/iet-opt.2016.0131. [Online]. Available: https://ietresearch.onlinelibrary.wiley.com/doi/abs/10.1049/iet-opt.2016.0131 (see page 3).
- [25] B. Majlesein, V. Matus, C. Jurado-Verdu, V. Guerra, J. Rabadan, and J. Rufo, Experimental characterization of sub-pixel underwater optical camera communications, in 2022 13th International Symposium on Communication Systems, Networks and Digital Signal Processing (CSNDSP), IEEE, 2022, 150–155 (see page 3).
- [26] E. Niarchou, V. Matus, R. Perez-Jimenez, J. Rabadan, and V. Guerra, Experimental evaluation of wearable LED strip for outdoor optical camera communications systems, in 2024 14th International Symposium on Communication Systems, Networks and Digital Signal Processing (CSNDSP), 2024, 621–625. DOI: 10.1109/CSNDSP60683.2024.10636549 (see pages 4, 5, 66).
- [27] O. I. Younus, E. Niarchou, S. R. Teli, Z. Ghassemlooy, S. Zvanovec, and H. Le Minh, Near-Infrared based optical camera communications, in 2022 13th International Symposium on Communication Systems, Networks and Digital Signal Processing (CSNDSP), 2022, 11–15. DOI: 10.1109/CSNDSP54353.2022.9907899 (see page 4).

- [28] Statcounter, https://gs.statcounter.com/screen-resolution-stats/mobile/worldwide, Accessed: 2024-12-04 (see page 9).
- [29] R.-A. Dobre, R.-O. Preda, and R.-A. Badea, Robust OCC system optimized for low-frame-rate receivers, Sensors, vol. 22:no. 16, ISSN: 1424-8220. DOI: 10.3390/s22165938. [Online]. Available: https://www.mdpi.com/1424-8220/22/16/5938 (see page 9).
- [30] V. H. Nguyen, M. D. Thieu, H. Nguyen, and Y. M. Jang, Design and implementation of the mimo-cook scheme using an image sensor for long-range communication, Sensors, vol. 20:no. 8, ISSN: 1424-8220. DOI: 10.3390/s20082258. [Online]. Available: https://www.mdpi.com/1424-8220/20/8/2258 (see page 9).
- [31] D. Antolín, N. Medrano, B. Calvo, and F. Pérez, A wearable wireless sensor network for indoor smart environment monitoring in safety applications, Sensors, vol. 17:no. 2, ISSN: 1424-8220. DOI: 10.3390/s17020365. [Online]. Available: https://www.mdpi.com/1424-8220/17/2/365 (see page 9).
- [32] Y. Wang, S. Cang, and H. Yu, A survey on wearable sensor modality centred human activity recognition in health care, Expert Systems with Applications, vol. 137, 167–190, ISSN: 0957-4174. DOI: https://doi.org/10.1016/j.eswa.2019.04.057. [Online]. Available: https://www.sciencedirect.com/science/article/pii/S0957417419302878 (see page 9).
- [33] S. Majumder, T. Mondal, and M. J. Deen, Wearable sensors for remote health monitoring, Sensors, vol. 17:no. 1, ISSN: 1424-8220. DOI: 10.3390/s17010130. [Online]. Available: https://www.mdpi.com/1424-8220/17/1/130 (see page 9).
- [34] J. S. Heo, M. F. Hossain, and I. Kim, Challenges in design and fabrication of flexible/stretchable carbon- and textile-based wearable sensors for health monitoring: A critical review, Sensors, vol. 20:no. 14, ISSN: 1424-8220. DOI: 10.3390/s20143927. [Online]. Available: https://www.mdpi.com/1424-8220/20/14/3927 (see page 9).
- [35] S. Nasiri and M. R. Khosravani, Progress and challenges in fabrication of wearable sensors for health monitoring, Sensors and Actuators A: Physical, vol. 312, 112105, ISSN: 0924-4247. DOI: https://doi.org/10.1016/j.sna.2020.112105. [Online]. Available: https://www.sciencedirect.com/science/article/pii/S0924424720306361 (see page 9).
- [36] S. Kharche and J. Kharche, 6G intelligent healthcare framework: A review on role of technologies, challenges and future directions, *Journal of Mobile Multimedia*, vol. 19, 603– 644. DOI: 10.13052/jmm1550-4646.1931 (see page 9).
- [37] A. D. Valentine, T. A. Busbee, J. W. Boley, J. R. Raney, A. Chortos, A. Kotikian, J. D. Berrigan, M. F. Durstock, and J. A. Lewis, **Hybrid 3D printing of soft electronics**, *Advanced Materials*, vol. 29:no. 40, 1703817. DOI: https://doi.org/10.1002/adma.201703817. eprint: https://advanced.onlinelibrary.wiley.com/doi/pdf/10.1002/adma.201703817. [Online]. Available: https://advanced.onlinelibrary.wiley.com/doi/abs/10.1002/adma.201703817 (see page 9).
- [38] N.-W. Lo and A. Yohan, BLE-based authentication protocol for micropayment using wearable device, Wireless Personal Communications, vol. 112:no. 4, 2351–2372, ISSN: 1572-834X. DOI: 10.1007/s11277-020-07153-0. [Online]. Available: https://doi.org/10.1007/s11277-020-07153-0 (see page 10).
- [39] T. Hoang, S. Sahuguede, and A. Julien-Vergonjanne, Optical wireless network design for off-body-sensor based monitoring, Wireless Communications and Mobile Computing, vol. 2019, 1–13. DOI: 10.1155/2019/5473923 (see page 10).
- [40] J. Hasan, M.-A. Khalighi, J. Garcia-Marquez, and B. Béchadergue, Performance analysis of optical-CDMA for uplink transmission in medical Extra-WBANs, IEEE Access, vol. 8, 171672. DOI: 10.1109/ACCESS.2020.3025005 (see page 10).
- [41] M. F. Ahmed, M. K. Hasan, M. Shahjalal, M. M. Alam, and Y. M. Jang, Design and implementation of an OCC-based real-time heart rate and pulse-oxygen saturation monitoring system, *IEEE Access*, vol. 8, 198740–198747. DOI: 10.1109/ACCESS.2020. 3034366 (see page 10).

- [42] V. P. Rachim, J. An, P. N. Quan, and W.-Y. Chung, A novel smartphone camera-LED communication for clinical signal transmission in mhealth-rehabilitation system, in 2017 39th Annual International Conference of the IEEE Engineering in Medicine and Biology Society (EMBC), 2017, 3437–3440. DOI: 10.1109/EMBC.2017.8037595 (see page 10).
- [43] H. Herfandi, O. S. Sitanggang, M. R. A. Nasution, H. Nguyen, and Y. M. Jang, Real-time patient indoor health monitoring and location tracking with optical camera communications on the internet of medical things, *Applied Sciences*, vol. 14:no. 3, ISSN: 2076-3417. DOI: 10.3390/app14031153. [Online]. Available: https://www.mdpi.com/2076-3417/14/3/1153 (see pages 10, 15).
- [44] M. K. Hasan, M. Shahjalal, M. Z. Chowdhury, and Y. M. Jang, Real-time healthcare data transmission for remote patient monitoring in patch-based hybrid OCC/BLE networks, Sensors, vol. 19:no. 5, ISSN: 1424-8220. DOI: 10.3390/s19051208. [Online]. Available: https://www.mdpi.com/1424-8220/19/5/1208 (see page 11).
- [45] M. K. Hasan, M. Shahjalal, M. Chowdhury, and Y. M. Jang, Access point selection in hybrid OCC/RF eHealth architecture for real-time remote patient monitoring, in, Oct. 2018. DOI: 10.1109/ICTC.2018.8539582 (see page 11).
- [46] H. Mohammadi-Abdar, A. L. Ridgel, F. M. Discenzo, R. S. Phillips, B. L. Walter, and K. A. Loparo, Test and validation of a smart exercise bike for motor rehabilitation in individuals with parkinson's disease, *IEEE Transactions on Neural Systems and Rehabilitation Engineering*, vol. 24:no. 11, 1254–1264. DOI: 10.1109/TNSRE.2016.2549030 (see page 12).
- [47] C. Tan, C. Xiao, and W. Wang, Camera-based cardiovascular screening based on heart rate and its variability in pre- and post-exercise conditions, in 2023 45th Annual International Conference of the IEEE Engineering in Medicine & Biology Society (EMBC), 2023, 1–5. DOI: 10.1109/EMBC40787.2023.10340871 (see page 12).
- [48] K. Xie, C.-H. Fu, H. Liang, H. Hong, and X. Zhu, Non-contact heart rate monitoring for intensive exercise based on singular spectrum analysis, in 2019 IEEE Conference on Multimedia Information Processing and Retrieval (MIPR), 2019, 228–233. DOI: 10.1109/ MIPR.2019.00048 (see page 12).
- [49] M. Mertens, G. Debard, J. Davis, E. Devriendt, K. Milisen, J. Tournoy, T. Croonenborghs, and B. Vanrumste, Motion sensor-based detection of outlier days supporting continuous health assessment for single older adults, Sensors, vol. 21:no. 18, ISSN: 1424-8220. DOI: 10.3390/s21186080. [Online]. Available: https://www.mdpi.com/1424-8220/21/18/6080 (see page 12).
- [50] L. Huang and G. Liu, Functional motion detection based on artificial intelligence, The Journal of Supercomputing, vol. 78:no. 3, 4290–4329, ISSN: 1573-0484. DOI: 10.1007/s11227-021-04037-3. [Online]. Available: https://doi.org/10.1007/s11227-021-04037-3 (see page 12).
- [51] R.-E. Mastoras, D. Iakovakis, S. Hadjidimitriou, V. Charisis, S. Kassie, T. Alsaadi, A. Khandoker, and L. J. Hadjileontiadis, Touchscreen typing pattern analysis for remote detection of the depressive tendency, *Scientific Reports*, vol. 9:no. 1, 13414, ISSN: 2045-2322. DOI: 10.1038/s41598-019-50002-9. [Online]. Available: https://doi.org/10.1038/s41598-019-50002-9 (see page 12).
- [52] A. Hoeijmakers, G. Licitra, K. Meijer, K.-H. Lam, P. Molenaar, E. Strijbis, and J. Killestein, Disease severity classification using passively collected smartphone-based keystroke dynamics within multiple sclerosis, *Scientific Reports*, vol. 13:no. 1, 1871, ISSN: 2045-2322. DOI: 10.1038/s41598-023-28990-6. [Online]. Available: https://doi.org/10.1038/s41598-023-28990-6 (see page 12).
- [53] S. Lim, C. Kim, B. H. Cho, S.-H. Choi, H. Lee, and D. P. Jang, Investigation of daily patterns for smartphone keystroke dynamics based on loneliness and social isolation, *Biomedical Engineering Letters*, vol. 14:no. 2, 235–243, ISSN: 2093-985X. DOI: 10.1007/s13534-023-00337-0. [Online]. Available: https://doi.org/10.1007/s13534-023-00337-0 (see page 12).

- [54] V. L. Nguyen, D. H. Tran, H. Nguyen, and Y. M. Jang, An experimental demonstration of MIMO C-OOK scheme based on deep learning for optical camera communication system, Applied Sciences, vol. 12:no. 14, ISSN: 2076-3417. DOI: 10.3390/app12146935. [Online]. Available: https://www.mdpi.com/2076-3417/12/14/6935 (see pages 13, 15).
- [55] D. K. Vishwakarma and T. Singh, A visual cognizance based multi-resolution descriptor for human action recognition using key pose, AEU International Journal of Electronics and Communications, vol. 107, 157–169, ISSN: 1434-8411. DOI: https://doi.org/10.1016/j.aeue.2019.05.023. [Online]. Available: https://www.sciencedirect.com/science/article/pii/S1434841119303942 (see page 13).
- [56] M. Nallasivam and V. Senniappan, Moving human target detection and tracking in video frames, Studies in informatics and control, vol. 30:no. 1, 119–129 (see page 13).
- [57] P. Ma, C. Li, M. M. Rahaman, Y. Yao, J. Zhang, S. Zou, X. Zhao, and M. Grzegorzek, A state-of-the-art survey of object detection techniques in microorganism image analysis: From classical methods to deep learning approaches, *Artificial Intelligence Review*, vol. 56:no. 2, 1627–1698 (see page 14).
- [58] S. Minaee, Y. Boykov, F. Porikli, A. Plaza, N. Kehtarnavaz, and D. Terzopoulos, Image segmentation using deep learning: A survey, IEEE transactions on pattern analysis and machine intelligence, vol. 44:no. 7, 3523–3542 (see page 14).
- [59] W. Luo, J. Xing, A. Milan, X. Zhang, W. Liu, and T.-K. Kim, Multiple object tracking: A literature review, Artificial intelligence, vol. 293, 103448 (see page 14).
- [60] K. Hu, J. Jin, F. Zheng, L. Weng, and Y. Ding, Overview of behavior recognition based on deep learning, Artificial intelligence review, vol. 56:no. 3, 1833–1865 (see page 14).
- [61] X. Zhao, L. Wang, Y. Zhang, X. Han, M. Deveci, and M. Parmar, A review of convolutional neural networks in computer vision, Artificial Intelligence Review, vol. 57:no. 4, 99 (see pages 14, 19).
- [62] L. Chen, S. Wang, W. Fan, J. Sun, and S. Naoi, Beyond human recognition: A CNN-based framework for handwritten character recognition, in 2015 3rd IAPR Asian Conference on Pattern Recognition (ACPR), IEEE, 2015, 695–699 (see page 14).
- [63] M. A. Haque, A. Verma, J. S. R. Alex, and N. Venkatesan, Experimental evaluation of CNN architecture for speech recognition, in First International Conference on Sustainable Technologies for Computational Intelligence: Proceedings of ICTSCI 2019, Springer, 2020, 507–514 (see page 14).
- [64] M. Ramesh and K. Mahesh, A performance analysis of pre-trained neural network and design of CNN for sports video classification, in 2020 International Conference on Communication and Signal Processing (ICCSP), 2020, 0213–0216. DOI: 10.1109/ICCSP48568.2020.9182113 (see page 14).
- [65] S. Pagare and R. Kumar, Human activity recognition and classification systems using yolov9, in 2024 International Conference on Intelligent Systems and Advanced Applications (ICISAA), 2024, 1–8. DOI: 10.1109/ICISAA62385.2024.10829230 (see pages 14, 15).
- [66] G. L. Santos, P. T. Endo, K. H. d. C. Monteiro, E. d. S. Rocha, I. Silva, and T. Lynn, Accelerometer-based human fall detection using convolutional neural networks, Sensors, vol. 19:no. 7, ISSN: 1424-8220. DOI: 10.3390/s19071644. [Online]. Available: https://www.mdpi.com/1424-8220/19/7/1644 (see page 14).
- [67] É. Zablocki, H. Ben-Younes, P. Pérez, and M. Cord, Explainability of deep vision-based autonomous driving systems: Review and challenges, International Journal of Computer Vision, vol. 130:no. 10, 2425–2452 (see page 14).
- [68] J. Xiong, E.-L. Hsiang, Z. He, T. Zhan, and S.-T. Wu, Augmented reality and virtual reality displays: Emerging technologies and future perspectives, Light: Science & Applications, vol. 10:no. 1, 1–30 (see page 14).
- [69] C. Huang, Z. Wu, J. Wen, Y. Xu, Q. Jiang, and Y. Wang, Abnormal event detection using deep contrastive learning for intelligent video surveillance system, IEEE Transactions on Industrial Informatics, vol. 18:no. 8, 5171–5179 (see page 14).

- [70] T. L. Pham, H. Nguyen, T. Nguyen, and Y. M. Jang, A novel neural network-based method for decoding and detecting of the DS8-PSK Scheme in an OCC system, Applied Sciences, vol. 9:no. 11, ISSN: 2076-3417. DOI: 10.3390/app9112242. [Online]. Available: https://www.mdpi.com/2076-3417/9/11/2242 (see page 14).
- [71] W. A. Cahyadi and Y. H. Chung, Smartphone camera-based device-to-device communication using neural network-assisted high-density modulation, Optical Engineering, vol. 57:no. 9, 096102–096102 (see page 14).
- [72] M. S. Ifthekhar, N. Saha, and Y. M. Jang, Neural network based indoor positioning technique in optical camera communication system, in 2014 International Conference on Indoor Positioning and Indoor Navigation (IPIN), 2014, 431–435. DOI: 10.1109/IPIN.2014.7275513 (see page 14).
- [73] S. R. Teli, W. A. Cahyadi, and Y. H. Chung, Trained neurons-based motion detection in optical camera communications, Optical Engineering, vol. 57:no. 4, 040501. DOI: 10.1117/1.OE.57.4.040501. [Online]. Available: https://doi.org/10.1117/1.OE.57.4.040501 (see page 14).
- [74] M. S. Ifthekhar, N. Saha, and Y. M. Jang, Stereo-vision-based cooperative-vehicle positioning using OCC and neural networks, Optics Communications, vol. 352, 166–180, ISSN: 0030-4018. DOI: https://doi.org/10.1016/j.optcom.2015.04.067. [Online]. Available: https://www.sciencedirect.com/science/article/pii/S0030401815003569 (see page 14).
- [75] A. Islam, M. T. Hossan, and Y. M. Jang, Convolutional neural networks scheme–based optical camera communication system for intelligent internet of vehicles, International Journal of Distributed Sensor Networks, vol. 14:no. 4, 1550147718770153. DOI: 10.1177/1550147718770153. eprint: https://doi.org/10.1177/1550147718770153. [Online]. Available: https://doi.org/10.1177/1550147718770153 (see page 14).
- [76] K. Yu, J. He, and Z. Huang, Decoding scheme based on CNN for mobile optical camera communication, Appl. Opt., vol. 59:no. 23, 7109–7113. DOI: 10.1364/AO.395717. [Online]. Available: https://opg.optica.org/ao/abstract.cfm?URI=ao-59-23-7109 (see page 14).
- [77] S. Park and H. Lee, Deep learning approach to optical camera communication receiver design, in 2021 IEEE Region 10 Symposium (TENSYMP), 2021, 1–5. DOI: 10.1109 / TENSYMP52854.2021.9550896 (see page 14).
- [78] J. Redmon, You only look once: Unified, real-time object detection, in Proceedings of the IEEE conference on computer vision and pattern recognition, 2016 (see page 15).
- [79] J. Redmon, S. Divvala, R. Girshick, and A. Farhadi, You only look once: Unified, real-time object detection, in 2016 IEEE Conference on Computer Vision and Pattern Recognition (CVPR), 2016, 779–788. DOI: 10.1109/CVPR.2016.91 (see page 15).
- [80] T. Ahmad, Y. Ma, M. Yahya, B. Ahmad, S. Nazir, and A. u. Haq, Object detection through modified YOLO neural network, Scientific Programming, vol. 2020:no. 1, 8403262. DOI: https://doi.org/10.1155/2020/8403262. eprint: https://onlinelibrary.wiley.com/doi/pdf/10. 1155/2020/8403262. [Online]. Available: https://onlinelibrary.wiley.com/doi/abs/10.1155/2020/8403262 (see page 15).
- [81] H. H. Nguyen, T. N. Ta, N. C. Nguyen, H. M. Pham, D. M. Nguyen, et al., Yolo based real-time human detection for smart video surveillance at the edge, in 2020 IEEE eighth international conference on communications and electronics (ICCE), IEEE, 2021, 439–444 (see page 15).
- [82] L. Zhao and S. Li, Object detection algorithm based on improved YOLOv3, Electronics, vol. 9:no. 3, ISSN: 2079-9292. DOI: 10.3390/electronics9030537. [Online]. Available: https://www.mdpi.com/2079-9292/9/3/537 (see page 15).
- [83] C. Kumar B., R. Punitha, and Mohana, YOLOv3 and YOLOv4: Multiple object detection for surveillance applications, in 2020 Third International Conference on Smart Systems and Inventive Technology (ICSSIT), 2020, 1316–1321. DOI: 10.1109/ICSSIT48917.2020.9214094 (see page 15).

- [84] M. T. Kim and B. W. Kim, DeepCCB-OCC: Deep learning-driven complementary color barcode-based optical camera communications, Applied Sciences, vol. 12:no. 21, ISSN: 2076-3417. DOI: 10.3390/app122111239. [Online]. Available: https://www.mdpi.com/2076-3417/12/21/11239 (see page 15).
- [85] C. Gupta, N. S. Gill, P. Gulia, and J. M. Chatterjee, A novel finetuned YOLOv6 transfer learning model for real-time object detection, Journal of Real-Time Image Processing, vol. 20:no. 3, 42, ISSN: 1861-8219. DOI: 10.1007/s11554-023-01299-3. [Online]. Available: https://doi.org/10.1007/s11554-023-01299-3 (see page 15).
- [86] H. Zhenyu, Research on small target detection in optical remote sensing based on YOLOv7, in 2023 IEEE International Conference on Sensors, Electronics and Computer Engineering (ICSECE), 2023, 804–809. DOI: 10.1109/ICSECE58870.2023.10263365 (see page 15).
- [87] O. S. Sitanggang, V. L. Nguyen, H. Nguyen, R. F. Pamungkas, M. M. Faridh, and Y. M. Jang, Design and implementation of a 2D MIMO OCC system based on deep learning, Sensors, vol. 23:no. 17, 7637 (see pages 15, 19).
- [88] H. Nguyen and Y. M. Jang, An experimental demonstration of 2D-MIMO based deep learning for OCC system, in 2024 Fifteenth International Conference on Ubiquitous and Future Networks (ICUFN), 2024, 165–168. DOI: 10.1109/ICUFN61752.2024.10624750 (see page 15).
- [89] A. R. Khekan, H. S. Aghdasi, and P. Salehpour, The impact of YOLO algorithms within fall detection application: A review, IEEE Access, vol. 13, 6793–6809. DOI: 10.1109/ACCESS. 2024.3496823 (see pages 15, 21).
- [90] V. Breive and T. Sledevic, Person detection in thermal images: A comparative analysis of YOLOv8 and YOLOv9 models, in 2024 IEEE Open Conference of Electrical, Electronic and Information Sciences (eStream), 2024, 1–4. DOI: 10.1109/eStream61684.2024.10542600 (see page 15).
- [91] M. Bakirci and I. Bayraktar, **YOLOv9-enabled vehicle detection for urban security and forensics applications**, in *2024 12th International Symposium on Digital Forensics and Security (ISDFS)*, 2024, 1–6. DOI: 10.1109/ISDFS60797.2024.10527304 (see page 15).
- [92] Y. Li, W. Leong, and H. Zhang, YOLOv10-based real-time pedestrian detection for autonomous vehicles, in 2024 IEEE 8th International Conference on Signal and Image Processing Applications (ICSIPA), 2024, 1–6. DOI: 10.1109/ICSIPA62061.2024.10686546 (see page 15).
- [93] S. Sriram, A. P., A. K. T. P., N. Vijayaraj, and T. Murugan, Enhanced YOLOv10 framework featuring dpam and dalsm for real-time underwater object detection, *IEEE Access*, vol. 13, 8691–8708. DOI: 10.1109/ACCESS.2025.3527315 (see page 16).
- [94] X. Ji, Z. Yue, H. Yang, and Z. Zhang, Infrared image classification and detection algorithm for power equipment based on improved YOLOv10, IEEE Access, vol. 12, 184976–184988. DOI: 10.1109/ACCESS.2024.3514103 (see page 16).
- [95] Y. Li, H. Yan, D. Li, and H. Wang, Robust miner detection in challenging underground environments: An improved YOLOv11 approach, Applied Sciences, vol. 14:no. 24, ISSN: 2076-3417. DOI: 10.3390/app142411700. [Online]. Available: https://www.mdpi.com/2076-3417/14/24/11700 (see pages 16, 21).
- [96] N. Chi, LED-based visible light Communications. Springer, 2018, vol. 245 (see pages 17, 23).
- [97] N. D. Mankowska, A. B. Marcinkowska, M. Waskow, R. I. Sharma, J. Kot, and P. J. Winklewski, Critical flicker fusion frequency: A narrative review, Medicina (Kaunas), vol. 57:no. 10, 1096. DOI: 10.3390/medicina57101096 (see page 17).
- [98] T.-C. Bui, R. Cusani, G. Scarano, and M. Biagi, Metameric MIMO-OOK transmission scheme using multiple RGB LEDs, Opt. Express, vol. 26:no. 11, 14038–14050. DOI: 10.1364/OE.26. 014038. [Online]. Available: https://opg.optica.org/oe/abstract.cfm?URI=oe-26-11-14038 (see page 17).

- [99] P. Luo, M. Zhang, Z. Ghassemlooy, S. Zvanovec, S. Feng, and P. Zhang, Undersampled-based modulation schemes for optical camera communications, IEEE Communications Magazine, vol. 56:no. 2, 204–212 (see page 18).
- [100] C. Danakis, M. Afgani, G. Povey, I. Underwood, and H. Haas, Using a CMOS camera sensor for visible light communication, in 2012 IEEE Globecom Workshops, 2012, 1244–1248. DOI: 10.1109/GLOCOMW.2012.6477759 (see pages 18, 24).
- [101] N. Rajagopal, P. Lazik, and A. Rowe, **Visual light landmarks for mobile devices**, in *IPSN-14 Proceedings of the 13th International Symposium on Information Processing in Sensor Networks*, 2014, 249–260. DOI: 10.1109/IPSN.2014.6846757 (see page 18).
- [102] V. N. Yokar, Hoa-Le-Minh, F. Ghassemlooy, and W. L. Woo, A novel blur reduction technique for QR and ASCII coding in smartphone visible light communications, in 2022 13th International Symposium on Communication Systems, Networks and Digital Signal Processing (CSNDSP), 2022, 428–433. DOI: 10.1109/CSNDSP54353.2022.9907993 (see page 18).
- [103] V. Nguyen, Y. Tang, A. Ashok, M. Gruteser, K. Dana, W. Hu, E. Wengrowski, and N. Mandayam, High-rate flicker-free screen-camera communication with spatially adaptive embedding, in IEEE INFOCOM 2016 The 35th Annual IEEE International Conference on Computer Communications, 2016, 1–9. DOI: 10.1109/INFOCOM.2016.7524512 (see page 18).
- [104] D. Wang and M. Zhang, Artificial intelligence in optical communications: From machine learning to deep learning, Frontiers in Communications and Networks, vol. 2, ISSN: 2673-530X. DOI: 10.3389/frcmn.2021.656786. [Online]. Available: https://www.frontiersin.org/journals/communications-and-networks/articles/10.3389/frcmn.2021.656786 (see page 19).
- [105] M. Amirabadi, S. Nezamalhosseini, M. Kahaei, and L. R. Chen, **A survey on machine and deep learning for optical communications**, arXiv preprint arXiv:2412.17826 (see page 19).
- [106] DeepMind, *Deepmind research*, Accessed: 2025-02-05, 2025. [Online]. Available: https://deepmind.google/research/ (see page 19).
- [107] T. Carneiro, R. V. Medeiros Da NóBrega, T. Nepomuceno, G.-B. Bian, V. H. C. De Albuquerque, and P. P. R. Filho, Performance analysis of Google colaboratory as a tool for accelerating deep learning applications, *IEEE Access*, vol. 6, 61677–61685. DOI: 10.1109/ACCESS.2018. 2874767 (see page 19).
- [108] IBM, *Neural processing unit (NPU)*, Accessed: 2025-02-05, 2025. [Online]. Available: https://www.ibm.com/think/topics/neural-processing-unit (see page 19).
- [109] K. Yadav, S. Bidnyk, and A. Balakrishnan, Artificial intelligence and machine learning in optics: Tutorial, J. Opt. Soc. Am. B, vol. 41:no. 8, 1739–1753. DOI: 10.1364/JOSAB.525182. [Online]. Available: https://opg.optica.org/josab/abstract.cfm?URI=josab-41-8-1739 (see page 19).
- [110] C. Jurado-Verdu, V. Guerra, J. Rabadan, and R. Perez-Jimenez, Deep learning for signal clock and exposure estimation in rolling shutter optical camera communication, *Opt. Express*, vol. 30:no. 12, 20261–20277. DOI: 10.1364/OE.458538. [Online]. Available: https://opg.optica.org/oe/abstract.cfm?URI=oe-30-12-20261 (see page 19).
- [111] P. Ling, M. Li, and W. Guan, Channel-attention-enhanced LSTM neural network decoder and equalizer for RSe-based optical camera communications, *Electronics*, vol. 11:no. 8, ISSN: 2079-9292. DOI: 10.3390/electronics11081272. [Online]. Available: https://www.mdpi.com/2079-9292/11/8/1272 (see page 19).
- [112] M. A. Chandra and S. Bedi, Survey on SVM and their application in image classification, International Journal of Information Technology, vol. 13:no. 5, 1–11 (see page 19).
- [113] M. F. Ansari and K. A. Lodi, A survey of recent trends in two-stage object detection methods, in *Renewable Power for Sustainable Growth*, A. Iqbal, H. Malik, A. Riyaz, K. Abdellah, and S. Bayhan, Eds., Singapore: Springer Singapore, 2021, 669–677, ISBN: 978-981-33-4080-0 (see page 20).

- [114] T. Diwan, G. Anirudh, and J. V. Tembhurne, Object detection using YOLO: Challenges, architectural successors, datasets and applications, Multimedia Tools and Applications, vol. 82:no. 6, 9243–9275, ISSN: 1573-7721. DOI: 10.1007/s11042-022-13644-y. [Online]. Available: https://doi.org/10.1007/s11042-022-13644-y (see page 20).
- [115] S. Patil, S. Waghule, S. Waje, P. Pawar, and S. Domb, Efficient object detection with YOLO: A comprehensive guide, International Journal of Advanced Research in Science, Communication and Technology, 519–531. DOI: 10.48175/IJARSCT-18483 (see page 20).
- [116] A. Vijayakumar and S. Vairavasundaram, YOLO-based object detection models: A review and its applications, *Multimedia Tools and Applications*, vol. 83:no. 35, 83535–83574, ISSN: 1573-7721. DOI: 10.1007/s11042-024-18872-y. [Online]. Available: https://doi.org/10.1007/s11042-024-18872-y (see page 20).
- [117] H. Rezatofighi, N. Tsoi, J. Gwak, A. Sadeghian, I. Reid, and S. Savarese, **Generalized** intersection over union: A metric and a loss for bounding box regression, in *Proceedings* of the IEEE/CVF conference on computer vision and pattern recognition, 2019, 658–666 (see page 21).
- [118] Z. Wang, Q. Wang, W. Huang, and Z. Xu, Visible light communications: modulation and signal processing. John Wiley & Sons, 2017 (see page 23).
- [119] Z. Ghassemlooy, L. N. Alves, S. Zvanovec, and M.-A. Khalighi, Visible light communications: theory and applications. CRC press, 2017 (see pages 23, 29).
- [120] N. Waltham, 423–442, in, *Observing Photons in Space: A Guide to Experimental Space Astronomy*, M. C. E. Huber, A. Pauluhn, J. L. Culhane, J. G. Timothy, K. Wilhelm, and A. Zehnder, Eds., New York, NY: Springer New York, 2013, ISBN: 978-1-4614-7804-1. DOI: 10.1007/978-1-4614-7804-1.23. [Online]. Available: https://doi.org/10.1007/978-1-4614-7804-1.23 (see page 23).
- [121] A. El Gamal and H. Eltoukhy, Cmos image sensors, IEEE Circuits and Devices Magazine, vol. 21:no. 3, 6–20. DOI: 10.1109/MCD.2005.1438751 (see page 23).
- [122] W. A. Cahyadi, Y. H. Chung, Z. Ghassemlooy, and N. B. Hassan, Optical camera communications: Principles, modulations, potential and challenges, *Electronics*, vol. 9:no. 9, 1339 (see page 23).
- [123] T. Le, N.-T. Le, and Y. M. Jang, Performance of rolling shutter and global shutter camera in optical camera communications, in 2015 International Conference on Information and Communication Technology Convergence (ICTC), 2015, 124–128. DOI: 10.1109/ICTC.2015. 7354509 (see page 24).
- [124] T. Nguyen, A. Islam, T. Hossan, and Y. M. Jang, Current status and performance analysis of optical camera communication technologies for 5G networks, *IEEE Access*, vol. 5, 4574–4594. DOI: 10.1109/ACCESS.2017.2681110 (see page 24).
- [125] B. W. Kim, J.-H. Yoo, and S.-Y. Jung, Design of streaming data transmission using rolling shutter camera-based optical camera communications, *Electronics*, vol. 9:no. 10, ISSN: 2079-9292. DOI: 10.3390/electronics9101561. [Online]. Available: https://www.mdpi.com/2079-9292/9/10/1561 (see page 24).
- [126] A. Nano, ATmega328 16 MHz, 2KB SRAM, 32KB flash, 1KB EEPROM. datasheet, Accessed: February 2025, 2023. [Online]. Available: https://docs.arduino.cc/resources/datasheets/ A000005-datasheet.pdf (see page 29).
- [127] Atmel, XIAO SAMD21, 32-bit 48MHz microcontroller (SAMD21G18) with 256KB flash, 32KB SRAM. datasheet, Accessed: February 2025, 2016 (see page 29).
- [128] Portable LED super bright flashlight USB rechargeable waterproof camping light magnet hook 5V output COB work light, Available online: https://es.aliexpress.com/item/1005003069560073.html?gatewayAdapt=glo2esp (Accessed on: February 2025) (see page 30).
- [129] L. Avenue, LA CW20WP6 LED chip cold white 20 mil. datasheet (see page 30).

- [130] SONY-semicon, *IMX477-AACK diagonal 7.853 mm (type 1/2.3) 12.3 mega-pixel CMOS image sensor with square pixel for color cameras*, Datasheet, 2018. [Online]. Available: https://www.sony-semicon.com/files/62/pdf/p-13\_IMX477-AACK\_Flyer.pdf (see page 31).
- [131] Roboflow, Roboflow, https://roboflow.com/, Accessed: 2024-09-20, 2024 (see page 33).
- [132] E. Niarchou, V. Matus, J. Rabadan, V. Guerra, and R. Perez-Jimenez, Optical camera communications in healthcare: A wearable LED transmitter evaluation during indoor physical exercise, Sensors, vol. 24:no. 9, ISSN: 1424-8220. DOI: 10.3390/s24092766. [Online]. Available: https://www.mdpi.com/1424-8220/24/9/2766 (see pages 37, 77).
- [133] E. Niarchou, V. Matus, J. Rabadan, V. Guerra, and R. Perez-Jimenez, Experimental evaluation of LED-based wearable transmitter for optical camera communications systems, in 2023 17th International Conference on Telecommunications (ConTEL), 2023, 1–5. DOI: 10.1109/ ConTEL58387.2023.10199043 (see page 38).
- [134] E. Niarchou, K. Eollos-Jarosikova, V. Matus, R. Perez-Jimenez, S. Zvanovec, M. Komanec, and J. Rabadan, Experimental evaluation of wearable LED strip and side-emitting fiber for optical camera communications systems, Opt. Express, vol. 32:no. 14, 25091–25103. DOI: 10.1364/OE.521967. [Online]. Available: https://opg.optica.org/oe/abstract.cfm?URI=oe-32-14-25091 (see pages 52, 77).
- [135] K. Eöllős-Jarošíková, V. Neuman, E. Niarchou, O. Gomez-Cardenes, S. Zvánovec, R. Perez-Jimenez, and M. Komanec, Pilot experiments of side-emitting fiber-based optical camera communication for wearable applications, in 2023 South American Conference On Visible Light Communications (SACVLC), 2023, 65–69. DOI: 10.1109/SACVLC59022.2023.10347578 (see page 52).
- [136] E. Niarchou, A. F. Usmani, V. Matus, J. Rabadan, V. Guerra, L. N. Alves, and R. Perez-Jimenez, Cnn-based human detection and identification in indoor optical camera communication systems using a wearable led strip, *IET Optoelectronics*, vol. 19:no. 1, e70005. DOI: https://doi.org/10.1049/ote2.70005. eprint: https://ietresearch.onlinelibrary.wiley.com/doi/pdf/10.1049/ote2.70005. [Online]. Available: https://ietresearch.onlinelibrary.wiley.com/doi/abs/10.1049/ote2.70005 (see pages 66, 77).
- [137] D. Moreno, V. Guerra, J. Rufo, J. Rabadan, and R. Perez-Jimenez, Multispectral optical camera communication links based on spectral signature multiplexing, *IET Optoelectronics*, vol. 17:no. 4, 91–100. DOI: https://doi.org/10.1049/ote2.12090. eprint: https://ietresearch.onlinelibrary.wiley.com/doi/pdf/10.1049/ote2.12090. [Online]. Available: https://ietresearch.onlinelibrary.wiley.com/doi/abs/10.1049/ote2.12090 (see page 80).
- [138] J. Aranda, V. Guerra, J. Rabadan, and R. Perez-Jimenez, Enhancing computational efficiency in event-based optical camera communication using N-pulse modulation, Electronics, vol. 13:no. 6, ISSN: 2079-9292. DOI: 10.3390/electronics13061047. [Online]. Available: https: //www.mdpi.com/2079-9292/13/6/1047 (see page 81).



## Conference proceedings

This appendix contains the author's articles, which were presented at conference proceedings during the thesis development. The following pages include the final camera-ready versions of these papers.

# Experimental Evaluation of LED-based Wearable Transmitter for Optical Camera Communications Systems

Eleni Niarchou\*, Vicente Matus\*, Jose Rabadan\*, Victor Guerra†, Rafael Perez-Jimenez\*

\*IDeTIC-ULPGC, Las Palmas de Gran Canaria, Spain

†Pi-Lighting, Valais, Switzerland

eleni.niarchou@ulpgc.es, vicente.matus@ulpgc.es, jrabadan@idetic.eu,

victor.guerra@pi-lighting.com, rperez@idetic.eu

Abstract-In this paper, we experimentally demonstrate an optical camera communications (OCC) system for wearable light-emitting diode (LED) as the transmitter. Wearable devices are powerful tools for supporting Internet of Things (IoT) systems because of their sensing, processing, and communication capability. The term "wearable devices" refers to a wide range of products that can be integrated into clothing and accessories, thus allowing real-time data detection, storage, and exchange without human intervention. This paper presents the practical evaluation of an LED-based wearable transmitter for an OCC system to demonstrate its feasibility. In particular, an LED array attached to the body is modulated using on-off keying to transmit data via visible light, and a smartphone camera captures video of the user wearing the device while slightly moving in a static position in the room. Finally, the data is decoded from the video frames using an image processing algorithm that tracks the source and demodulates the signal.

*Index Terms*—Optical camera communications (OCC), visible light communications (VLC), Internet of Things (IoT), wearable devices, image processing.

#### I. INTRODUCTION

Optical wireless communications (OWC) are an important field of research in mobile communication due to their low cost, high-speed, and reliable data transmission capability [1], and are already recognized as a complementary, and sometimes a viable alternative technology to radio-frequency (RF). Optical camera communications (OCC) is a promising OWC technology that uses a light-emitting diode as a transmitter  $(T_x)$ , an image sensor (IS) (i.e., camera) as receiver  $(R_x)$ , and light as the communication medium. OCC has several valuable features, including low cost, high security, low power consumption, and enhanced reliability. Furthermore, it is free from electromagnetic interference and thus entirely safe for human health [2]. The exponential growth in camera-mounted smart devices has enabled OCC to be utilized in innovative applications in both indoor and outdoor scenarios, such as in indoor positioning systems [3], and healthcare [2], [4]. The extensive deployment of smart devices (e.g., sensors, actuators, smartwatches, smartphones) connected to the Internet, represents a headstone for Internet of Things (IoT) systems [5].

Currently, smart clothes, smartwatches, and smartphones are considered conventional products that incorporate wearable technologies in human activity recognition [6]. Wearable devices can be integrated into clothes and accessories or directly attached to the human body, ensuring continuous, non-invasive, non-intrusive, and seamless surveillance of one's physiological condition and motion activities [7]. Wearable sensors can be defined as devices providing real-time data and biochemical monitoring, and biophysical tracking [6]. LEDs can be embedded in wearable devices and transmit data sensed from wearable sensors via visible or infrared light.

Up to now, only a few works have been done considering wearable sensors combined with LED as  $T_x$ . For instance, a medical sensor and an infrared LED are used for uplink transmission of medical data for patient monitoring in [8] and for indoor health monitoring assuming patient mobility in [9]. In addition, in [10], an all-optical bidirectional wireless communication system is used to evaluate the mobility and the position of the sensor on the body. Furthermore, in [11], the authors investigate the performance of optical code-division multiple access in asynchronous mode considering the effect of random transmitters' orientation.

Specifically, in OCC, a number of medical applications focused on wearable sensors for measuring health conditions have been developed. For instance, in [2] a system is implemented for real-time remote monitoring of patient's heart rate and oxygen saturation data, for monitoring the health conditions of the patient using a pulse oximeter sensor [4], and for transmission of multiple clinical data such as electrocardiogram, photoplethysmogram, and respiration signal [12]. In addition, OCC can be combined with other technologies, thus creating hybrid systems that complement the capabilities of each technology, making the systems more resilient [13]. In particular, in [14], it is combined with Bluetooth Low Energy (BLE) to ensure efficient, remote, and real-time transmission of a patient's electrocardiogram signal to a monitor, and in [15] for real-time health monitoring from the body sensors to the gateway. The authors consider that the motion of nodes in OCC can cause outage in the link and, therefore, BLE substitutes the communication in those cases.

Despite the several advances of the proposed systems, some challenges require further research and development to improve the performance of the monitoring system. First and foremost, the hardware design of the wearable device. The device must be adjustable to the human body, allowing data transmission without interfering user's activity. In addition, the characteristics of the commercially available LED device may limit the system's performance. For instance, the LED's power and size determine the maximum link distance. Therefore, the more power it has (e.g., high-intensity illumination) and the larger the illuminating area it is, the more easily it is detected by the camera. Furthermore, the smartphone's camera exposure time levels are limited compared with those provided by professional cameras. Hence, high-intensity LEDs can be captured by standard smartphone's camera.

In this work, we experimentally evaluate an LED-based wearable transmitter for OCC system assuming user's controlled movement, doing physical exercise in an indoor environment. Wearable LEDs have been modulated in intensity to transmit binary data to a smartphone camera at a frequency that is not detected by the human eye but is captured by the camera. The camera performs the tracking process produced by the user's movement and detects the data. The obtained results are focused on the transmitter detection and tracking challenge. For this purpose, we propose the use of a template signal that is transmitted by the LED  $T_x$  and detected in the image by a correlation process. The complexity of this process can be reduced by taking into account the characteristics of the movement generated by the controlled exercise activity, bounding the tracking process to a smaller area of the image.

The possible applications of the proposed activity monitoring system are home-based seated exercise, stationary bike, or treadmill, among others. The primary contribution of this work is the use of conventional and commercially available wearable devices (e.g., LEDs) and a smartphone for communication purposes. The proposed system could potentially allow people to lead independent and active lives in their familiar home environment in rehabilitation, sports, early detection of musculoskeletal or cognitive diseases, and fall and balance assessment.

The structure of the paper is organized as follows. In Section II, the methodology, materials, and methods that are used are analyzed. The experimental results obtained are discussed in Section III. Finally, Section IV draws the conclusions of this work.

#### II. PROPOSED SYSTEM

In this section, the equipment of both transmitting and receiving nodes implemented for the experimental setup is summarized. The methods (i.e., modulation, demodulation, and image processing) applied for the experimental setup are also explained.

The system implemented for the proposed experiment consisted of digital signal processing hardware and optical frontends. The  $T_x$  comprised of a regular LED device [16] with a diffuser connected to the digital output of a micro-controller

unit (MCU) (Seeeduino Xiao [17]), while the  $R_x$  by a smartphone [18] which is capturing video in a distance of 10-15 cm approximately. The  $T_x$  is worn by a person as shown in Fig. 1a, standing in a fixed position inside a room while slightly moving. Note all the measurements are performed under the indoor ambient light condition. The block diagram of the proposed OCC link is illustrated in Fig. 2. The most

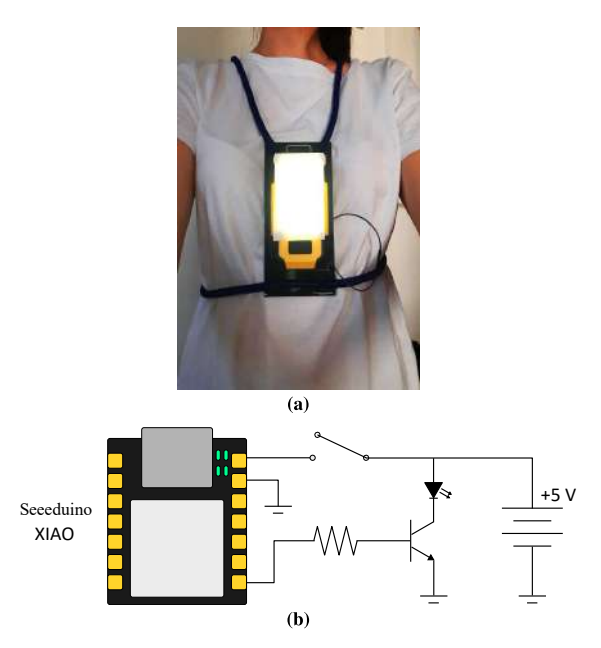


Fig. 1. (a) Wearable transmitter device. (b) Transmitter circuit.

relevant parameters of the experimental setup are summarized in Table I.

 $\label{eq:table I} \textbf{TABLE I}$  Parameters of the system and their values

Module	Parameter	Value	
$T_x$	Light source	LED array	
	Device dimensions	$11 \times 6.5 \times 3.5$ cm	
	Power supply	5 V	
	Transistor	NPN	
	Microcontroller	Seeeduino XIAO	
	Modulation frequency $f_{T_x}$	2.5 kHz	
	Data packet size	6b/packet [110100]	
$R_x$	Smartphone camera	Samsung Galaxy A51	
	Image sensor	Sony IMX582	
	Exposure time $t_{exp}$	Manually set to min.	
	Frame rate	30 fps	
	Resolution	$1080 \times 1920 \text{ px}$	
Channel	Link distance d	10-15 cm	

The proposed system uses data transmission with non-return-to-zero on-off keying (NRZ-OOK) modulation technique to send data over a short-range line-of-sight (LoS) free-space wireless channel. OOK is the simplest modulation scheme and is specialized for OCC [19]. Low '0' binary data will be represented by no carrier signal, which means the

Fig. 2. Block diagram of the transmitting and receiving node.

LED is OFF, while high '1' binary data will be represented by a carrier signal, which means the LED is ON [8]. This modulation exploits the switching digital outputs available in most MCUs, where the packet data is converted into a voltage signal that drives the LED directly. If the LED's current exceeds the MCU's maximum, a transistor connected to the power source must be implemented for driving the LED [20].

On the transmitting node, a regular LED device (comprised of 30 white LEDs) with rechargeable batteries is modified accordingly in order to drive the LED with a transistor powered directly from the battery terminals. Fig. 1b illustrates the transmitter's circuit implemented with an amplifier transistor circuit. The micro-controller generates a 6-bit data packet [110100] at a frequency  $f_{T_x}$  of 2.5 kHz (per bit) using a repeat-packet strategy to improve the link performance.

The smartphone camera captures a 30 fps frame-rate video, with exposure time  $t_{exp}$  manually set to minimum, using full resolution (1080  $\times$  1920 px) in rolling shutter (RS) mode. The RS-based cameras can capture the image row-by-row of pixels, which means that different lines of the image array are exposed at various times to read the light intensity through the sensor. This can cause motion blur when capturing fast-moving objects, but multiple states of LEDs (ON and OFF) can be obtained in a single frame [21]. The captured video is processed offline with Python, as presented in the  $R_x$ 's diagram in Fig. 2. First, the video is divided into frames. Then, one frame is selected and plotted, as shown in Fig. 3, and one template of 3 consecutive packets is generated.

Each packet on the template is a sequence of [110100] bits. Both template and frame images are converted into grayscale to retrieve the pixels' intensity profile. The correlation process slides the generated template image over the frame (as in 2D convolution) to detect the 2D position in the frame of the signal captured from the transmitting source. The blue line plot is the average row value and the red line is the plot of the template signal. The region of interest (ROI) in the frame where the template matches is drawn in Fig. 4. The same process is followed in all the frames. Afterward, the ROI is used for data decoding, as shown in Fig. 5. Following thresholding and binarization of the data acquired, we efficiently decode the received signal, Fig. 6. Finally, we calculate the signal to noise ratio (SNR) (1) as the ratio of the power of the obtained signal to the power of background noise, where  $\mu$  is the signal mean

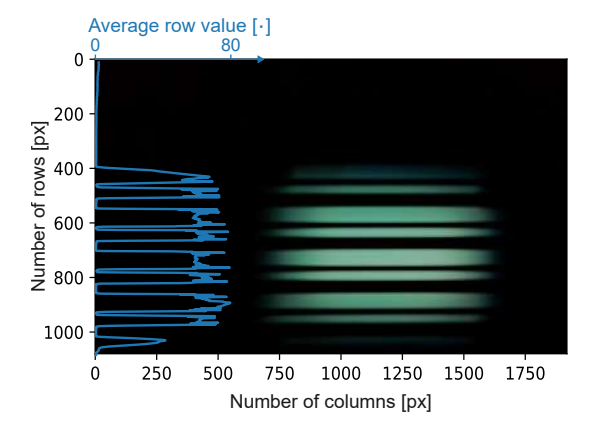


Fig. 3. Representation of the received signal in one image frame.

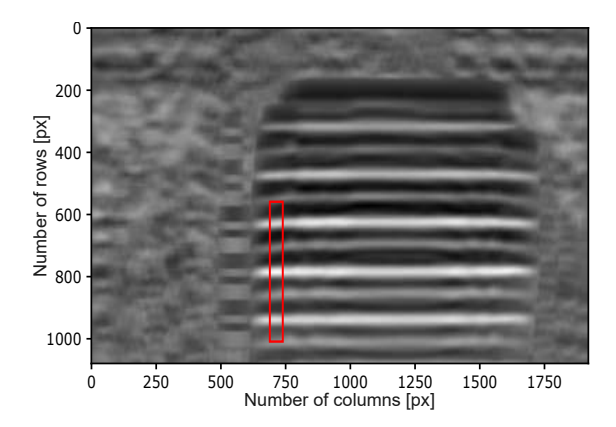


Fig. 4. Frame showing values obtained from the correlation coefficient between a random frame and the template. The region of interest (ROI) is highlighted in red.

value and  $\sigma$  the standard deviation of the noise. Note, the obtained power is the amplitude of the received signal over a certain threshold since the low received signal level values are zero. Therefore, the mean value and the standard deviation of high received signal level values are the average received

signal power and the noise power, respectively.

$$SNR_{dB} = 10 \log_{10}(\frac{\mu^2}{\sigma^2})$$
 (1)

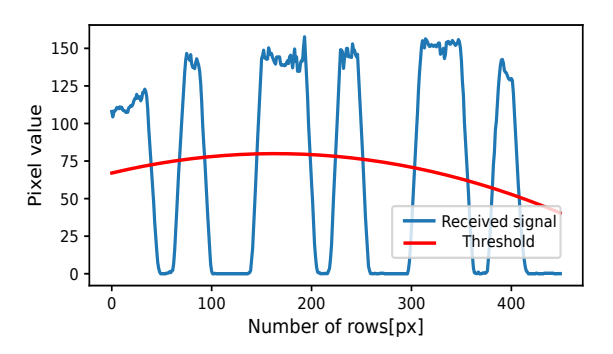


Fig. 5. Received signal and Threshold.

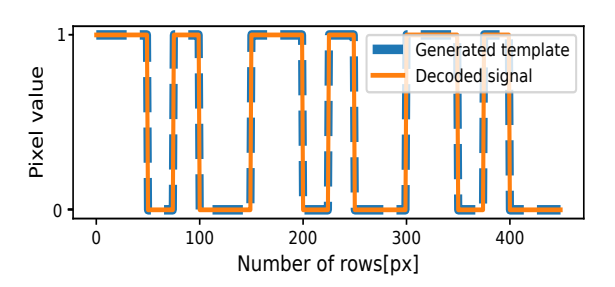


Fig. 6. Generated template and decoded signal.

#### III. RESULTS

In this section, we summarize the results obtained from the image processing algorithm applied to the video frames captured in the experiment described before.

From the obtained results, we can efficiently detect the transmitting source within all the frames and hence decode the received signal. The average calculated SNR is 22 dB. Moreover, the ROI can be bounded to a smaller region of the image frame as the source is detected in an area limited by the user's movement. For segregating the ROI, we used the detected coordinates of each template obtained by the correlation process in all the frames. The minimum and maximum values on the x and y-axis, as well as the width and height of the template, define the dimensions of the segregated ROI, which, for this case, it is  $734 \times 992$  px. Consequently, the correlation process can be focused on the vertical direction, as in the horizontal direction, the movement in the frames covers 2.6 times less area.

Note, the template transmission does not represent a real data transmission, but could become a header of a packet of real data collected by a sensor.

#### IV. CONCLUSION

In this paper, we experimentally evaluated a LED-based wearable  $T_x$  for an OCC link. The proposed system was tested using conventional devices, thus making it available for general use. This device could be a potential transmitter of health data of people in a medical, gym or home environment. Moreover, we proved that, despite the  $T_x$ 's movement, it is feasible to detect the transmitting source and thus reduce the ROI in the frames by achieving a significantly high average SNR.

Future research will include the implementation of wavelength division multiplexing technique where the template could serve as a beacon to send data with multiple light wavelengths. The  $T_x$ 's design could also be improved in terms of weight and seamless integration with the clothing piece, thus making it more convenient for the user. Last but not least, using the latest version of the smartphone, which captures video in less exposure time and with higher frame rates, could allow lower power consumption  $T_x$  in longer distances.

#### ACKNOWLEDGMENTS

This work has been supported by OCCAM project (PID2020-114561RB-100) and SUCCESS (TED2021-130049B-C21) from Agencia Estatal de Investigación (Spain Government), by Grant Catalina Ruiz (APCR2022010014) by the Agencia Canaria de Investigación, Innovación y Sociedad de la Información (ACIISI) under European Social Fund and by the European Union COST Action NEWFOCUS (CA19111).

#### REFERENCES

- M. Uysal, C. Capsoni, A. Boucouvalas, and E. Udvary, Optical Wireless Communications – An Emerging Technology, 01 2017.
- [2] M. F. Ahmed, M. K. Hasan, M. Shahjalal, M. M. Alam, and Y. M. Jang, "Design and implementation of an occ-based real-time heart rate and pulse-oxygen saturation monitoring system," *IEEE Access*, vol. 8, pp. 198 740–198 747, 2020.
- [3] B. Lin, Z. Ghassemlooy, C. Lin, X. Tang, Y. Li, and S. Zhang, "An indoor visible light positioning system based on optical camera communications," *IEEE Photonics Technology Letters*, vol. 29, no. 7, pp. 579–582, 2017.
- [4] M. F. Ahmed, M. O. Ali, M. H. Rahman, and Y. M. Jang, "Real-time health monitoring system design based on optical camera communication," in 2021 International Conference on Information Networking (ICOIN). IEEE, 2021, pp. 870–873.
- [5] A. Hamza and T. Tripp, "Optical Wireless Communication for the Internet of Things: Advances, Challenges, and Opportunities," 7 2020. [Online]. Available: https://www.techrxiv.org/articles/preprint/Optical\_ Wireless\_Communication\_for\_the\_Internet\_of\_Things\_Advances\_ Challenges and Opportunities/12659789
- [6] S. Nasiri and M. R. Khosravani, "Progress and challenges in fabrication of wearable sensors for health monitoring," *Sensors and Actuators A: Physical*, vol. 312, p. 112105, 2020.
- [7] S. Majumder, T. Mondal, and M. J. Deen, "Wearable sensors for remote health monitoring," *Sensors*, vol. 17, no. 1, p. 130, 2017.
- [8] T. Adiono, R. F. Armansyah, S. S. Nolika, F. D. Ikram, R. V. W. Putra, and A. H. Salman, "Visible light communication system for wearable patient monitoring device," in 2016 IEEE Region 10 Conference (TENCON), 2016, pp. 1969–1972.
- [9] C. Le Bas, T. B. Hoang, S. Sahuguede, and A. Julien-Vergonjanne, "Lighting fixture communicating in infrared and visible for indoor health monitoring," in 2017 IEEE 19th International Conference on e-Health Networking, Applications and Services (Healthcom), 2017, pp. 1–6.

#### **Chapter A** Conference proceedings

- [10] T. B. Hoang, S. Sahuguede, and A. Julien-Vergonjanne, "Optical wireless network design for off-body-sensor based monitoring," Wireless Communications and Mobile Computing, vol. 2019, 2019.
- [11] M. J. Hasan, M. A. Khalighi, J. García-Márquez, and B. Béchadergue, "Performance analysis of Optical-CDMA for uplink transmission in medical extra-WBANs," *IEEE Access*, vol. 8, pp. 171672–171685, 2020.
- [12] V. P. Rachim, J. An, P. N. Quan, and W.-Y. Chung, "A novel smartphone camera-LED communication for clinical signal transmission in mhealthrehabilitation system," in 2017 39th Annual International Conference of the IEEE Engineering in Medicine and Biology Society (EMBC). IEEE, 2017, pp. 3437–3440.
- [13] S. R. Teli, P. Chvojka, S. Vítek, S. Zvanovec, R. Perez-Jimenez, and Z. Ghassemlooy, "A simo hybrid visible-light communication system for optical iot," *IEEE Internet of Things Journal*, vol. 9, no. 5, pp. 3548–3558, 2022.
- [14] M. K. Hasan, M. Shahjalal, M. Z. Chowdhury, and Y. M. Jang, "Real-time healthcare data transmission for remote patient monitoring in patch-based hybrid OCC/BLE networks," *Sensors*, vol. 19, no. 5, p. 1208, 2019.

- [15] M. K. Hasan, M. Shahjalal, M. Chowdhury, and Y. M. Jang, "Access point selection in hybrid OCC/RF ehealth architecture for real-time remote patient monitoring," 10 2018.
- [16] Portable LED Super Bright Flashlight USB Rechargeable Waterproof Camping Light Magnet Hook 5V Output COB Work Light.
- [17] Atmel, XIAO SAMD21, 32bit 48MHz microcontroller(SAMD21G18) with 256KB Flash,32KB SRAM, Datasheet. Atmel, 2016.
- [18] Samsung Galaxy A51 Dual SIM (4GB/128GB). SAMSUNG.
- [19] V. Matus, V. Guerra, C. Jurado-Verdu, S. Zvanovec, and R. Perez-Jimenez, "Wireless sensor networks using sub-pixel optical camera communications: Advances in experimental channel evaluation," *Sensors*, vol. 21, no. 8, p. 2739, 2021.
- [20] V. Matus, V. Guerra, C. Jurado-Verdu, J. Rabadan, J. Rufo, and R. Perez-Jimenez, "Development of an experimental optical camera communication research setup," in 2022 4th West Asian Symposium on Optical and Millimeter-wave Wireless Communications (WASOWC), 2022, pp. 1-4.
- [21] T. Le, N.-T. Le, and Y. M. Jang, "Performance of rolling shutter and global shutter camera in optical camera communications," in 2015 International Conference on Information and Communication Technology Convergence (ICTC). IEEE, 2015, pp. 124–128.

2024 14th International Symposium on Communication Systems, Networks and Digital Signal Processing (CSNDSP)

## Experimental Evaluation of Wearable LED Strip for Outdoor Optical Camera Communications Systems

Eleni Niarchou\*, Vicente Matus\*, Rafael Perez-Jimenez\*, Jose Rabadan\*, Victor Guerra†

\*IDeTIC-ULPGC, Las Palmas de Gran Canaria, Spain

†Pi-Lighting, Valais, Switzerland

eleni.niarchou@ulpgc.es, vicente.matus@ulpgc.es, rperez@idetic.eu,

jrabadan@idetic.eu, victor.guerra@pi-lighting.com

Abstract—In this paper, we experimentally demonstrate an outdoor optical camera communications (OCC) system utilizing a wearable light-emitting diode (LED) as the transmitter. We explore the practicality of employing commercial devices, such as an LED strip and a smartphone, in OCC links for simultaneous monitoring and communication purposes. In particular, a strip of red-green-blue (RGB) LEDs is modulated to transmit data for user identification via visible light. Each color (red, green, blue and yellow) serves as an indicator of the user's status. Our system exhibits potential applications in high-risk environments where monitoring the physical well-being of individuals is crucial.

Index Terms—Optical camera communications (OCC), outdoor optical communications, wearable devices, image processing.

#### I. INTRODUCTION

Digital cameras are widespread consumer devices that not only perform tasks related to images, but also receive data from optical sources. The technology that uses a light-emitting diode (LED) as the transmitter  $(T_x)$ , an image sensor (IS) (i.e., camera) as the receiver  $(R_x)$ , and light as the communication medium, is known as optical camera communications (OCC) and has been studied within optical wireless communications (OWC), particularly within the IEEE 802.15.7a framework [1]. The plethora of cameras in end-user devices, such as smartphones and public infrastructure surveillance cameras, offers diverse functionalities, including data communications, localization, and motion identification within indoor and outdoor Internet of Things (IoT) [2].

OCC has been extensively studied in indoor scenarios with medical applications of great interest due to concerns about interference of radiofrequency (RF) signals with proper instrumentation performance. For instance, in [3], a home-based rehabilitation OCC system facilitates the transmission of various clinical data types, including electrocardiogram, photoplethysmogram, and respiration signals. In addition, in [4], a real-time remote monitoring OCC system has been developed to monitor a patient's heart rate and oxygen saturation data. Moreover, in [5] standard closed-circuit television (CCTV) setups incorporate deep learning-based OCC for the simultaneous monitoring of multiple patients. Other applications include smart homes [6] and industrial facilities [7].

In outdoor environments, OCC holds promise for supporting data reception in sensor networks, a use case often requiring low data rates, a large number of nodes, and a restricted energy budget. However, it can be affected by environmental phenomena. The feasibility of OCC in emulated outdoor conditions, such as fog and heat-induced turbulence, using commercially

available LEDs and cameras, has been demonstrated in [8]. Furthermore, in [9], subpixel OCC exhibits particularly suitable capabilities for wireless sensor network (WSN) applications, overcoming attenuation caused by various atmospheric conditions such as rain, turbulence, and the presence of aerosols. Moreover, [10] presents a practical implementation of a surveil-lance system capable of simultaneous video and data acquisition.

In the field of wearables, devices such as smartwatches, smartphones, or those seamlessly integrated into clothing or directly attached to the body (like glucose sensor patches) have become integral to our daily lives. These devices incorporate sensors for monitoring health and fitness data. When combined with LEDs, they have the potential to serve as transmitters in both indoor and outdoor OCC systems. In our earlier studies, we have evaluated the performance of a wearable LED array [11] and a fiber attached on T-shirt [12] as distributed transmitters.

This work exploits the feasibility of using commercial devices like LED strip and a smartphone in outdoor OCC links, for communication and monitoring purposes. The LED strips utilize various colors (red, green, blue, and yellow), with each color indicating the status of the user. Specifically, red signifies risk, green denotes safety, blue conveys other information, and yellow serves as a warning indicator. Each color encompasses details for user identification.

Our system has potential applications in high-risk environments where monitoring the physical well-being of individuals is crucial. This includes professions such as mining workers, factory workers, construction workers, ground crew in airports, and public safety personnel. Additionally, our technology is of relevance in rehabilitation centers and elderly care facilities. Integration of LEDs within uniforms not only enhances visibility and provides user comfort, but also enables seamless transmission of vital health metrics.

The structure of the paper is organized as follows. Section II provides details of the OCC system design and the experimental setup. Section III analyzes the experimental methodology and the results obtained. Lastly, Section IV presents the conclusions drawn from this work.

#### II. PROPOSED SYSTEM

In this section, we introduce the equipment utilized in the experimental setup for both transmitting and receiving nodes, as well as the modulation employed on the transmitting node.



2024 14th International Symposium on Communication Systems, Networks and Digital Signal Processing (CSNDSP)

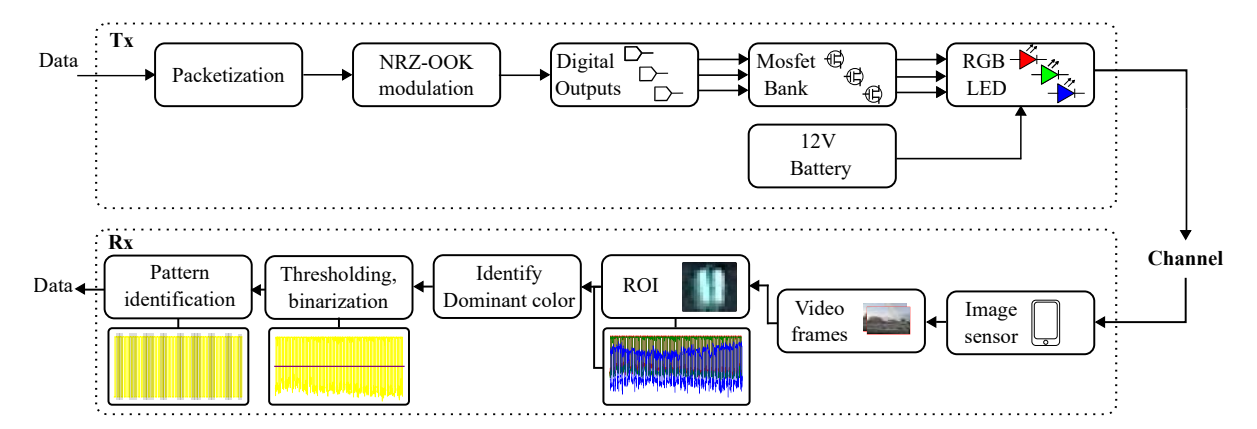


Fig. 1. Block diagram of the transmitting and receiving node.

The transmitting and receiving nodes that comprise the OCC link are illustrated in the block diagram in Fig. 1 and their key parameters are listed in Table I.

TABLE I EXPERIMENT KEY PARAMETERS.

Module	Parameter	Value	
	Light source	RGB LED strip (SMD 5050)	
$T_x$	Power supply	12 V	
	Microcontroller	Arduino Nano	
Modulation	Modulation frequency	3.8 Hz	
Modulation	Data pattern	[11010]	
	Smartphone camera	Samsung Galaxy S23	
$R_x$	Image sensor	S5KGN3	
$n_x$	Frame rate	60 fps	
	Resolution	1920 × 1080 px	
Channel	Link distance (static)	90 m	
Chamiei	Link distance (walking)	90 m to 120 m	

The  $T_x$  unit was built using a 10 mm wide strip of redgreen-blue (RGB) LEDs connected to the digital outputs of a microcontroller (Arduino Nano [13]) through a switching circuit based on transistors (mosfet bank). A 12 V rechargeable battery supplied power to both the LED strip and the circuit. The RGB LED strip was affixed to the front and back sides of a yellow safety jacket worn by an individual, as seen in Fig. 2. The circuitry induces the RGB channels to emit a repetitive beacon, characterized by a sequence of on-off pulses in the pattern [11010] at a frequency of 3.8 Hz for each of the RGB channels, including yellow.



Fig. 2. The wearable transmitter device.

On the receiving node, a smartphone camera of Samsung S23 [14], captures a 60 fps frame-rate video in  $1920 \times 1080$  px resolution. Typically, OCC systems take advantage of the rolling shutter (RS) acquisition mechanism of the camera, capturing images row-by-row [15]. However, in this experimental setup, we took advantage of the global shutter (GS) acquisition capability of the camera. This allowed for simultaneous communication during the actual video capture process.

#### III. EXPERIMENTAL METHODOLOGY AND RESULTS

In this section, we detail the types of measurements conducted and the image processing algorithm applied to the video frames captured. Finally, we present a summary of the results obtained from the image processing algorithm.

In this work, we conducted two types of measurements in an outdoor environment. Initially, static measurements involved the user with the wearable  $T_x$  standing at a distance of 90 m. Following that, walking measurements were performed with the user walking a distance of 500 m, maintaining a distance of 90 m to 120 m from the camera.

The output videos from the smartphone were processed of-fline using Python and segmented into 3000 frames. Each frame was cropped based on the type of measurement, specifically focusing on the transmitter's location within the frame. In static measurements, a region of interest (ROI) of  $18 \times 18$  px within the video frame sample was selected, as illustrated in Fig. 3 (a). For walking measurements, an ROI of  $690 \times 120$  px was chosen, covering the walking area within the frame, Fig. 3 (b). The map footprint is also included.

The RGB pixel values extracted from all ROIs in the frame samples to identify the dominant color of the transmission. For instance, the RGB pixel values corresponding to yellow color transmission are depicted in Fig. 4 (a) and in Fig. 5 (a) for static and walking measurements, respectively. Note that the yellow color in RGB is a combination of the red and green channels. Once the dominant color, in this case yellow, is identified, the pixel values corresponding to that color are utilized for data decoding. The pixel values for the yellow color in the static and walking measurements are respectively displayed in Fig. 4 (b) and Fig. 5 (b). Following color identification from all frame samples, a threshold and binarization of the received signal are applied to recognize the transmitted pattern. The frame samples where this pattern is successfully identified, are highlighted in Fig. 4 (c) for static measurement and in Fig. 5 (c) for walking measurement.

Repeating that process for each color transmission (red, green, blue, yellow), the results demonstrate efficient identification of the transmitted pattern for both static and walking measurements, as depicted in Table II. The 3000 frame samples, correspond to 50 s of transmission and a total of 38 patterns.

TABLE II
NUMBER OF PATTERN IDENTIFICATIONS IN EVERY COLOR TRANSMISSION,
FOR STATIC AND WALKING MEASUREMENTS.

Color	Static	Walking
Red	20	19
Green	19	20
Blue	20	20
Yellow	19	22

Regarding color transmission, based on the obtained values, we conclude that all colors exhibit a high level of effectiveness in pattern identification, in both static and walking measurements. Despite the fact that cameras have heightened sensitivity to red light, the yellow color, formed by a combination of red and green channels, shows the highest efficiency, with 22 instances of pattern identification.

Specifically, in static measurements, we observe that the efficiency of red and blue colors surpasses that of green and yellow. In contrast, during walking measurements, the yellow color slightly outperforms all other colors, while green, blue and red follow closely with 20 and 19 instances of pattern identification, respectively. Overall, the numbers of pattern identifications correspond to one pattern detection approximately every 2.5 s. The numbers of received patterns out of the total 38 transmitted patterns result in a success of reception (SoR) of 50 % [16].



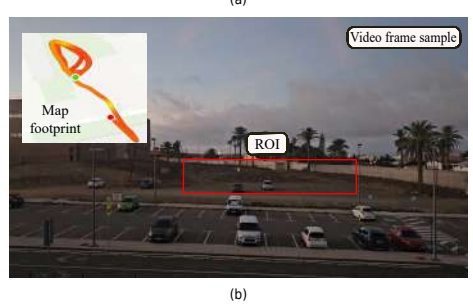


Fig. 3. The region of interest (ROI) corresponding to the transmitter's location in one video frame sample, is highlighted in red for (a) static measurements and (b) walking measurements.

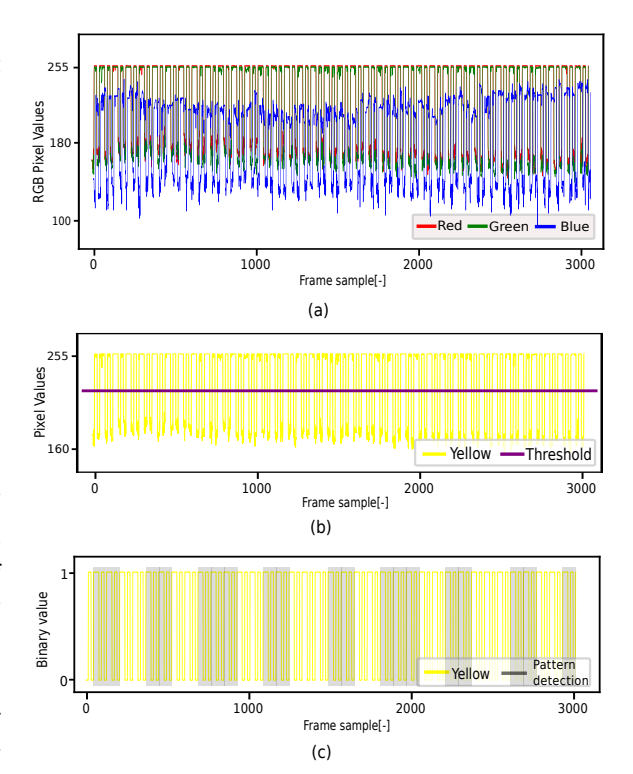


Fig. 4. Static measurement plots. (a) The red-green-blue (RGB) pixel values corresponding to the transmission of the yellow color, extracted from all frame samples. (b) Pixel values representing the yellow color, extracted from all frame samples with the threshold. (c) Binary values of yellow color, extracted from all frame samples, with highlighted the frames where the pattern is detected.

2024 14th International Symposium on Communication Systems, Networks and Digital Signal Processing (CSNDSP)

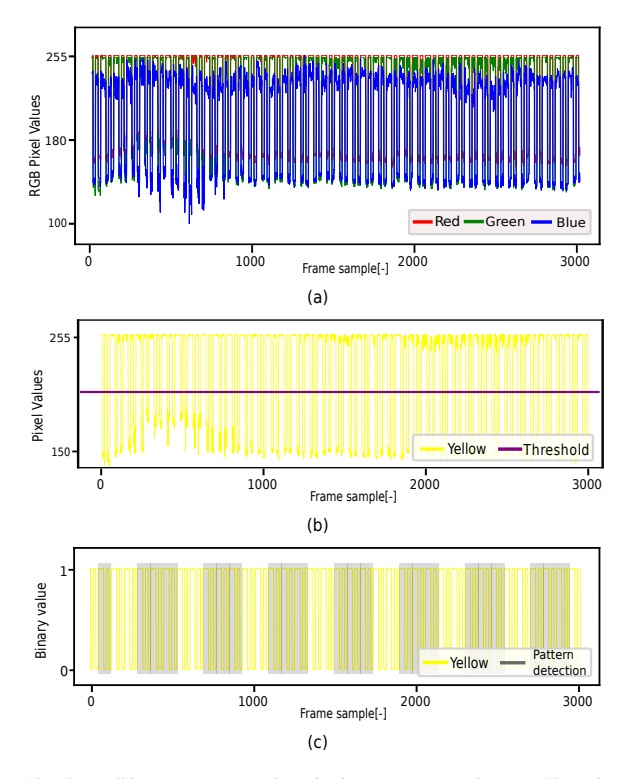


Fig. 5. Walking measurement plots. Static measurement plots. (a) The redgreen-blue (RGB) pixel values corresponding to the transmission of the yellow color, extracted from all frame samples. (b) Pixel values representing the yellow color, extracted from all frame samples with the threshold. (c) Binary values of yellow color, extracted from all frame samples, with highlighted the frames where the pattern is detected.

#### IV. CONCLUSION

In this paper, we explore the practicality of employing commercially available devices, such as LED strip and smartphone, in outdoor OCC for communication and monitoring applications. The LED strip incorporates different colors (red, green, blue, and yellow), each signifying the user's status. Within each color, the data includes information for user identification. The obtained results indicate that all colors exhibit a high level of effectiveness in pattern identification in both static and walking measurements. However, the SoR of 50%, is insufficient for bit error rate (BER) calculation. This can be improved by applying a matched filter in the signal processing.

For the implementation of an outdoor or indoor OCC system for simultaneous video streaming and data acquisition, there are several challenges that should be addressed. The transmitting nodes require long-term battery life and a waterproof design to ensure functionality in different environmental conditions. Additionally, on the receiving node the main challenge is the real-time monitoring of multiple users and simultaneous data decoding. This includes the real-time processing of the streamed video, the identification of multiple users, the isolation of their signals from other ambient lighting sources, and the continuous tracking of their movements over time. Addressing these challenges requires the implementation of cloud-based architectures and complex computer vision models. Although

such systems offer great potential in environments where the continuous monitoring of individuals' physical well-being is of vital importance.

#### ACKNOWLEDGMENTS

This work has been supported by OCCAM project (PID2020-114561RB-100) and SUCCESS (TED2021-130049B-C21) from Agencia Estatal de Investigación (Spain Government), by Grant Catalina Ruiz (APCR2022010014) by the Agencia Canaria de Investigación, Innovación y Sociedad de la Información (ACIISI) under European Social Fund. This work is based upon work from COST Action CA19111 (European Network on Future Generation Optical Wireless Communication Technologies, NEWFOCUS), supported by COST (European Cooperation in Science and Technology).

#### REFERENCES

- [1] "IEEE standards association," https://standards.ieee.org/ieee/802.15.7a/ 10367/, accessed: 2023-09-15.
- [2] S. R. Teli, S. Zvanovec, and Z. Ghassemlooy, "Optical internet of things within 5G: Applications and challenges," in 2018 IEEE International Conference on Internet of Things and Intelligence System (IOTAIS), 2018, pp. 40–45.
- [3] V. P. Rachim, J. An, P. N. Quan, and W.-Y. Chung, "A novel smartphone camera-LED communication for clinical signal transmission in mhealthrehabilitation system," in 2017 39th Annual International Conference of the IEEE Engineering in Medicine and Biology Society (EMBC). IEEE, 2017, pp. 3437–3440.
- [4] M. F. Ahmed, M. K. Hasan, M. Shahjalal, M. M. Alam, and Y. M. Jang, "Design and implementation of an occ-based real-time heart rate and pulse-oxygen saturation monitoring system," *IEEE Access*, vol. 8, pp. 198740–198747, 2020.
- [5] H. Herfandi, O. S. Sitanggang, M. R. A. Nasution, H. Nguyen, and Y. M. Jang, "Real-time patient indoor health monitoring and location tracking with optical camera communications on the internet of medical things," *Applied Sciences*, vol. 14, no. 3, p. 1153, 2024.
- [6] S. Teli, W. A. Cahyadi, and Y. H. Chung, "Optical camera communication: Motion over camera," *IEEE Communications Magazine*, vol. 55, no. 8, pp. 156–162, 2017.
- [7] M. F. Ahmed, M. K. Hasan, M. Z. Chowdhury, N. C. Hoan, and Y. M. Jang, "Continuous status monitoring of industrial valve using occ-enabled wireless sensor network," *IEEE Transactions on Instrumentation and Measurement*, vol. 71, pp. 1–10, 2022.
- [8] V. Matus, E. Eso, S. R. Teli, R. Perez-Jimenez, and S. Zvanovec, "Experimentally derived feasibility of optical camera communications under turbulence and fog conditions," *Sensors*, vol. 20, no. 3, p. 757, 2020.
- [9] V. Matus, V. Guerra, C. Jurado-Verdu, S. Zvanovec, and R. Perez-Jimenez, "Wireless sensor networks using sub-pixel optical camera communications: Advances in experimental channel evaluation," *Sensors*, vol. 21, no. 8, p. 2739, 2021.
- [10] V. Matus, J. Rabadán, and R. Perez-Jimenez, "Practical implementation of outdoor optical camera communication systems with simultaneous video and data acquisition," OPTICAL WIRELESS COMMUNICATION TECHNOLOGIES, p. 31, 2023.
- [11] E. Niarchou, V. Matus, J. Rabadan, V. Guerra, and R. Perez-Jimenez, "Experimental evaluation of led-based wearable transmitter for optical camera communications systems," in 2023 17th International Conference on Telecommunications (ConTEL). IEEE, 2023, pp. 1–5.
- [12] K. Eöllős-Jarošíková, V. Neuman, E. Niarchou, O. Gomez-Cardenes, S. Zvánovec, R. Perez-Jimenez, and M. Komanec, "Pilot experiments of side-emitting fiber-based optical camera communication for wearable applications," in 2023 South American Conference On Visible Light Communications (SACVLC). IEEE, 2023, pp. 65–69.
- [13] A. Nano, "ATmega328 16 MHz, 2KB SRAM, 32KB flash, 1KB EEPROM," Datasheet, 2023. [Online]. Available: https://docs.arduino.cc/ resources/datasheets/A000005-datasheet.pdf
- [14] Samsung, "Samsung galaxy S23," https:// www.samsung.com/us/smartphones/galaxy-s23/buy/ galaxy-s23-256gb-unlocked-sm-s911uzkexaa/, 2023, accessed: [2024-02-09].

2024 14th International Symposium on Communication Systems, Networks and Digital Signal Processing (CSNDSP)

- [15] T. Le, N.-T. Le, and Y. M. Jang, "Performance of rolling shutter and global shutter camera in optical camera communications," in 2015 International Conference on Information and Communication Technology Convergence (ICTC). IEEE, 2015, pp. 124–128.
   [16] S. R. Teli, K. Eollosova, S. Zvanovec, Z. Ghassemlooy, and M. Komanec,

"Optical camera communications link using an led-coupled illuminating optical fiber," *Opt. Lett.*, vol. 46, no. 11, pp. 2622–2625, Jun 2021. [Online]. Available: https://opg.optica.org/ol/abstract.cfm?URI=ol-46-11-2622

B

## Collaborations

This appendix contains the articles in which the author has participated as a collaborator.

2022 13th International Symposium on Communication Systems, Networks and Digital Signal Processing (CSNDSP)

### Near-Infrared based Optical Camera Communications

Othman Isam Younus<sup>1</sup>, Eleni Niarchou<sup>2</sup>, , Shivani Rajendra Teli<sup>3</sup>, Zabih Ghassemlooy<sup>1</sup>, Stanislav Zvanovec<sup>3</sup>, and Hoa Le Minh<sup>1</sup>

- <sup>1</sup> Optical Communications Research Group, Faculty of Engineering and Environment, Northumbria University, Newcastle upon Tyne NE1 8ST, U.K.
- <sup>2</sup> Institute for Technological Development and Innovation in Communications, Universidad de Las Palmas de Gran Canaria, 35001 Las Palmas
- <sup>3</sup> Department of Electromagnetic Field, Faculty of Electrical Engineering, Czech Technical University in Prague, Prague 16627, Czech Republic

Corresponding author: Othman Isam Younus (e-mail: othman.younus@outlook.com)

Abstract— We report, for the first time in the literature, an optical camera communications (OCC) link leveraging a near-infrared band at a wavelength of 850 nm that is visible to a standard camera and undetectable by the human eye. An experimental test-bed is developed and evaluated for the proposed system. The quality of the proposed communication link is measured in terms of the eye diagram and the bit error rate (BER) for different signal bandwidths. We demonstrated that, an acceptable BER (below the forward error correction limit) can be achieved with a data rate of ~2 kbps using a single near-infrared light-emitting diode, a commercially available camera with a 30-frame rate. This work paves the way to enable the use of the OCC links to many internet of things applications with low cost and no additional complexity.

Keywords— Near-Infrared, optical camera communications (OCC), LED, optical wireless communications

#### I. INTRODUCTION

Optical wireless communications (OWC) as a subset of optical communication, which involves infrared (IR), ultraviolet, and visible light signals[1]. The wavelength of infrared light is longer than that of visible light, since it may be harmless for humans when used at low levels, yet undetectable to the naked eye [2]. This feature distinguishes it from visible light in terms of prospective applications.

The vast majority of works reported on light positioning systems use the visible light band, even though very high (subcentimetre or even submillimeter) accuracies are also possible by adopting the IR band [3]. Remarkably, even though the IR technology is rather a niche, its implementations vary widely. In general, IR signals are used mainly to provide positioning services [4]. For instance, active beacon systems have fixed infrared receivers (Rxs) or transmitters (Txs) placed at known locations in indoor environments, and mobile Txs or Rxs whose positions are unknown. The IR pulse streams sent from the Txs are used to determine the location of the mobile nodes. An example of this technology is the HTC VIVE [5], wherein, a virtual reality system uses two IR base stations (i.e., access points) to determine the 60 of freedom position of the headset and the controller. Another example is Microsoft Kinect, which uses a continuously projected IR structured light to detect the environment using an IR camera [6].

The use of these wavelength ranges has some additional advantages compared to the visible light communications (VLC) links. For instance, light dimming is not an issue in IR-based systems, and the uplink implementation using IR is much more convenient as it avoids the use of a bright visible light next to the user's equipment. In addition, IR-based links

can (i) provide much higher transmission data rates compared to the VLC systems [7]; (ii) offer a longer transmission range via both non-directed diffused and line-of-sight paths [8], [9]. Therefore, IR or near-IR wavelength ranges could be the potential candidates for data communications, in which, the IR light emitting diodes (LEDs) are employed as the Tx. As for the detection, an image sensor (IS)-based Rx can be utilised to spatially receive the transmitted information using a single or multiple Tx (i.e., LEDs). This technology is best known as VLC and optical camera communications (OCC).

The OCC technology leverages the use of off-the-shelf ISs, which were addressed and standardized under the IEEE 802.15.7m [10]. The ISs represent the fastest-growing semiconductor product category in the last decade with a revenue quadrupling between 2010 and 2019 to reach over \$18 billion [11]. Hence, the ISs may be considered the main key sensor for the Internet of things (or the Internet of everything) applications as part of the fifth- and sixth-generation wireless networks [12], [13]. The application includes data communication [14], intelligent transport systems [15], indoor positioning, digital signage, drone-to-drone communication, augmented/virtual reality, motion capture [16], mobile and security application communication.

Consequently, OCC combined with IR may find potential applications as a part of IoTs advancement. For instance, the use of the off-the-shelf camera to detect information from an IR-LED on the ground, which is already available in most indoor and outdoor environments [18]. Hence, integrating available cameras for a dual-use of communication and vision purposes can lead to higher energy efficiency, and lower costs. In [19], the IR optical communication exploited the advantages of OCC and proposed both practical indoor wireless communication and positioning. In [4], by using steered narrow IR beams, high capacity and accurate localization were offered to individual user devices. Upstream signaling can be applied for identifying a large number of active user devices, thus keeping track of their movements, and monitoring the channel behaviour.

Alike the previous works, we have implemented an OCC link to capture the transmitted invisible light with a wavelength of 850 nm for the first time, to the best of authors' knowledge. The Tx was characterised to investigate its suitability and functionality for data communications. An

experimental test-bed is developed for the proposed system, and the quality of the communication link is measured in terms of eye-opening and therefore the bit error rate (BER) for range of bandwidth of the transmitted signal.

The remainder of the paper is organised as follows: Section II introduces the system model. The numerical results and discussion are presented in Section III. Finally, Section IV draws the final conclusion.

#### II. SYSTEM MODEL

Figure 1 illustrates the block diagram of the proposed OCC link, in which, a pseudorandom binary sequence (PRBS) with a length of 2  $^{13}-1$  is generated using Matlab® at the Tx side. The data is then up-sampled with  $n_{\rm samp}$  of 50 prior to being encoded in the non-return to zero (NRZ)-Manchester line code (MLC) format. The MLC signal is utilised to ensure a uniform distribution of 1 and 0 symbols and facilitates both decoding and synchronisation processes of the signal. The PRBS signal s(t) is split into sub-sequences with effective symbols per packet with the length of  $P_{\rm bir}$ -symbol. The effective symbols are packetized to ensure accurate detection at the Rx. The formed packet  $Q^{\rm th}$  contains a  $P_{\rm bir}$ -symbol size of 20 symbols and 5-bit for each pre-amble  $P_{\rm rc}$  and post-amble  $P_{\rm ost}$  with the sequences of [11100] and [00111], respectively.

The patterns of the header and footer are designed such that they never occur in the MLC pattern in the payload. To investigate the link performance, the Tx bandwidth  $f_{\rm Tx}$  is set to vary between 300 and 700 Hz. The data is then loaded into a signal generator (Teledyne LeCroy T3AWG3252) to generate the electrical signal for intensity modulation of the LED via a LED driver. Note, at the Tx, an optical lens is used to focus the transmitted beams before transmission over a 50 cm free space channel.

At the Rx side, the intensity-modulated optical signal is captured using a CMOS IS-based Rx (Thorlabs DCC1645C) via an optical diffuser. The rolling shutter (RS)-based camera is modelled using a single convex lens with a focal length f. The transmission speed in the RS-based OCC system is defined by the amount of the information that can be captured by an image at the distance transmission range d, which depends on the acquired number of samples (i.e., pixel rows) and is given by [20]:

$$N_{row} = 2 f \times tan\left(\frac{FoV}{2}\right) = 2 f \times \frac{L}{2d},$$
 (1)

where FoV is the angular field of view, and L is the Tx normalized length (i.e., the diameter). Note that, the acquired  $N_{\text{row}}$  is incorporated with the sampling frequency of the IS,

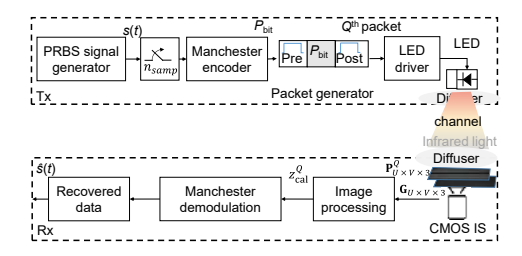


Fig. 1. Block diagram for OCC system.

known as the rolling rate of IS,  $F_s$  (i.e., the frequency at which the row pixels are sampled at the image plane).

Therefore, the maximum frequency of the transmitted signal is limited to  $\frac{F_s}{2}$  according to Nyquist's theorem.  $F_s$  value depends on the pixel clock and  $T_{\rm exp}$  (i.e., the time that every sample (pixel) of the IS is exposed to the light). Note,  $T_{\rm exp}$  acts as a moving-average filter with the frequency resolution given by [21]:

$$\Delta f = \frac{1}{T_{exp}} = \frac{F_{s}}{N_{row}(d)},\tag{2}$$

where  $F_s$  is defined in terms of the bandwidth of the transmitted signal  $f_{\text{Tx}}$  and the number of received pixels per symbol  $N_{\text{pps}}$ , which is given by:

$$F_s = N_{pps} \cdot f_{Tx} \,. \tag{3}$$

Note, (i)  $N_{\rm pps}$  varies with the payload  $P_{\rm bit}$ ; and (ii) the maximum transmission distance is proportional to both  $\Delta f$  and the size (diameter) of the light source. Higher  $T_{\rm exp}$  results in increased signal intensity levels, and, therefore, higher signal-to-noise-ratio (SNR) at the cost of reduced Rx bandwidth.

The RGB captured frame  $\mathbf{P}^Q_{U \times V \times 3}$  of  $Q^{\text{th}}$  Tx packets are processed off-line in Matlab®, in which, the adopted flow chart shown in Fig. 2 is applied to detect the received information via the IR and VLC channels.  $\mathbf{P}^Q_{U \times V \times 3}$  is initially converted to the grayscale to eliminate the hue and saturation information while retaining the luminance of the image plane. It is noted that, the channel within the invisible range for the human eye (i.e., only observed by the IS), higher absorption of longer wavelengths will help to reduce the risk of causing any damage to the human eye as compared with other technologies. The intensities for all pixels are aggregated together at each row since they are exposed to the incident light at the same time. This increases the SNR of the signal by the number of row pixels.

Furthermore, the DC gain of the optical signal is measured to overcome the non-uniformity of the IS captured signal using a calibration matrix. The calibration matrix is constructed by acquiring  $20 \times \mathbf{G}_{U \times V \times 3}$ , which represents the DC signal (i.e., captured frame without applying the baseband signal).

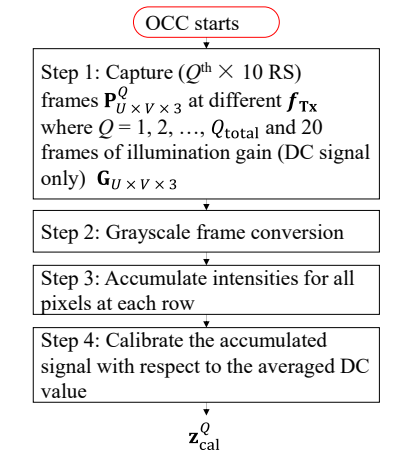


Fig. 2. Signal extraction flow chart.

2022 13th International Symposium on Communication Systems, Networks and Digital Signal Processing (CSNDSP)

Table 1. System parameters.			
Description		Value	
	LED type  • Wavelength	Vishay (VSMY1850X01) 850 nm	
	<ul> <li>Bandwidth</li> </ul>	9.4 MHz	
Tx	Tx signal bandwidth $f_{Tx}$ (Hz)	300-700 Hz	
	Tx bias current	100 mA	
	Optical lens	Condenser (ACK25416U	
	Camera model	Thorlabs DCC1645C-HQ	
	Exposure time $T_{\text{exp}}$	2 ms	
	Maximum SNR of IS	44 dB	
Camera Rx	Lens type	Navitar 12 mm F/1.8 2/3" 10 MP	
Camera Kx	Pixel clock	10 MHz	
	Camera raw image resolution	1280 × 1024 pixels	
	Diffuser type	Glass with diameter of 2.0", 220 GRIT	
	Data format	MLC	
Packet	Symbol per packet Pbit	20 symbols	
Generator	Packet generator sample rate	11.125 kHz	
	Number of samples $n_{\text{samp}}$	p50	
Channel	Channel length	50 cm	

Note, none of the pixels of the region of interest in the calibration matrix should be over/under exposed. The received signal was normalized using the measured  $\mathbf{G}_{U \times V \times 3}$  and the calibrated signals  $\mathbf{Z}_{cal}^Q$  is then estimated for the optical channel.

In order to ensure the full packet inclusion in the captured frame (i.e., contains both pre- and post-ambles), a  $10 \times P_{U \times V \times 3}^Q$  is captured at each  $Q^{th}$  transmitted packet. A resampling process is then applied to resize the signal length based on the packet size observed in pixels. Next, a correlation algorithm is used to maintain the synchronization between the transmitted  $Q^{th}$  transmitted packet and the received  $\mathbf{z}_{cal}^Q$  signals, where a filtered version of  $\mathbf{z}_{cal}^Q$  is simulated based on the encoded  $Q^{th}$  packet using a moving average filter. Note, the window size of the filter is set to  $n_{samp}$  since it provides an optimal match compared with the observed signal. All the key system parameters are listed in Table 1.

#### III. RESULTS AND DISCUSSION

The experimental work is focused on establishing an OCC link to capture near-infrared signals using a regular IS. The optoelectronic characteristics of the Tx in terms of the voltage, current, and output power are firstly presented in Fig. 3.

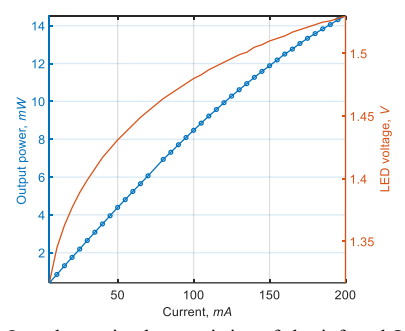


Fig. 3. Optoelectronic characteristics of the infrared LED in terms of Current-voltage (I-V) and the Output optical power;

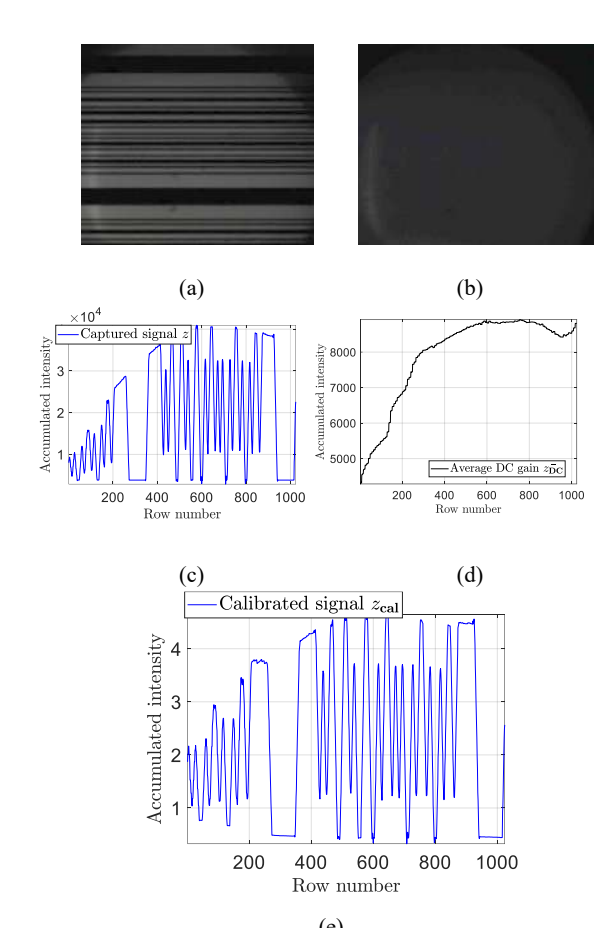


Fig. 4. Examples of received  $Q^{\text{th}}$ Tx packet signal at a  $T_{\text{exp}}$  of 2 ms: (a) Received frame  $\mathbf{P}_{U\times V\times 3}^Q$ , (b) Received DC gain frame  $\mathbf{G}_{U\times V\times 3}$ , (c) calibrated signal  $\mathbf{z}$  without the DC gain normalization, (d) the average DC gain  $\mathbf{z}_{\text{DC}}$ , and (e)  $\mathbf{z}_{\text{cal}}$  signals with the DC gain  $\mathbf{z}_{\text{DC}}$  normalization.

Next, the captured  $\mathbf{P}_{U\times V\times 3}^Q$  of  $\mathcal{Q}^{\text{th}}$  transmitted packets as well as  $\mathbf{G}_{U\times V\times 3}$  frames are processed as described in section II. Figure 4 (a and b) depicts samples of captured frames  $\mathbf{P}_{U\times V\times 3}^Q$  and  $\mathbf{G}_{U\times V\times 3}$  in a respective way. The signals are then detected based on the summation of pixel intensities at each row for both  $\mathbf{P}_{U\times V\times 3}^Q$  and  $\mathbf{G}_{U\times V\times 3}$ , see Fig. 4 (c and d). Subsequently, the calibrated signal  $\mathbf{z}_{\text{cal}}^Q$  is estimated as shown in Fig. 4 (e).

The communication channel is investigated for a range of bandwidth  $f_{\rm Tx}$  between 300 and 700 Hz for a fixed exposure time as well as the payload size. Fig. 5 depicts examples of the acquired frames for the transmitted packets for  $f_{\rm Tx}$  of 300, 350, 400, 500, 600, and 700 Hz. Increasing  $f_{\rm Tx}$  decreases the number of received pixels for each MLC symbol, thus, reducing the quality of the communications link. The IS sampling frequency of 13.31 kHz is recorded based on the demodulated signal, see Fig. 4.

The recorded number of pixels used for each MLC symbol is shown in Table 2. The regenerated signal quality is measured by means of eye-diagrams, see Fig. 6, where the eye

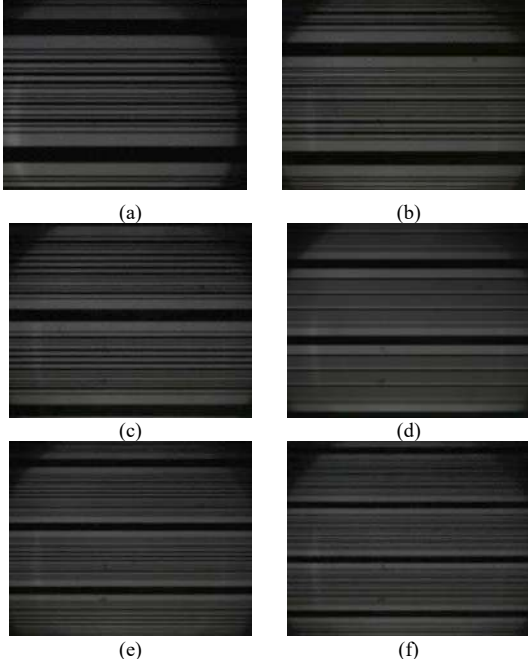


Fig. 5. Examples of the frame acquisition based on CIS for MLC packets and  $f_{\rm Tx}$  of: (a) 300 Hz, (b) 350 Hz, (c) 400 Hz, (d) 500 Hz, (e) 600 Hz, and (f) 700 Hz.

opening indicates the decision threshold and the impact of the intersymbol interference (ISI) on the received signal. The threshold can be easily differentiated for  $f_{\rm Tx}$  of 300, 400, and 500 Hz, see Figs. 6(a) and (b), while it is difficult to retrieve the signal beyond 500 Hz, see Fig. 6(c).

Table 2. I of 1024 p	Results with $R_f$ ox	of 30 fp	s, P <sub>bit</sub> of 20	) symbols,	and IS width
Total number of symbols/ packet	Number of pixels/symbol $(N_{\rm pps})$	f <sub>Tx</sub> (Hz)	Symbols per frame	R <sub>b</sub> obtained (kbps)	Normalized eye height (a.u.)
30	44.39	300	23.07	1.38	0.36
30	33.30	400	30.76	1.85	0.21
30	26.64	500	38.44	2.31	0.15
30	22.20	600	46.13	2.77	~0

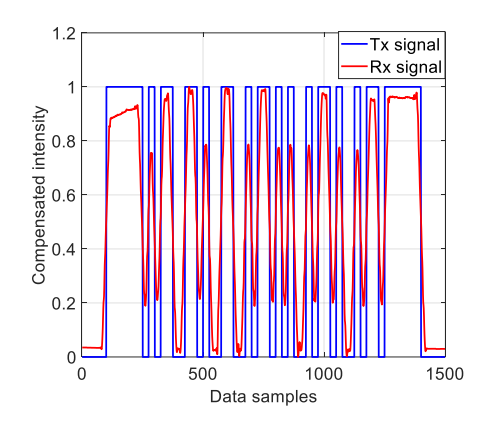


Fig. 7. An example of the transmitted and received signal for MLC signal with  $P_{\rm bit}$  of 20 symbols/packet and  $f_{\rm Tx}$  of 300 Hz

Figure 7 shows an example of transmitted and received signals for  $P_{\rm bit}$  of 70 bits. Consequently, the eye's heights and the data rate  $R_b$  obtained is shown in Table 2. Note that, the recorded BER shows that the system is capable of achieving an error free transmission (i.e., a BER <  $10^{-4}$ ) for  $f_{\rm Tx}$  of 300, and 400 Hz, whereas the quality of the communication link is reduced at  $f_{\rm Tx}$  of 600 Hz and the BER observed is  $17 \times 10^{-3}$ . The experimental work shows that  $R_b$  of  $\sim$ 2 kbps can be obtained using a single LED and a regular IS.

#### IV. CONCLUSION

We proposed, for the first time in literature, an OCC link-based infrared signal with a wavelength of 850 nm. The Tx was characterised to investigate it is suitability and functionality for data communications. An experimental testbed is developed for the proposed system, and the quality of the communication link was measured in terms of eye-opening and the bit error rates via different Tx signal bandwidths. The quality of received signals was measured based on the eye-diagram opening. We demonstrated that, an acceptable BER (below the forward error correction limit) can be achieved with a data rate of ~2 kbps using a single LED, CIS with a 30 frame rate and a commercially available camera. This work paves the way to enable the use of the OCC links to many IoT applications with low cost and no additional complexity.

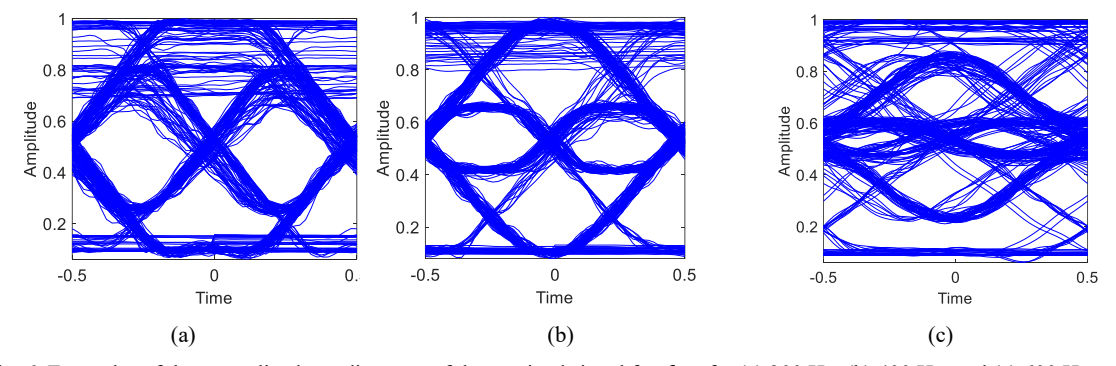


Fig. 6. Examples of the normalized eye diagrams of the received signal for  $f_{\text{Tx}}$  of: (a) 300 Hz, (b) 400 Hz, and (c) 600 Hz.

2022 13th International Symposium on Communication Systems, Networks and Digital Signal Processing (CSNDSP)

#### ACKNOWLEDGEMENT

This work is supported by Northumbria University Ph.D. Scholarship, and the EU COST Action NEWFOCUS CA19111.

#### REFERENCES

- [1] Z. Ghassemlooy, P. Luo, and S. Zvanovec, "Optical Camera Communications," in Optical Wireless Communications, M. Uysal, C. Capsoni, Z. Ghassemlooy, A. Boucouvalas, and E. Udvary, Eds. Cham: Springer International Publishing, 2016, pp. 547-568. doi: 10.1007/978-3-319-30201-0 25.
- [2] M. F. Keskin, O. Erdem, and S. Gezici, "Cooperative Localization in Hybrid Infrared/Visible Light Networks: Theoretical Limits and Distributed Algorithms," IEEE Trans. Signal Inf. Process. Netw., vol. 5, no. 1, pp. 181-197, Mar. 2019, doi: 10.1109/TSIPN.2018.2866344.
- [3] G. M. Mendoza-Silva, J. Torres-Sospedra, and J. Huerta, "A Meta-Review of Indoor Positioning Systems," Sensors, vol. 19, no. 20, 2019, doi: 10.3390/s19204507.
- [4] N. Q. Pham, K. Mekonnen, E. Tangdiongga, A. Mefleh, and T. Koonen, "User Localization and Upstream Signaling for Beam-Steered Infrared Light Communication System," IEEE Photonics Technol. Lett., vol. 33, no. 11, pp. 545-548, Jun. 2021, doi: 10.1109/LPT.2021.3075080.
- [5] HTC Corporation, "Discover Virtual Reality Beyond Imagination," *Vive. VIVETM*, 2018. https://www.vive.com/us/
- [6] Z. Zhang, "Microsoft kinect sensor and its effect," IEEE Multimed., vol. 19, no. 2, pp. 4-10, 2012.
- [7] M. Alresheedi, A. Hussein, J. Elmirghani, and A. Taha Hussein, "Uplink Design in VLC Systems with IR Sources and Beam Steering," IET Commun., vol. 11, Oct. 2016, doi: 10.1049/ietcom 2016.0495.
- [8] M. Alresheedi, A. Taha Hussein, and J. Elmirghani, Hybrid diffuse IR transmitter supporting VLC systems with imaging receivers. 2016, p. 6. doi: 10.1109/ICTON.2016.7550290.
- [9] O. Z. Alsulami, M. T. Alresheedi, and J. M. H. Elmirghani, "Infrared Uplink Design for Visible Light Communication (VLC) Systems with Beam Steering," in 2019 IEEE International Conference on Computational Science and Engineering (CSE) and IEEE International Conference on Embedded and Ubiquitous Computing (EUC), Aug. 2019, 57-60. pp. 10.1109/CSE/EUC.2019.00020.
- [10] T. Nguyen, A. Islam, T. Yamazato, and Y. M. Jang, "Technical Issues on IEEE 802.15.7m Image Sensor Communication Standardization," IEEE Commun. Mag., vol. 56, no. 2, pp. 213-218, Feb. 2018, doi: 10.1109/MCOM.2018.1700134.
- [11] IC Insights, "A Market Analysis and Forecast for the Optoelectronics, Sensors/Actuators, and Discretes," May 2021. [Online]. Available: icinsights.com

- [12] N. Van Hoa, H. Nguyen, C. H. Nguyen, and Y. Min Jang, "OCC Technology-based Developing IoT Network," in 2020 International Conference on Information and Communication Technology Convergence (ICTC), Oct. 2020, pp. 670-673. 10.1109/ICTC49870.2020.9289552.
- [13] M. Z. Chowdhury, T. Hossan, A. Islam, and Y. M. Jang, "A Comparative Survey of Optical Wireless Technologies: Architectures and Applications," vol. 6, p. 22, 2018.
- [14] O. I. Younus et al., "Data Rate Enhancement in Optical Camera Communications Using an Artificial Neural Network Equaliser," IEEE Access, vol. 8, pp. 42656–42665, 2020, doi: 10.1109/ACCESS.2020.2976537.
- [15] E. Eso et al., "Experimental Demonstration of Vehicle to Road Side Infrastructure Visible Light Communications," in 2019 2nd West Asian Colloquium on Optical Wireless Communications (WACOWC), Tehran, Iran, Apr. 2019, pp. 85-89. doi: 10.1109/WACOWC.2019.8770186.
- [16] S. Teli and Y.-H. Chung, "Selective capture based high-speed optical vehicular signaling system," Signal Process. Image Commun., vol. 68, Sep. 2018, doi: 10.1016/j.image.2018.08.009.
- [17] O. I. Younus, H. Le Minh, P. T. Dat, N. Yamamoto, A. T. Pham, and Z. Ghassemlooy, "Dynamic Physical-Layer Secured Link in a Mobile MIMO VLC System," IEEE Photonics J., vol. 12, no. 3, pp. 1-14, Jun. 2020, doi: 10.1109/JPHOT.2020.2990798.
- [18] T.-C. Bui and S. Kiravittaya, "Demonstration of using camera communication based infrared LED for uplink in indoor visible light communication," in 2016 IEEE Sixth International Conference on Communications and Electronics (ICCE), Ha-Long City, Quang Ninh Province, Vietnam, Jul. 2016, pp. 71-76. 10.1109/CCE.2016.7562615.
- [19] W. A. Cahyadi and Y. H. Chung, "Experimental demonstration of indoor uplink near-infrared LED camera communication," p. 8,
- [20] H. Nguyen, T. L. Pham, H. Nguyen, and Y. M. Jang, "Tradeoff Communication distance and Data rate of Rolling shutter OCC," in 2019 Eleventh International Conference on Ubiquitous and Future Networks (ICUFN), Jul. 2019, pp. 148-151. doi: 10.1109/ICUFN.2019.8806101.
- [21] O. I. Younus, N. B. Hassan, Z. Ghassemlooy, S. Zvanovec, L. N. Alves, and H. Le-Minh, "The Utilization of Artificial Neural Network Equalizer in Optical Camera Communications," Sensors, vol. 21, no. 8, 2021, doi: 10.3390/s21082826.

110

## Pilot Experiments of Side-Emitting Fiber-Based Optical Camera Communication for Wearable Applications

#### Klára Eöllős-Jarošíková

Department of Electromagnetic Field Faculty of Electrical Engineering Czech Technical University in Prague Prague, Czech Republic eollokla@fel.cvut.cz

## Oscar Gomez-Cardenes Department of Industrial Engineering University of La Laguna Santa Cruz de Tenerife, Spain ogomezca@ull.edu.es

#### Matěj Komanec

Department of Electromagnetic Field
Faculty of Electrical Engineering
Czech Technical University in Prague
Prague, Czech Republic
komanmat@fel.cvut.cz

#### Vojtěch Neuman

Department of Electromagnetic Field Faculty of Electrical Engineering Czech Technical University in Prague Prague, Czech Republic vojtech.neuman@fel.cvut.cz

#### Stanislav Zvánovec

Department of Electromagnetic Field
Faculty of Electrical Engineering
Czech Technical University in Prague
Prague, Czech Republic
xzvanove@fel.cvut.cz

#### Eleni Niarchou

Technological Centre for Innovation in Communications University of Las Palmas de Gran Canaria Las Palmas, Spain eleni.niarchou101@alu.ulpgc.es

#### Rafael Perez-Jimenez

Institute for Technological Development and Innovation in Communications
Universidad de Las Palmas de Gran Canaria
Las Palmas de Gran Canaria, Spain rperez@idetic.eu

Abstract—We demonstrate for the first time the application of LED-based optical camera communication using a side-emitting fiber in wearable applications. A 1.2-m long plastic side-emitting fiber with a 4-mm outer diameter acts as a distributed transmitter. The side-emitting fiber is attached to a T-shirt over the shoulder with a 50-cm section of the fiber both on the front and back side of the T-shirt. This expands the possibilities of data detection by the rolling shutter camera. The light from a white LED is coupled into the side-emitting fiber with LED on-off keying (OOK) modulation frequencies of 2.64 kHz, 3.54 kHz, and 5.31 kHz. The results show bit error rate bellow  $3.8\cdot 10^{-3}$  for up to 200 cm fiber to camera distance.

Index Terms—light emitting diode, optical camera communication, rolling shutter camera, side-emitting fiber, visible light communication, wearable applications

#### I. INTRODUCTION

Optical camera communication (OCC) systems have been growing rapidly as a part of visible light communication (VLC). The OCC technology uses a visible light source as a transmitter (Tx), e.g., a light-emitting diode (LED), and

The research has been supported by the CTU in Prague SGS23/168/OHK3/3T/13 and CELSA-22-205 project POWER. Oscar Gomez-Cardenes has been supported by the 'Catalina Ruiz training aid program for research personnel' of the Regional Ministry of Economy, Knowledge, and Employment, as well as the European Social Fund.

a rolling-shutter camera as a receiver (Rx), which captures a set of image frames with dark and bright stripes representing logical zeros and ones [1]–[3]. We recently demonstrated, how the traditional OCC systems can be expanded by using a side-emitting fiber acting as a distributed transmitter [4], [5]. We explored the possibilities of side-emitting fibers as a part of OCC systems in general, and on top of these foundations, we would like to extend the technology toward wearable systems in this paper.

The idea of wearable systems has been well studied e.g. in [6] and the OCC wearable systems can be built on these foundations. In [7], a microwave radiation-free system for wireless transmission of electroencephalogram (EEG) signals was proposed using a wearable EEG and transmitter with an OCC detector – a mobile phone camera. A hybrid OCC/Bluetooth Low Energy (BLE) system of a wearable sensor for an electrocardiogram (ECG) was described in [8]. The system uses a patch circuit with an integrated LED array and a BLE chip and ensures remote and real-time transmission of data. An OCC-based system for real-time monitoring of heart rate and pulse-oxygen saturation was described in [9], where a wearable LED array is used as a transmitter and a closed-circuit television (CCTV) camera as a receiver. The LEDs were modulated using color intensity modulation and

security in the form of data encoding using a unique key is implemented.

In this paper, we present the first application study of sideemitting fiber-based optical camera communication (OCC) in wearable applications. For this experiment, we attached a 1.2m-long polymethyl methacrylate (PMMA) side-emitting fiber of a 4 mm diameter on a T-shirt and experimentally analyzed the OCC performance. First, the experiment is introduced, describing the used approach, materials, and measurement setup. Next, the results are shown and explained. And last, the impact and importance in the OCC field are discussed and concluded.

#### II. SIDE-EMITTING FIBERS FOR OCC

The side-emitting optical fiber, as opposed to a conventional optical fiber, is specially designed to emit light gradually along the fiber length. The emission of visible light alongside the fiber's length may be described as a side- or glowstick-like emission. The side-emitting fibers can be made of polymer (e.g., PMMA) or silica material or by combining a silica core and a polymer cladding. To achieve side-emission, modifications in the fiber cladding or the fiber core are carried out. The cladding changes include the already mentioned use of polymer cladding over silica core [10] or particles working as scattering centers may be distributed within the cladding [11]. These cladding-embedded particles cause the evanescent wave to scatter, which leads to a transfer of energy away from the core and out from the fiber surface. Alternatively, a variety of particles may be added directly into the core of the fiber causing the passing-through light to scatter and, finally, emit from the fiber [12].

An important parameter describing a side-emitting fiber, besides the fiber diameter and material, is the diffusion length DL, which is defined as the fiber length over which  $90\,\%$  of the coupled optical power is lost. For example, for  $DL=1\,\mathrm{m}$ , there will be  $10\,\%$  of the coupled light at the output of a 1-mlong section of the side-emitting fiber [13] while the rest of the power is mainly radiated along the fiber length and partially attenuated in the fiber structure. The illuminating power P(l) of the side-emitting fiber, the power illuminated from the fiber surface, is then defined in [14] as

$$P(l) = P_0 \cdot 10^{-\alpha l/10},\tag{1}$$

where  $P_0 = P(0)$  is the illuminating power coupled from the light source into the fiber,  $\alpha$  is the attenuation coefficient, which illustrates the attenuation over the length of the side-emitting fiber, and l is the distance on the side-emitting fiber from the point of the light coupling.

With changes in the fiber diameter, the properties of the side-emitting fiber vary as well [12], [15], [16]— the thinner the fiber, the more flexible it is. On the other hand, with the increasing thickness of the fiber, the light is easier and thus more efficiently coupled from an LED into the fiber.

The side-emitting fibers open up new application possibilities as it is effectively a distributed light source. Thanks to the flexible nature of the side-emitting fibers, they can be used

in places where LEDs and LED strips would not be practical [11]. The outer diameter of side-emitting fibers varies from hundreds of micrometers up to 30 mm, which gives us a wide variety of diameters [15] for particular applications. Another advantage of side-emitting fiber over an LED or an LED strip is its radiation pattern. Usually, the radiation pattern of an LED is about 120°, whereas the radiation pattern of a side-emitting fiber is 360° [17].

We have selected a 4-mm diameter PMMA side-emitting fiber for a proof-of-concept validation of the OCC wearable application. The 4-mm fiber diameter offers us a good trade-off between flexibility and pixel width of the side-emitting fiber in the captured image frames.

#### III. SYSTEM OVERVIEW AND MEASUREMENT SETUP

The block diagram of the proposed experiment is illustrated in Fig. 1a). A data packet of non-return to zero (NRZ) on-off keying (OOK) modulation scheme is generated using an Arduino Nano. The 6-bit packet of [011001] pattern is used. The LED has an embedded lens providing a narrow 20° beam pattern which allows low-loss coupling into the side-emitting fiber. A 3D-printed holder is used to fix the LED to one end of the side-emitting fiber.

We use a 1.2-m long PMMA side-emitting fiber with an outer diameter of 4 mm (ZDEA, Super-Bright Side Glow) stitched to a white T-shirt using a white thread, see Fig. 1b) with the white thread in a zig-zag pattern attaching the side-emitting fiber.

Figure 1c) shows how the side-emitting fiber is attached to the T-shirt. The side-emitting fiber is bent over the shoulder with 50 cm sections of the fiber on each side (front and back) of the T-shirt. The segment of the fiber that is lying on the shoulder is about 20 cm long. This offers us more options for how the fiber can be captured in real situations. Since the side-emitting fiber is radiating in a 360° radiation pattern and is attached on top of the T-shirt, it can be captured from multiple angles, from the front, the back, and also from the side. Furthermore, the side view on the side-emitting fiber allows us to capture both the front and back part of the fiber in one image increasing the amount of data pixel width captured in a single image. This would be nearly impossible to achieve while using an LED strip since most LED strips have only 120° radiation pattern. The LED was coupled to the front section of the side-emitting fiber, meaning the illumination level of the fiber gradually decreases as the fiber goes up towards the shoulder, over the shoulder, and down away from the shoulder on the backside.

As a receiver, we use a Raspberry Pi Camera Module 2 to capture the data signal. In Fig. 1d), the camera mounted on a tripod can be seen in the foreground capturing the fiber on the T-shirt. The camera is facing the fiber perpendicularly. The orientation of the camera RS is also perpendicular to the fiber. A summary of used equipment and its fundamental parameters is listed in Table I.

For the experimental part, we calculated the proper parameters to achieve a captured bit size of 20, 15, and 10 pixel

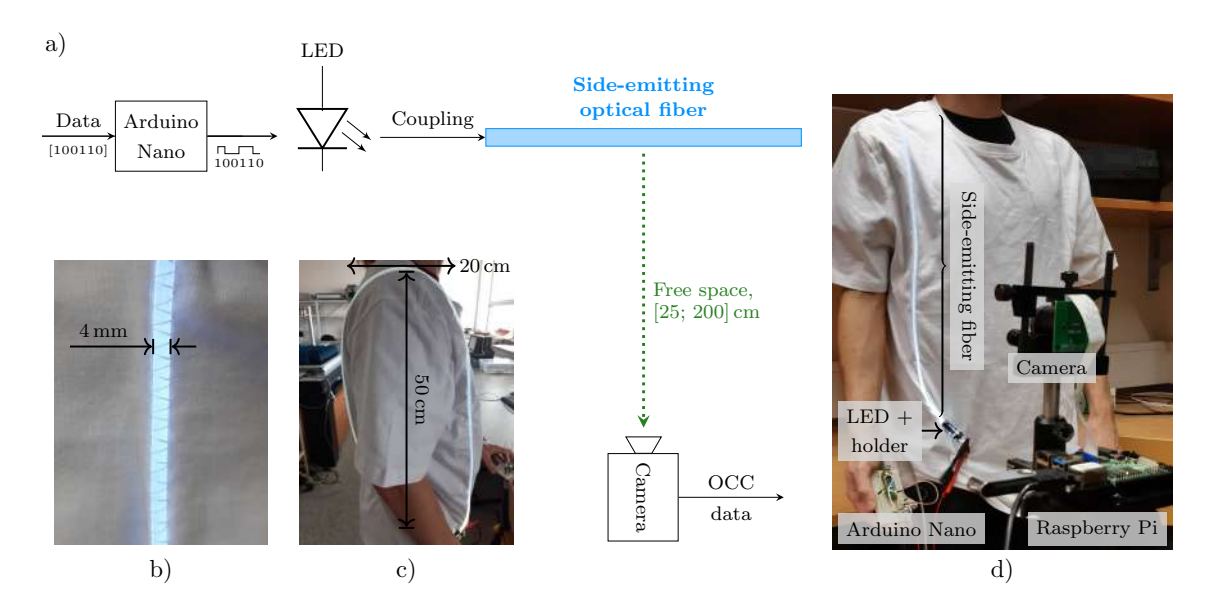


Fig. 1: a) Block diagram of the proposed optical camera communication system in wearable applications using a side-emitting fiber. b) Detail of the side-emitting fiber stitched to a T-shirt. c) The side-emitting fiber is bent over the shoulder. d) Optical camera capturing data (in the front) and the transmitting fiber on the T-shirt (in the back).

TABLE I: Equipment list with key parameters.

Parameter	Value
LED	LA CW20WP6, white
Surface area	$500 \times 500 \mu\mathrm{m}$
Signal generator	Arduino Nano
$f_{ m Tx}$	2.64, 3.54, 5.31 kHz
Data packet size	6 b/packet [011001]
Side-emitting fiber	ZDEA, Super bright
Diameter	4 mm
Material	PMMA
Diffusion length	1 m
Tx-Rx distance d	from 25 to 200 cm
Camera	Raspberry Pi Camera 2
Lens	HX-27227 4 mm f/1.4
Sensor	Sony IMX219
Resolution	$1920 \times 1080$ pixels
$t_{\rm exp}$	$190, 140, 90 \mu s$
$N_{ m pps}$	20, 15, 10  px/symbol

rows per symbol (pps), which corresponds to the values used in our previous paper [5]. First, we calculated the modulation frequencies  $f_{\mathrm{Tx}}$  as

$$f_{\rm Tx} = \frac{1}{\rm N_{\rm pps} \cdot T_{\rm s}} = \frac{1}{t_{\rm symbol}},$$
 (2)

where  $N_{\rm pps}$  is the theoretically expected number of pixel rows per symbol (pps),  $T_{\rm s}$  is the sampling period of the camera, defined as the time between the activation of two consecutive rows [18], and  $t_{\rm symbol}$  is the symbol duration, i.e., the time in which the rolling shutter (RS) camera captures one logical bit. Based on the parameters of our camera and selected  $N_{\rm pps}$ , we determined three transmitter modulation frequencies  $f_{\rm Tx}$ 

of 2.64 kHz, 3.54 kHz, and 5.31 kHz. Camera exposure time  $t_{\rm exp}$  can be calculated using  $t_{\rm symbol}$  as

$$t_{\rm exp} \le \frac{t_{\rm symbol}}{2}.$$
 (3)

By setting a specific  $t_{\rm exp}$  according to used  $t_{\rm symbol}$  intersymbol interference (ISI) is minimized [18].

Each of the three modulation frequencies  $f_{\rm Tx}$  is tested with corresponding exposure time  $t_{\rm exp}$  (190  $\mu{\rm s}$ , 140  $\mu{\rm s}$ , and 90  $\mu{\rm s}$ ) in a set of side-emitting fiber-camera distances d ranging from 25 cm up to 200 cm. A set of 30 to 50 image frames was captured for each setting (measurement).

The camera was facing directly to the side-emitting fiber attached to the T-shirt. The person wearing the T-shirt was standing with their front, or their back towards the camera for the measurements of the front and the back section of the fiber, respectively.

First, captured images are turned into gray-scale images. See Fig. 2 for examples of captured images. Second, a region of interest (ROI) is found. In our experiment, the ROI is represented by a mask that covers the data-transmitting side-emitting fiber in the image frames.

An individual image mask is found for each individual image frame. The mask needs to be found separately, because the wearer of the T-shirt moved slightly during the measurements to mimic standard human motion, e.g., in an office. Due to this slight motion, there was a difference in the position of the ROI in each image and a simple time difference algorithm would not be sufficient. When the ROI is determined

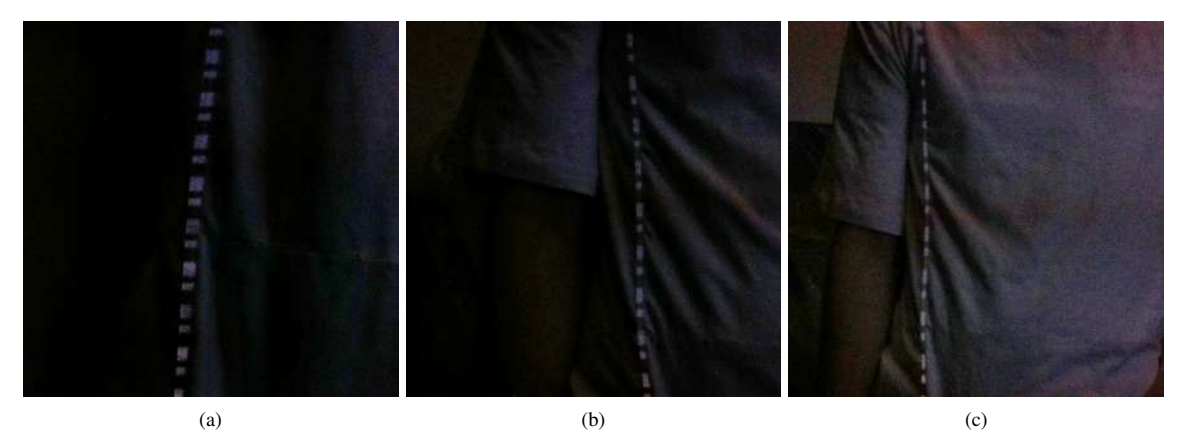


Fig. 2: Examples of captured images of the front of the T-shirt with visible data ( $f_{\rm Tx}=2.64\,{\rm kHz}$ ) on the fiber at different distances: a) 0.5 m, b) 1.0 m, and c) 1.5 m. Note, how the bit size  $N_{\rm pps}$  remains constant with increasing distance. The contrast in these images was increased for presentation purposes to better show the ROI.

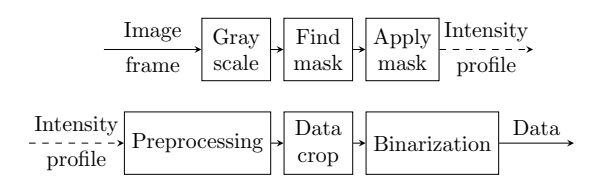


Fig. 3: Block diagram of data processing.

the found mask is applied to each image. Next, the images are preprocessed, they are cropped to eliminate only partially captured bits, and finally, they are binarized. The binarized data are then evaluated. This image processing procedure is outlined in Fig. 3.

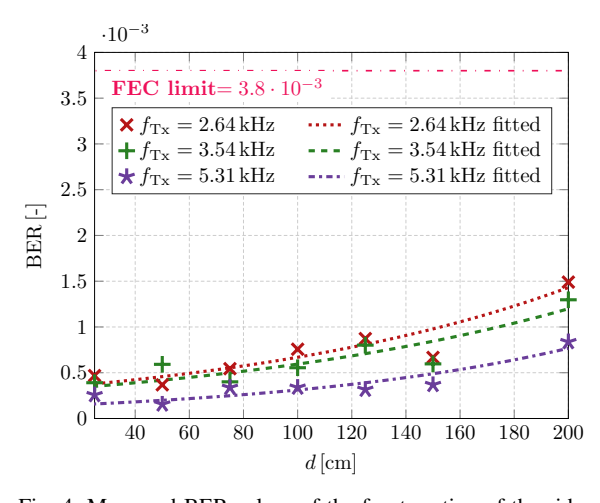


Fig. 4: Measured BER values of the front section of the sideemitting fiber.

### IV. EVALUATION OF OCC LINK PERFORMANCE AND MEASUREMENTS RESULTS

First of all, we experimentally confirmed that the white thread partially covering the side-emitting fiber does not negatively affect the data transmission performance. Though the thread does partially cover the fiber which is visible in the captured image frames, due to the direction of the thread (it overlaps the fiber on a slant) there is enough pixel width of the fiber uncovered to ensure undisturbed data transmission. The performance of the side-emitting fiber-based OCC link was evaluated in terms of bit-error-rate (BER) and reviewed in context to the forward-error-correction (FEC) limit [19], which is  $3.8\cdot 10^{-3}.$ 

Figures 4 and 5 show the resulting BER of the front and the back view on the side-emitting fiber, respectively, with the

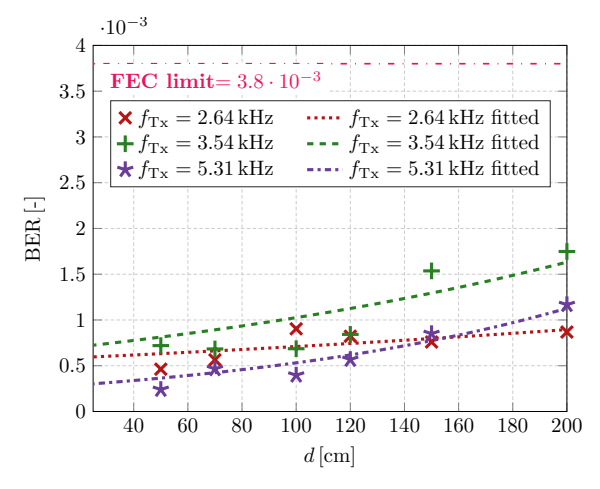


Fig. 5: Measured BER values of the back section of the sideemitting fiber.

T-shirt wearer front-facing (Fig. 4) and rear-facing (Fig. 5) the camera. From the figures, it is evident that the FEC limit of  $3.8\cdot 10^{-3}$  is met for all  $f_{\rm Tx}$ , for the Tx-Rx distances of 25 cm up to 200 cm, and for both front and back view on the fiber.

When we take a closer look at Fig. 4 and 5, the BER is better the closer to the camera the Tx is. The highest  $f_{\rm Tx}$  of 5.31 kHz gives us the best BER results. And when comparing the two variations of the T-shirt wearer, the front view on the side-emitting fiber gives us better results compared to the back view which is due to the side-emitting fiber power loss, since the LED is coupled to the far end of the fiber.

#### V. CONCLUSIONS

We have experimentally evaluated the performance of a side-emitting fiber acting as a distributed transmitter in OCC for wearable applications. We used a 4 mm diameter, 1.2 m long PMMA side-emitting fiber stitched to a white T-shirt as a proof of concept. The resulting OCC link provided BER below the FEC limit for LED modulation frequencies 2.6 to 5.3 kHz for up to 200 cm fiber-camera distance.

Since side-emitting fibers are flexible and lightweight they can be easily attached to clothing (or even integrated fully). Such a wearable side-emitting fiber-based OCC holds significant potential across diverse applications. For example, in the context of first responders, such as firefighters and police, where integration of side-emitting fibers within their uniforms not only augments visibility but also facilitates the real-time transmission of vital health metrics. Moreover, side-emitting fibers can find practical deployment in various headgear.

In the future, we aim to broaden the scope by testing various side-emitting fiber shapes and diameters. Additionally, the wearable side-emitting fiber-based OCC could be measured in different contexts such as with different colors of the T-shirt or using different methods of attaching the side-emitting fiber to the garment.

#### REFERENCES

- P. Luo, M. Zhang, Z. Ghassemlooy, H. L. Minh, H.-M. Tsai, X. Tang, L. C. Png, and D. Han, "Experimental demonstration of RGB LEDbased optical camera communications," *IEEE Photonics Journal*, vol. 7, no. 5, pp. 1–12, 10 2015.
- [2] H.-Y. Lee, H.-M. Lin, Y.-L. Wei, H.-I. Wu, H.-M. Tsai, and K. C.-J. Lin, "RollingLight," in Proceedings of the 13th Annual International Conference on Mobile Systems, Applications, and Services. ACM, 5 2015.
- [3] X. Li, N. B. Hassan, A. Burton, Z. Ghassemlooy, S. Zvanovec, and R. Perez-Jimenez, "A simplified model for the rolling shutter based camera in optical camera communications," in 2019 15th International Conference on Telecommunications (ConTEL). IEEE, 7 2019.
- [4] S. R. Teli, K. Eollosova, S. Zvanovec, Z. Ghassemlooy, and M. Komanec, "Optical camera communications link using an LED-coupled illuminating optical fiber," *Optics Letters*, vol. 46, no. 11, p. 2622, 5 2021.
- [5] K. Eöllős-Jarošíková, V. Neuman, C. M. Jurado-Verdú, S. R. Teli, S. Zvánovec, and M. Komanec, "Long-distance indoor optical camera communication using side-emitting fibers as distributed transmitters," *Optics Express*, vol. 31, no. 16, p. 26980, jul 2023.
  [6] R. D. Fazio, M. D. Vittorio, and P. Visconti, "Innovative IoT solutions
- [6] R. D. Fazio, M. D. Vittorio, and P. Visconti, "Innovative IoT solutions and wearable sensing systems for monitoring human biophysical parameters: A review," *Electronics*, vol. 10, no. 14, p. 1660, jul 2021.
- [7] V. P. Rachim, Y. Jiang, H.-S. Lee, and W.-Y. Chung, "Demonstration of long-distance hazard-free wearable EEG monitoring system using mobile phone visible light communication," *Optics Express*, vol. 25, no. 2, p. 713, jan 2017.
- [8] M. Hasan, M. Shahjalal, M. Chowdhury, and Y. Jang, "Real-time healthcare data transmission for remote patient monitoring in patchbased hybrid OCC/BLE networks," Sensors, vol. 19, no. 5, p. 1208, mar 2019.
- [9] M. F. Ahmed, M. K. Hasan, M. Shahjalal, M. M. Alam, and Y. M. Jang, "Design and implementation of an OCC-based real-time heart rate and pulse-oxygen saturation monitoring system," *IEEE Access*, vol. 8, pp. 198740–198747, 2020.
- [10] M. Lanzarini-Lopes, S. Garcia-Segura, K. Hristovski, M. Messerly, A. J. Simon, and P. Westerhoff, "Particle-modified polymeric cladding on glass optical fibers enhances radial light scattering," *Journal of the Optical Society of America B*, vol. 36, no. 6, p. 1623, may 2019.
- [11] M. Lanzarini-Lopes, Z. Zhao, F. Perreault, S. Garcia-Segura, and P. Westerhoff, "Germicidal glowsticks: Side-emitting optical fibers inhibit pseudomonas aeruginosa and escherichia coli on surfaces," Water Research, vol. 184, p. 116191, 10 2020.
- [12] D. Kremenakova, J. Militky, B. Meryova, and V. Ledl, "Characterization of side emitting plastic optical fibers light intensity loss," pp. 223–228, 7 2013.
- [13] W. S. Klubben, S. L. Logunov, E. J. Fewkes, J. Mooney, P. M. Then, P. G. Wigley, H. Schreiber, K. Matias, C. J. Wilson, and M. Ocampo, "Novel light diffusing fiber for use in medical applications," in SPIE Proceedings, I. Gannot, Ed. SPIE, mar 2016.
- [14] A. W. Snyder and J. Love, Optical Waveguide Theory. Springer US, Dec. 2012.
- [15] M. Zajkowski, "Emission of flux light in side-light fiber optic," in SPIE Proceedings, R. S. Romaniuk and K. T. Pozniak, Eds. SPIE, 10 2003.
- [16] A. Endruweit, A. Alobaidani, D. Furniss, A. Seddon, T. Benson, M. Johnson, and A. Long, "Spectroscopic experiments regarding the efficiency of side emission optical fibres in the UV-A and visible blue spectrum," Optics and Lasers in Engineering, vol. 46, no. 2, pp. 97–105, 2 2008.
- [17] P. Imperatore, G. Testa, G. Persichetti, and R. Bernini, "Power coupling between light diffusing fibers: Modelling and validation," *Journal of Lightwave Technology*, vol. 40, no. 3, pp. 813–821, 2 2022.
- [18] C. Jurado-Verdu, V. Guerra, V. Matus, J. Rabadan, and R. Perez-Jimenez, "Convolutional autoencoder for exposure effects equalization and noise mitigation in optical camera communication," *Optics Express*, vol. 29, no. 15, p. 22973, 6 2021.
- [19] T. Mizuochi, Forward Error Correction. Berlin, Heidelberg: Springer Berlin Heidelberg, 2010, vol. 6, pp. 303–333.